8-2012

IDENTIFICATION AND ANALYSIS OF A NOVEL ROLE FOR THE TOUSLED-LIKE KINASE IN REGULATING MITOTIC SPINDLE DYNAMICS

Jason R. Ford

IDENTIFICATION AND ANALYSIS OF A NOVEL ROLE FOR THE TOUSLED-LIKE KINASE IN REGULATING MITOTIC SPINDLE DYNAMICS

by

Jason Robert Ford, M.S.

APPROVED:

_____
Jill Schumacher, Ph.D., Supervisory Professor

_____
Sharon Dent, Ph.D.

_____
Swathi Arur, Ph.D.

_____
Lei Li, Ph.D.

_____
Xiangwei He, Ph.D.

APPROVED:

_____
Dean, The University of Texas Health Sciences Center at Houston Graduate School of Biomedical Sciences

IDENTIFICATION AND ANALYSIS OF A NOVEL ROLE FOR THE TOUSLED-LIKE KINASE IN REGULATING MITOTIC SPINDLE DYNAMICS

A

DISSERTATION

Presented to the Faculty of

The University of Texas

Health Science Center at Houston

and

The University of Texas

MD Anderson Cancer Center

Graduate School of Biomedical Sciences

in Partial Fulfillment

of the Requirements

for the Degree of

DOCTOR OF PHILOSOPHY

by

Jason Robert Ford, M.S.

Houston, Texas

August 2012

This Thesis is dedicated to my Emma Bear, from whom attention was diverted in order to complete this work.

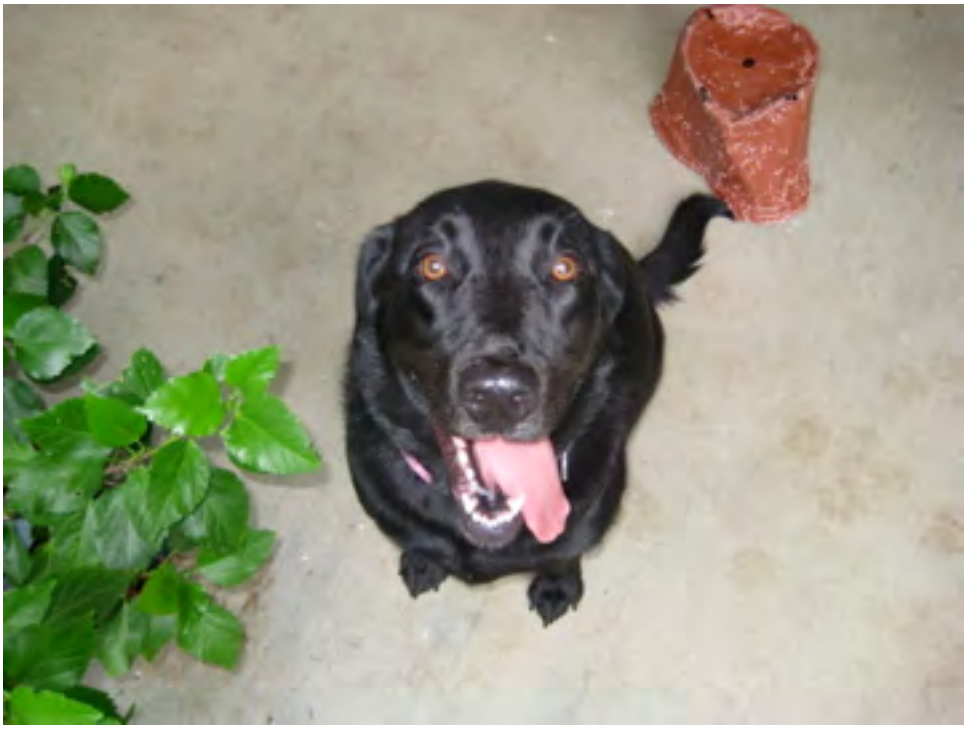

ACKNOWLEDGEMENTS

There are many to whom thanks should be given for their help in completing this Dissertation. First, I would like to acknowledge and thank my supervisor, Dr. Jill Schumacher, whose seemingly limitless support and guidance has helped me grow and mature as a scientist. Additionally, I am grateful to have had such an amazing supervisory committee to direct my training and progress as an independent scientist. Many students fear their committee meetings, but my committee always made me feel at ease and held my education as a top priority. A very special thanks goes to my labmates Tokiko Furuta and Jessica De Orbeta who made everyday in the lab both a pleasure and an adventure, and whose advice and knowledge aided in my scientific growth. I could not have made it through the most challenging points in graduate school without Dr. Swathi Arur, Dr. Victoria Knutson, and Elisabeth Lindheim, and I am grateful for their unyielding support and leadership. I developed some extremely close friends through my tenure at the UT-H GSBS, and I want Dr. Rachid Karam, Dr. Becky MacAllister, Dr. Chris Cassara, and Jessica De Orbeta to know how important they are in my life, and how much they have influenced me over the past several years. Finally, I would like to thank my family for their continuous support and love through my graduate training. They have helped me survive two burglaries, a flooded car, and a large Labrador retriever, and for that I am very grateful.

ABSTRACT

IDENTIFICATION AND ANALYSIS OF A NOVEL ROLE FOR THE TOUSLED-LIKE KINASE IN REGULATING MITOTIC SPINDLE DYNAMICS

Publication No. _____

Jason R. Ford, Ph.D.

Supervisory Professor: Jill M. Schumacher, Ph.D.

Deregulation of kinase activity is one example of how cells become cancerous by evading evolutionary constraints. The Tousled kinase (Tsl) was initially identified in *Arabidopsis thaliana* as a developmentally important kinase. There are two mammalian orthologues of Tsl and one orthologue in *C. elegans*, TLK-1, which is essential for embryonic viability and germ cell development. Depletion of TLK-1 leads to embryonic arrest large, distended nuclei, and ultimately embryonic lethality. Prior to terminal arrest, TLK-1-depleted embryos undergo aberrant mitoses characterized by poor metaphase chromosome alignment, delayed mitotic progression, lagging chromosomes, and supernumerary centrosomes.

I discovered an unanticipated requirement for TLK-1 in mitotic spindle assembly and positioning. Normally, in the newly-fertilized zygote (P_0) the maternal pronucleus migrates toward the paternal pronucleus at the posterior end of the embryo. After pronuclear meeting, the pronuclear-centrosome complex rotates 90° during centration to align on the anteroposterior axis followed by nuclear envelope breakdown (NEBD). However, in TLK-1-depleted P_0 embryos,

the centrosome-pronuclear complex rotation is significantly delayed with respect to NEBD and chromosome congression, Additionally, centrosome positions over time in *tlk-1(RNAi)* early embryos revealed a defect in posterior centrosome positioning during spindle-pronuclear centration, and 4D analysis of centrosome positions and movement in newly fertilized embryos showed aberrant centrosome dynamics in TLK-1-depleted embryos.

Several mechanisms contribute to spindle rotation, one of which is the anchoring of astral microtubules to the cell cortex. Attachment of these microtubules to the cortices is thought to confer the necessary stability and forces in order to rotate the centrosome-pronuclear complex in a timely fashion. Analysis of a microtubule end-binding protein revealed that TLK-1-depleted embryos exhibit a more stochastic distribution of microtubule growth toward the cell cortices, and the types of microtubule attachments appear to differ from wild-type embryos. Additionally, fewer astral microtubules are in the vicinity of the cell cortex, thus suggesting that the delayed spindle rotation could be in part due to a lack of appropriate microtubule attachments to the cell cortex. Together with recently published biochemical data revealing the Tousled-like kinases associate with components of the dynein microtubule motor complex in humans, these data suggest that Tousled-like kinases play an important role in mitotic spindle assembly and positioning.

TABLE OF CONTENTS

LIST OF FIGURES

LIST OF TABLES

LIST OF ABBREVIATIONS

AIR-2 – Aurora/Ipl1-related kinase 2

APC/C – Anaphase Promoting Complex and Cyclosome

AP – anteroposterior

ATM – Ataxia-telangiectasia Mutated kinase

ATR – Ataxia and Rad3-related kinase

C. elegans – Caenorhabditis elegans

CAK – Cyclin-dependent kinase Activating Kinase

CDKs – Cyclin-Dependent Kinases

CPC – Chromosomal Passenger Complex

DAPI – 4',6-Diamidino-2-phenylindole

DDR – DNA Damage Response

DNA - Deoxyribonucleic acid

DSB – Double-stranded DNA breaks

dsDNA – Double-stranded DNA

dsRNA – Double-stranded RNA

e.g. - exempli gratia

GFP – Green Fluorescent Protein

H3S10 – histone H3 serine 10

i.e. – id est

K-MT – kinetochore-microtubule

L4 – 4th larval stage in *C. elegans* development

MCC – Mitotic Checkpoint Complex

MPF – Maturation Promoting Factor

mRNA – Messenger RNA

MSP – Major Sperm Proteins

NCC – (Pro)nuclear Core Complex

NEBD – Nuclear Envelope Breakdown

PAR – abnormal embryonic PARtitioning of cytoplasm

PBD - Polo-box Domain

PLKs – Polo-like Kinases

PNM – Pronuclear Meeting

RNA - Ribonucleic acid

RNAi – RNA-mediated interference

SAC – Spindle Assembly Checkpoint

SEM – Standard Error of the Means

ssDNA – Singe-stranded DNA

ts – temperature sensitive

TLK-1 – Tousled-like kinase

UV – Ultraviolet

YFP – Yellow Fluorescent Protein

Forgive me my nonsense
as I also forgive the nonsense of those who think they talk sense

~Robert Frost

The whole problem with the world is that fools and fanatics are always so certain of themselves, but wiser men so full of doubts.

~Bertrand Russell

Chapter I: Introduction and Background

BACKGROUND

Cænorhabditis elegans as a system to study cellular dynamics

Model organisms have been used for decades to study how multicelluar organisms develop and to test hypotheses *in vivo*. In 1965, Sydney Brenner began using the soil nematode *Cænorhabditis elegans* as a model organism to research molecular and developmental biology, which he recognized as a useful tool for research due to its genetic tractability (Wood, 1988, Altun, 2002-2006, Basto et al., 2008, Zhang et al., 2009). *C. elegans* are approximately one millimeter in length with a simple anatomy, thus making it an ideal system for analyzing features such as cell biology, neuroscience, and aging (Altun, 2002-2006). *C. elegans* has two sexes: self-fertilizing hermaphrodites (XX) and males (XO). Hermaphrodites can produce on average 300 genetically-identical progeny by self-or cross-fertilization that develop quickly and have a relatively short lifespan of around three weeks. Fertilized eggs develop into adult worms in approximately three days at ambient temperatures. Males arise at a frequency of 0.1% by spontaneous nondisjunction of the X chromosome during oogenesis. In addition, they arise at a much higher frequency in male-hermaphrodite mating due to the lack of a paternal X chromosome. In addition, male sperm out-compete hermaphrodite sperm, resulting in greater genetic diversity in this species (Altun, 2002-2006).

The sequencing of the *C. elegans* genome increased the usefulness of the nematode as an easily-accessible genetic asset; all 100,291Mbs and ~19,735 protein coding genes were thoroughly detailed (Hillier et al., 2005). Additionally, this system has a repertoire of advantages for studying metazoan cell division, including genetic tractability, translucent embryo cytology, and ease of maintenance. The entire somatic cell lineages of both sexes are

amazingly invariant and have been precisely mapped: adult hermaphrodites have 959 somatic nuclei versus 1,031 male somatic nuclei (Altun, 2002-2006). Apropos its usefulness as a genetic model, *C. elegans* is amenable to both forward and reverse genetic techniques, in particular RNA-mediated interference (RNAi) (Timmons and Fire, 1998). The ease with which forward genetic screens are employed in *C. elegans* largely drove its acceptance as a powerful model organism. A variety of screens are routinely employed by *C. elegans* researchers to identify mutations that disrupt or alter particular biological processes of interest (Jorgensen and Mango, 2002). Conversely, the powerful reverse genetic technique of RNA-mediated interference (RNAi) was first described in *C. elegans*, and this unbelievably useful technique has been extrapolated and is now applied regularly to biological research in a number of different model organisms (Timmons and Fire, 1998, Maddox et al., 2006). RNAi in *C. elegans* is largely facilitated by one of two methods: feeding the worms *Escherichia coli* expressing specific double-stranded RNAs (dsRNAs) (Timmons and Fire, 1998) or via microinjection of the dsRNA directly into the hermaphroditic gonad (Maddox et al., 2006, Oegema and Hyman, 2006). Additionally, *C. elegans* is particularly well-suited for RNAi-based studies, as introduction of gene-specific dsRNA to the syncytial gonad reproducibly depletes oocytes of >95% of the target gene product and also persists to interfere with the zygotic contribution as well (Timmons and Fire, 1998, Poulin et al., 2004, Oegema and Hyman, 2006).

Another advantage for using *C. elegans* to study development is that cellular structures are easily discerned in their large embryos, especially in the newly-fertilized single-cell zygote. A single nematode embryo is approximately 50μm in length, 30μm in width, and 15μm in height (Goldstein and Hird, 1996), and maintains these approximate dimensions throughout embryonic development (Oegema and Hyman, 2006). This fascinating property allows for the

ready observation of the nuclear envelope, mitotic spindle, chromatin, cytoskeleton, and other organelles in the very early embryo. Furthermore, the rapid and invariant nature of the early mitotic divisions within the embryo provide an excellent resource for quickly assessing and exploring the nature of novel genes vis-à-vis cell cycle functions. Many *in vivo* techniques, such as Normarski/brightfield or fluorescence microscopy, have been developed to quantitatively study cellular events during embryonic development, including pronuclear migration (Albertson, 1984, O'Connell, 2000), anaphase chromosome segregation, spindle elongation (Grill et al., 2001, Cheeseman et al., 2004, Labbe et al., 2004), and asymmetric positioning of the spindle (Tsou et al., 2002, Colombo et al., 2003, Labbe et al., 2004, Oegema and Hyman, 2006). Several recent landmark genome-wide RNAi-based screens utilizing the beauty and power of confocal microscopy have unearthed thousands of essential genes necessary for accurate execution of the early mitotic divisions (Gonczy et al., 2000, Piano et al., 2000, Sonnichsen et al., 2005, Green et al., 2011).

To more closely study *C. elegans* embryos and their cellular structures during development, fixed immunofluorescence analysis or live-cell imaging of *C. elegans* embryos are indispensible resources for visually observing cellular processes at specific time points or through development. Microscopy has become especially useful as the number of transgenic worm strains expressing proteins tagged with fluorescent reporters (*e.g*, green fluorescent protein (GFP)) continues to increase since the development of the microparticle bombardment (Praitis et al., 2001) and Mos transposase single-copy insertion (Frokjaer-Jensen et al., 2008) methods of transgenesis. These strains are useful for following embryonic development and for testing developmental defects after employing RNAi against genes of interest. Additionally,

many genes are highly conserved from *C. elegans* to humans, including important developmental pathways whose dysfunction can lead to human disease (Beitel et al., 1990).

Altogether, these are several reasons why *C. elegans* is suitable for use as a genetic model for studying embryogenesis and development. The work presented in this dissertation utilizes the advantages of the *C. elegans* embryo to study and further elucidate the regulatory events required for embryonic development.

Meiosis in *Cænorhabditis elegans*

An important characteristic of sexual reproduction is the ability of an organism to produce haploid gametes, canonically through the process of meiosis. As male and female gametes proceed through meiosis, they are regulated in different ways and often vary between organisms. Spermatogenesis occurs through uninterrupted meiosis, while oocytes typically arrest at various points during meiosis depending on the species (Greenstein, 2005a). The distinct mechanisms by which each type of gamete develops and matures have been extensively studied in *C. elegans*, leading to a greater understanding of mechanics involved in sexual reproduction in hermaphroditic species. Since the wild-type *C. elegans* hermaphrodite harbors both sperm and oocytes – thus making it capable of self-fertilization – it is an extraordinarily useful model by which to study gonad formation and structure, gamete development and maturation, and ultimately embryogenesis.

In the hermaphrodite, the sex-determination cascade specifies gamete sex in the distal germline, while physiological sperm signaling activates MPK-1/ERK in the proximal germline to control oocyte maturation. Recently, it was reported that repeated utilization of a self-contained negative regulatory module consisting of NOS-3 translational repressor, FEM-CUL-

2, and TRA-1 (Gli transcriptional repressor) is responsible for coordinating both of these processes (Arur et al., 2009, Arur et al., 2011). Both sets of gametes in the *C. elegans* hermaphrodite come from a common set of germline precursor cells. Proliferation of these germ cell precursors takes place in the distal mitotic region of the hermaphroditic germline (Hubbard and Greenstein, 2005). Many different factors affect the outcome of whether these cells differentiate into sperm or oocytes, a process dubbed the sperm-oocyte switch, including the *fem-3, puf-8, fbf-1/2,* and *nos-1/2/3* genes (Ahringer and Kimble, 1991, Kuwabara, 1998, Kraemer et al., 1999, Crittenden et al., 2002, Bachorik and Kimble, 2005). Additionally, there are four key regulators that control entry into meiosis – GLD-1/2/3 and NOS-3 – primarily by overseeing a complex network of translationally-controlled gene products (Kadyk and Kimble, 1998, Eckmann et al., 2004, Hansen et al., 2004a, Hansen et al., 2004b).

In *C. elegans*, chromosomes are subject to the classically-described phases of meiotic prophase I. Upon commitment to meiosis, homologous recombination of chromosomes and synaptonemal complex (SC) formation occur in the transition zone of the gonad and is typically finished by the pachytene phase of meiosis (Hubbard and Greenstein, 2005). During this phase homologues are aligned and chromosomes localize to the nuclear periphery. Hermaphrodite (XX) pachytene nuclei contain six tripartite SCs while males (XO) only have five since their univalent X chromosome exists in a highly condensed heterochromatic state (Goldstein, 1982, Goldstein and Slaton, 1982). Advancement through pachytene to diplotene requires signaling from the mitogen-activated protein kinase (MAPK) pathway, which has pleiotropic activities during germline development (Church et al., 1995, Hsu et al., 2002, Arur et al., 2009), as well as the *daz-1* and *skr-1/2* genes (Karashima et al., 2000, Nayak et al., 2002).

During diplotene, condensed chromosomes bound together by their chiasmata begin to desynapse, and eventually detach from the nuclear envelope to condense further as they move into diakinesis (Villeneuve, 1994, Albertson et al., 1997). Six bivalents are readily observed in oocytes at diakinesis, but in spermatocytes individual chromosomes or bivalents are difficult to distinguish (Villeneuve, 1994). At diakinesis, oocytes enter diapause. They resume meiosis and complete meiotic maturation and ovulation of the oocytes are triggered by major sperm protein (MSP) released from the sperm stored in the spermatheca (Wood, 1988, Greenstein, 2005b). As the oocyte passes through the spermatheca, it is fertilized and ejected into the uterus.

Interestingly, anteroposterior (AP) polarity in the one-cell *C. elegans* embryo is determined at fertilization when PAR proteins establish both the anterior (PAR-3/6) and posterior (PAR-1/2) cortical domains (Wallenfang and Seydoux, 2000, Zonies et al., 2010). Prior to fertilization, the *C. elegans* oocyte is unpolarized, and determination of the AP axis is set by the sperm entry point, which ultimately demarcates the posterior pole of the embryo (Goldstein and Hird, 1996). After fertilization, the maternal nucleus completes two meiotic divisions, generating a haploid pronucleus. Concomitantly, a sperm-donated centrosome duplicates, separates, and begin to nucleate microtubules to set up the mitotic spindle (O'Connell, 2000, O'Connell et al., 2000, Singson, 2001, Tsai and Ahringer, 2007). The proteins SPD-2, ZYG-1, and AIR-1 recruit γ-tubulin and constituents of the pericentriolar material to the centrioles and mediate centrosome maturation; ultimately, these will become the spindle asters during the first mitotic division of the embryo (Schumacher et al., 1998a, Hannak et al., 2001b, Kemp et al., 2004, Pelletier et al., 2004, Pelletier et al., 2006). The ability of mature centrosomes to nucleate spindle microtubules results from the presence of γ-tubulin and associated proteins, (Hannak et al., 2002); importantly, the centrioles/centrosomes are required

Figure 1: The first embryonic *C. elegans* mitotic division.

Maternal and paternal pronuclear migration occur post-fertilization concomitant with mitotic spindle nucleation. After pronuclear meeting, the chromosomes condense and the mitotic spindle begins to rotate and chromosomes align near the center of the cell. After nuclear envelope breakdown, kinetochores are attached to microtubules and sister chromosomes align at the metaphase plate before separating at anaphase. As chromosome decondense and nuclear envelope reassembly takes place in telophase, cleavage furrow ingression ensues and results in cell separation.

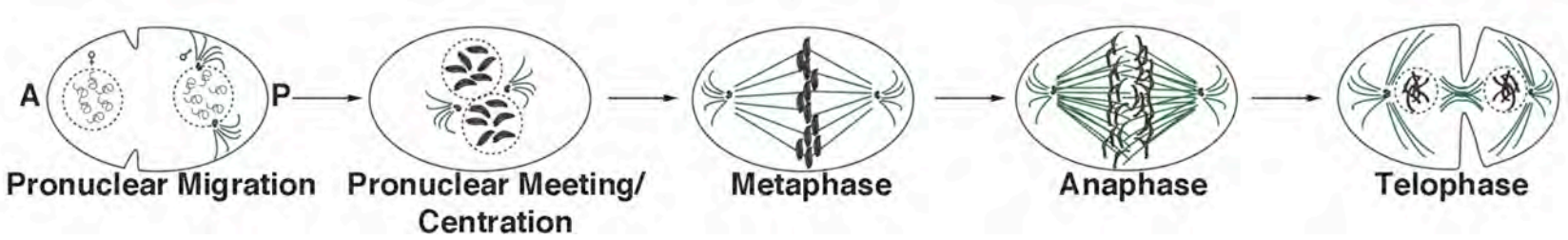
A
P
Pronuclear Migration
Pronuclear Meeting/
Centration
Metaphase
Anaphase
Telophase

to initiate the anterior-posterior polarity of the embryo but not to maintain it (Cowan and Hyman, 2004).

The first mitotic division in *Cænorhabditis elegans*

Cellular diversity is achieved in multicellular organisms when cells of different developmental potential arise by asymmetric cell division (Hyman and White, 1987, Skop and White, 1998, Pearson et al., 2004). Establishment of cellular polarity, accurate localization of cellular determinants, and correct positioning of the mitotic spindle prior to cytokinesis all are part of the recognized multifaceted paradigm for asymmetric cell division (Betschinger and Knoblich, 2004, Gonczy, 2008). In *C.elegans*, the first embryonic division is asymmetric and culminates in a larger anterior blastomere and a smaller posterior daughter cell (Figure 1). This difference in size is determined by the position of the mitotic spindle, which ultimately defines the cleavage plane during cytokinesis (Galli and van den Heuvel, 2008). Placement of the mitotic spindle is organized by microtubules nucleating from centrosomes and their associated motor proteins, which together act as generators and facilitators of the forces necessary for their accurate placement within cells, and centrosome positioning ultimately influences the positioning of the mitotic spindle.

Following fertilization by sperm and completion of meiosis by the oocyte nucleus, the paternal and maternal pronuclei form at the posterior and anterior poles of the embryo, respectively (Figure 2). These pronuclei begin migrating towards one another, with the maternal pronucleus moving significantly farther and faster than the paternal pronucleus, and eventually meet in the posterior half of the cell. During this time, both pronuclei begin to condense their chromosomes, hence this event is the first mitotic prophase (Wood, 1988).

The migration of the pronuclei is a result of microtubule-dependent spindle positioning and cytoplasmic reorganization. Internal cytoplasm begins to convect posteriorly, while cortical cytoplasm flows anteriorly (Goldstein et al., 1993, Hird and White, 1993) aiding in the overall process of pronuclear migration. Prior to completion of pronuclear migration, the anterior cortex undergoes actomyosin rearrangement as evidenced by wave-like cortical contractions, resulting in the formation of a pseudo-cleavage furrow (Kemphues and Strome, 1997). Concomitantly, embryonic polarity, which is discussed in more detail apropos cortical force generation and mitotic spindle positioning in a later section, is also established in this early phase of the first division (Cuenca et al., 2003).

The molecular motor dynein-dynactin complex has numerous important roles throughout cell division, including meiosis, centrosome separation, and pronuclear migration (Gonczy et al., 1999); two nuclear envelope-associated proteins required for the attachment of the centrosome to the nucleus, ZYG-12 and SUN-1, are necessary for recruitment of dynein to the sperm pronucleus (Malone et al., 2003). In addition, these centrosomal asters nucleate microtubules that interface with dynein on the surface of the oocyte pronucleus (Gonczy et al., 1999, O'Connell and Wang, 2000, O'Connell et al., 2000, Hamill et al., 2002, Schmidt et al., 2005). Dynein-mediated mechanical tension applied to the centrosomal microtubule asters is required for pronuclear migration toward the center of the zygote and accelerates the speed at which the pronuclei are pulled (Skop and White, 1998, Severson and Bowerman, 2003, Kimura and Onami, 2005). Upon successful culmination of pronuclear migration, pronuclear meeting (PNM) occurs slightly posterior to the center of the zygote while, simultaneously, chromosomes in each pronucleus are compacted under the direction of the condensin II complex, klesins, and topoisomerase enzymes responsible for decatenating DNA (Gassmann et al., 2004, Hirano, 2005).

Figure 2: Pronuclear migration after fertilization

Embryos expressing GFP::H2B;GFP::γ-tubulin subjected to live-cell spinning disc confocal microscopy. After fertilization (t=-330s), the maternal pronucleus migrates from the anterior to the posterior to meet with the paternal pronucleus. Times are relative to pronuclear meeting (PNM). Scale bar = 8μm

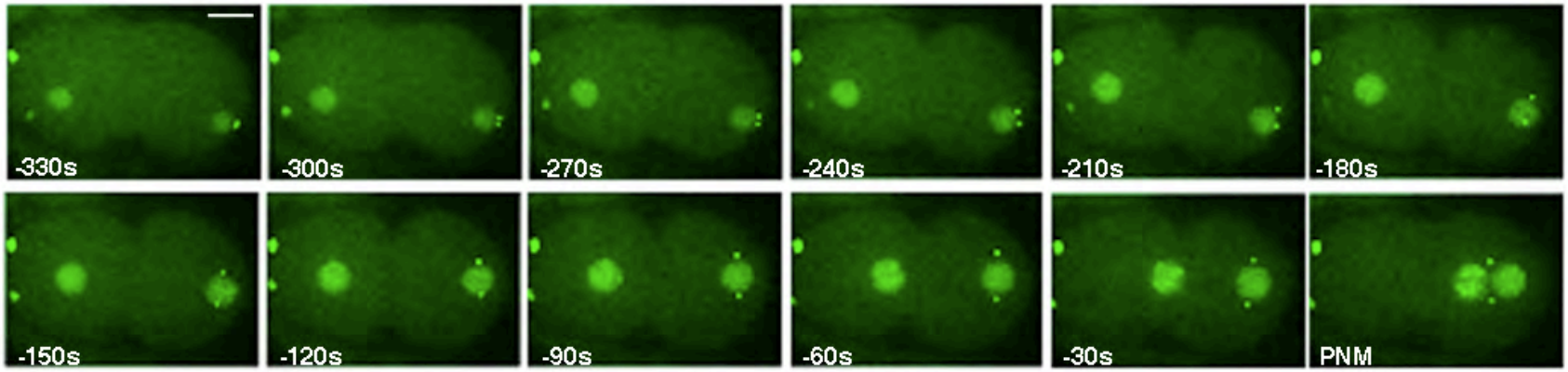
-330s
-300s
-270s
-240s
-210s
-180s
-150s
-120s
-90s
-60s
-30s
PNM

After PNM and the first embryonic mitotic prophase, the cell enters into prometaphase where the pronuclear envelopes are broken down and the bipolar mitotic spindle continues to form (Wood, 1988). Spindle microtubules emanating from centrosomes infiltrate the (pro)nuclear space to seek out kinetochores on each sister chromatid. Kinetochores are large proteinaceous structures harboring a trilaminar morphology (Cheeseman and Desai, 2008). They are highly ordered structures that are assembled on the region of the chromosome defined by the presence of the histone H3 variant CENP-A^{HCP-3}, which defines the centromere (Dernburg, 2001, Oegema et al., 2001, Maddox et al., 2004).

The *C. elegans* kinetochore is holocentric, which means that it is distributed along the entire outer face of sister chromatids, and consists of electron-dense inner and outer layers with an interceding electron-lucent middle layer, all of which cover the pole-ward face of each sister chromatid; importantly, the nematode kinetochore harbors many of the same structurally and functionally conserved properties as monocentric kinetochores (Kitagawa, 2009). As mentioned previously, the holocentric *C. elegans* kinetochore is a gigantic cellular structure, consisting of a vast array of members. Several outer kinetochore proteins serve as functional microtubule binding sites and can be classified into three groups: the kinetochore-null (KNL) proteins required for kinetochore assembly, one of which, KNL-1, interacts directly with microtubules plus-ends; the MIS12 complex, of which the namesake member MIS-12 interacts with KNL-1 to generate a binding site for the final complex, NDC80, which subsequently interacts with both KNL-1 and MIS-12 to anchor microtubules to the assembled kinetochore (Cheeseman et al., 2004, Cheeseman and Desai, 2008, Kitagawa, 2009).

Attachment of microtubules (MT) to kinetochores (K) is a stochastic process whereby incorrect attachments are mitigated by the chromosomal passenger complex (CPC); the CPC is composed of the Aurora B kinase (*Ce*AIR-2), the inner centromere protein INCENP (*Ce*ICP-1), Survivin (*Ce*BIR-1), and Borealin (*Ce*CSC-1) (Ruchaud et al., 2007). A lack of mechanical tension across and within sister kinetochores is a hallmark of syntelic attachments, where both sister kinetochores attach to microtubules from the same spindle pole. The Aurora B kinase is most likely not directly regulated by this lack of tension; rather a lack of tension allows substrates to remain in the vicinity of an active CPC (Cheeseman and Desai, 2008, Pilyugin et al., 2009). Bipolar K-MT attachments (amphitelic) generate tension across and within kinetochore pairs, thus satisfying the mitotic Spindle Assembly Checkpoint (SAC) (Musacchio and Salmon, 2007).

Unattached or incorrect K-MT attachments activate the SAC and prevent mitotic progression into anaphase (Encalada et al., 2005). However, chromosomes align in a dense metaphase plate once all sister kinetochores are properly attached to spindle microtubules. At this point, separase is activated and recruited to mitotic chromosomes where it cleaves the cohesin subunit SCC1 (Hauf et al., 2001, Sun et al., 2009). Since *C. elegans* chromosomes are holocentric, the mechanisms by which cohesin is regulated are not well understood; however, they are likely to be analogous to higher eukaryotes given that cohesin subunits are conserved in the nematode (Mito et al., 2003). Separase initiates cohesin degradation after being released from securin by the Anaphase Promoting Complex and Cyclosome (APC/C) (Hagan et al., 2001), leading to anaphase onset where a host of proteins are necessary for faithful chromosome segregation, including the nematode condensin I complex (Csankovszki et al., 2009, Ford and Schumacher, 2009). Sister chromosomes are

then directed to their respective spindle poles by cortical and midzone spindle forces (Oegema et al., 2001).

As anaphase progresses into telophase, chromosomes begin to decondense concomitant with reformation of the nuclear envelope, centrosomes dissociate, and the spindle fibers begin to dissipate (Oegema and Hyman, 2006) (Figure 1). The process of cytokinesis occurs after anaphase onset and on into telophase; it is driven by the formation of an actomyosin contractile ring that is regulated by the CPC, the central spindle midzone, and microtubule-based signaling (Lewellyn et al., 2011). Cytokinesis is a highly orchestrated process involving many factors that can be conceptualized in five broad categories: the central spindle, the RhoA pathway, non-muscle myosin II, actin assembly into filaments, and the plasma membrane machinery (Glotzer, 2005). In *C. elegans*, early mitotic divisions are asymmetrical due to cortical forces positioning the microtubule asters toward the posterior pole; this positioning determines the site of cytokinesis that ultimately results in an asymmetric division (Labbe et al., 2004).

The central spindle is a set of antiparallel microtubules bundled between the separating chromosomes during anaphase and is regulated spatially by the CPC (Schumacher et al., 1998b, Fraser et al., 1999, Kaitna et al., 2000, Speliotes et al., 2000, Bishop and Schumacher, 2002, Romano et al., 2003) and the centralspindlin complexes (*Ce*ZEN-4/MKLP1 and *Ce*CYK-4/MgcRacGAP) (Powers et al., 1998, Raich et al., 1998, Jantsch-Plunger et al., 2000, Severson et al., 2000, Mishima et al., 2002). After cytokinesis is completed, the mother cell has successfully generated two daughter cells; importantly, in *C. elegans*, the molecular compositions of the two daughter cells generated after the first mitotic division differ in that the posterior cell (P1) inherits germline-specific factors such as

P-granules and the transcriptional regulator PIE-1 (Pellettieri and Seydoux, 2002, Labbe et al., 2004). The nascent two-cell embryo follows a pattern stereotypical for early *C. elegans* embryonic divisions. During the transient interphase following the first mitotic division, the DNA is rapidly replicated followed by a subsequent M-phase, essentially transitioning from S-phase to M-phase with no intermittent gap phases (Kipreos, 2005). However, the rapid transitions from M-phase to S-phase in the early *C. elegans* embryo remain poorly understood.

Cellular Polarity Determinants

As mentioned previously, the first embryonic division in *C.elegans* is asymmetric and culminates in a larger anterior blastomere and a smaller posterior daughter cell. This difference in size is determined by the position of the mitotic spindle, which ultimately defines the cleavage plane during cytokinesis (Galli and van den Heuvel, 2008). Several mechanisms are known to contribute to spindle orientation and positioning, one of which is correct establishment and distribution of cortical polarity cues (Cheng et al., 1995, Grill et al., 2001, Tsou et al., 2002, Schneider and Bowerman, 2003), and the anchoring of astral microtubules to the cell cortex.

Anteroposterior (AP) polarity in the one-cell *C. elegans* embryo is determined at fertilization. At this point, PAR proteins establish both the anterior (PAR-3/6) and posterior (PAR-1/2) cortical domains (Wallenfang and Seydoux, 2000, Zonies et al., 2010) (Figure 3). The anterior PAR domain consists of the conserved PAR-3/PAR-6/PKC-3 complex, while PAR-1/PAR-2 establish the posterior domain (Cuenca et al., 2003). After polarity cues are

set up, microtubule-dependent forces promote the migration of the maternal pronucleus posteriorly, where it ultimately meets with the paternal pronucleus near the posterior pole (Strome and Wood, 1983).

Recent work has defined a "three domain model" for cortical forces in the one-cell *C. elegans* embryo (Krueger et al., 2010), which includes the anterior domain (0% to ~50% embryonic length), the posterior-lateral band (~50%-75% EL), and the posterior domain (~75%-100% EL) (Figures 3 and 4). The forces that align the spindle to the AP axis are regulated in part by the PAR proteins, which comprise a pathway that also includes Gα subunits, their regulators GPR-1/2 (homologous to Pins, LGN, AGS-3), LIN-5 (homologous to Mud and NuMA), and the DEP domain-containing protein LET-99 (Zwaal et al., 1996, Gotta and Ahringer, 2001, Tsou et al., 2002, Colombo et al., 2003, Gotta et al., 2003, Srinivasan et al., 2003, Tsou et al., 2003, Goulding et al., 2007, Park and Rose, 2008) (Figure 3). Cortical levels of GPR-1/2 and LIN-5 are higher at the anterior cortex than the posterior during NCC rotation (Park and Rose, 2008), but this pattern switches by metaphase so that the posterior cortex has the highest enrichment of these proteins (Figure 3) (Colombo et al., 2003, Tsou et al., 2003, Park and Rose, 2008). However, GPR-1/2 and LIN-5 are not distributed along the posterior cortex uniformly, but instead exhibit lower levels at the lateral-posterior domain where LET-99 accumulates and is restricted to throughout the entire first cell division (Tsou et al., 2002). Thus, the strongest pulling forces emanate from the anterior and posterior domains where GPR-1/2 and LIN-5 levels are the highest, while accumulation of LET-99 at the lateral-posterior domain results in a net inhibition of force generation between astral microtubules and the cell cortex at this central posterior region (Tsou et al., 2002, Krueger et al., 2010) (Figure 3).

Figure 3: Representation of polarity-determining protein complexes in the single embryo

The localization of PAR proteins demarcate the anterior and posterior domains of the newly-fertilized embryo. Additional regulators of polarity are also pictured, including LET-99, and GPR-1/2 during the first mitotic division. In this, and all subsequent figures, 0% embryo length marks the anterior pole, and embryos are oriented with the anterior to the left.

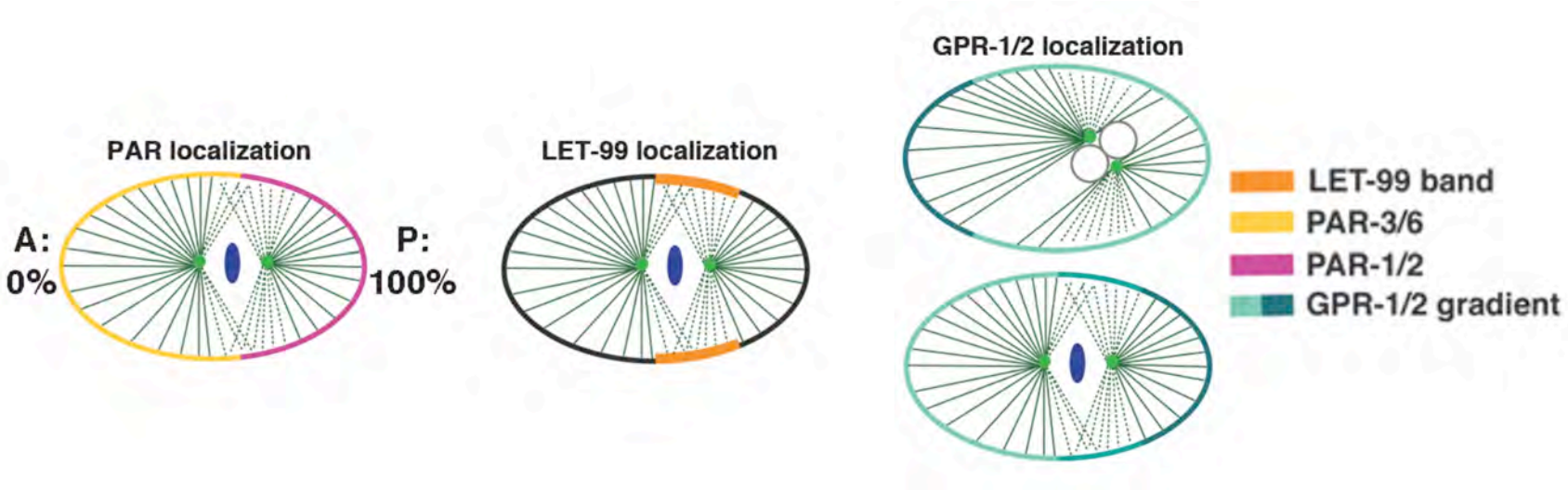
PAR localization
A:
0%
P:
100%
LET-99 localization
GPR-1/2 localization
LET-99 band
PAR-3/6
PAR-1/2
GPR-1/2 gradient

Figure 4: Schematic of the "three-domain" model of cortical force generation

The three force domain model for spindle positioning during the first asymmetric division is shown. Previous models predicted only two domains: the anterior and the posterior domains. Recent work has described a three-domain model instead, which is made up of the anterior domain (0-50% embryonic length), the posterior-lateral domain (50-75% EL) demarcated by accumulation of the LET-99 protein, and the absolute posterior domain (75-100% EL).

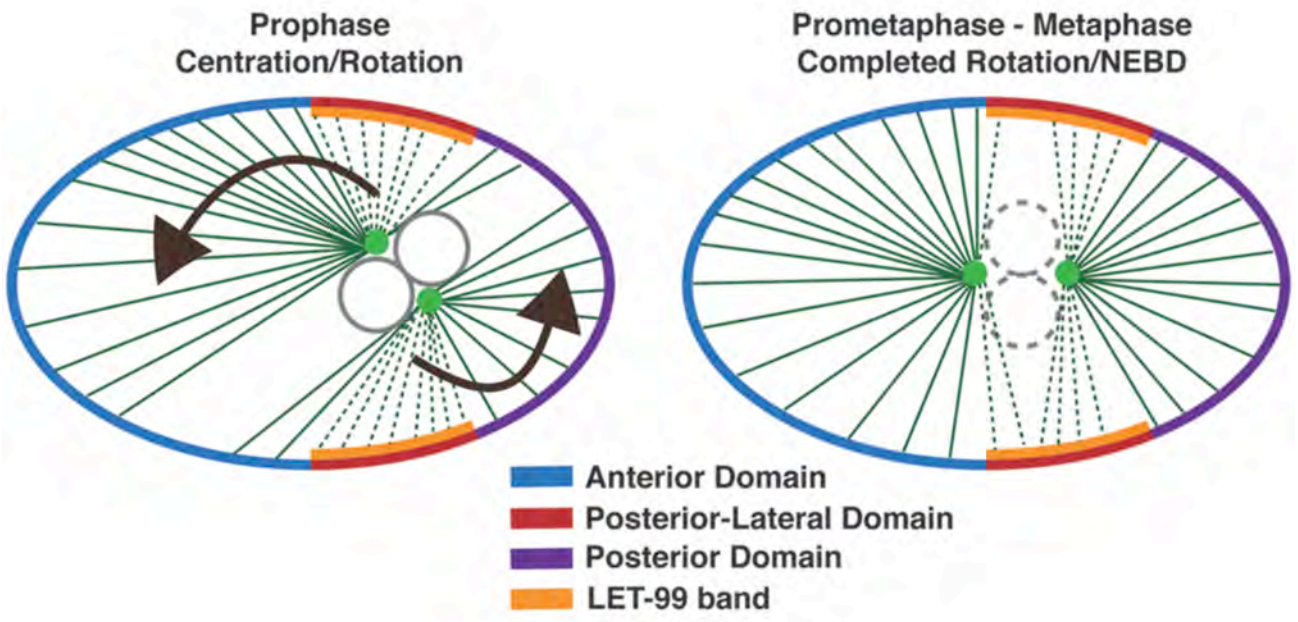
Prophase
Centration/Rotation
Prometaphase - Metaphase
Completed Rotation/NEBD
Anterior Domain
Posterior-Lateral Domain
Posterior Domain
LET-99 band

Figure 5: Cortical Forces generation in early mitotic dynamics

Three force domain model for spindle positioning during the first asymmetric division. The thickness of the arrows indicates magnitude of force acting on microtubules from the corresponding cortical region. Embryos from PNM through centration and rotation to posterior spindle displacement and anaphase onset are depicted.

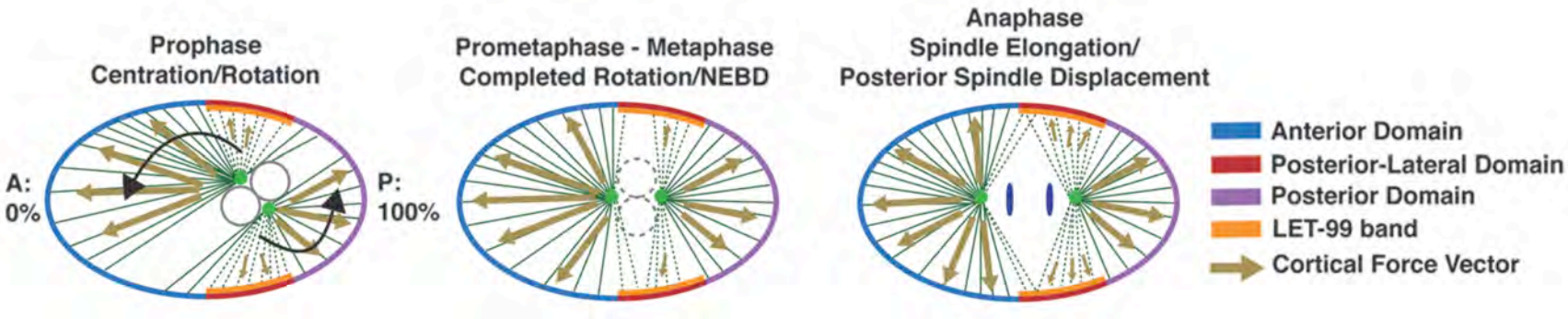
Prophase
Centration/Rotation
Prometaphase - Metaphase
Completed Rotation/NEBD
Anaphase
Spindle Elongation/
Posterior Spindle Displacement
A:
0%
P:
100%
Anterior Domain
Posterior-Lateral Domain
Posterior Domain
LET-99 band
Cortical Force Vector

Depletion of members of the Gα pathway results in reduced centration and rotation rates, as well as perturbed spindle displacement during anaphase. In *let-99* mutants, GPR-1/2 levels are uniformly distributed along cortical domains suggesting that restriction of GPR-1/2 localization to the anterior during rotation is regulated by LET-99 (Tsou et al., 2003, Park and Rose, 2008). Additionally, LET-99 is necessary for accurate NCC rotation and subsequent anaphase spindle displacement toward the posterior, as *let-99* mutants undergo abnormal hyperactive NCC rocking during prophase and do not rotate correctly (Krueger et al., 2010).

Mitotic spindle positioning

The cytoskeleton forms the basis for the internal stability and architecture of cells, and is dependent on microscopic fibres such as microtubules and actin filaments. These fibres are surprisingly mechanical in nature, and can withstand pico-Newtons of force exerted on them without being destroyed (Howard, 2001). However, these structures, in particular microtubules, are generated by the non-covalent assembly of α- and β-tubulin dimers and thus can be assembled and broken down quickly, which is an important factor in overall microtubule dynamics. Microtubule filament plus-ends can grow, shrink, or rapidly alternate between the two states in a process called dynamic instability (Desai and Mitchison, 1997, Garner et al., 2004).

Structurally, the monomers in microtubules assemble head to tail in a regular manner, and on the resulting lattice structures, molecular motors (*e.g.,* kinesins or dynein) use chemical energy to move directionally (Howard, 2001) or to spatially organize the microtubules. Additionally, specific enzymes control nucleation, assembly/disassembly, or

severing of the microtubules (Nedelec and Foethke, 2007). The cytoskeleton is involved in multiple cellular processes such as mitosis, polarity establishment, and motility of intercellular organelles (Skop and White, 1998, Severson and Bowerman, 2003). In this way, a set of dynamic microtubules form a stable larger assembly, the most obvious example of which is the mitotic spindle (Wittmann et al., 2001). The mitotic spindle is positioned by microtubules nucleating from centrosomes and their associated motor proteins, which together act as generators and facilitators of the forces necessary for their accurate placement within cells. Centrosome positioning ultimately influences the positioning of the mitotic spindle. Centrosomal abnormalities, defects in spindle-nuclear positioning, or failures in spindle rotation can lead to disruptions in embryonic polarity and cell fate differentiation (Basto et al., 2006, Basto et al., 2008), leading to embryonic lethality (Pihan et al., 1998, Lingle et al., 2002, Basto et al., 2008, Castellanos et al., 2008), and diseases such as cancer, microcephaly, or lissencephaly in humans (Bond et al., 2002, Tsai et al., 2007, Kumar et al., 2009, Nigg and Raff, 2009).

After pronuclear meeting (PNM), this (pro)nuclear-centrosome complex (NCC) migrates back anteriorly toward the center of the cell (centration) while rotating 90° to align itself with the AP axis (rotation). The orientation of the spindle during PNM, centration, and rotation is determined by cortical force generators that act on astral microtubule plus-end attachments to the cell cortex, while microtubule minus-ends remain embedded in the centrosomes (Kemphues et al., 1988, Cheng et al., 1995, Grill et al., 2001, Tsou et al., 2003, Gonczy and Rose, 2005). The resulting cortical pulling from these interactions act on centrosomes and determine their spatial positioning (Figure 5). During centration, stronger forces from the anterior pull the NCC away from the posterior, while differential pulling

forces on each centrosome are the major impetuses for rotation (Siller and Doe, 2009). After rotation and alignment of the mitotic spindle along the AP axis, nuclear envelope breakdown and metaphase alignment occur, followed by chromosome separation, spindle elongation and displacement to the posterior cortex, resulting in an asymmetric division. The entire spindle also oscillates rapidly during elongation and anaphase, which is due to inhibition of laterally-directed forces over the central portion of the posterior cortex (Tsou et al., 2002) (Figure 5).

The cell cycle

The sequence of events that generate genetically-identical daughter cells from a mother cell is appropriately referred to as the "cell cycle". The cell cycle classically comprises four phases demarcated by the molecular activities occurring during each specific phase, and a plethora of regulatory events oversee faithful cell cycle progression. Ultimately, the *raison d'être* of the cell cycle is to reliably and stably transmit genetic information to allow for continued propagation of life. Deregulation of the cell cycle has dire consequences, one of which is the inappropriate distribution of DNA during cell division, called aneuploidy. Aneuploidy contributes to maladies ranging from embryonic lethality to tumor formation and developmental defects in humans and other organisms.

In order to progress through the cell cycle and cell division in a timely manner, DNA must be tightly packaged from its nascent decondensed form to a highly ordered structure called chromatin. During chromatin packaging in eukaryotes, 147 basepairs of DNA is wrapped around an octamer of histone proteins comprised of two copies each of histone H2A, H2B, H3 and H4. The resulting structure is called a nucleosome, which is further

compacted to form higher-order chromatin structures (Margueron and Reinberg, 2010). Chromatin can be thought of as a dynamically-adjusted structure that adapts to cellular regulatory cues depending on what particular functions need to be carried out at a certain point during the cell cycle – an ideal example of the structure-function paradigm so often seen in biology. Each histone has an amino(N)-terminal tail that protrudes from the so-called globular domain of the nucleosome and can be subject to post-translational modifications (PTMs), including but not limited to acetylation, methylation, phosphorylation and monoubiquitylation (Trojer and Reinberg, 2006, Berger et al., 2009, Margueron and Reinberg, 2010). These various modifications act as a so-called "histone code", altering chromatin structure and conferring new functions to it. Location-specific chromatin can also be defined by the presence of histone variants, nucleosome spacing, or the nuclear position of chromatin (Eitoku et al., 2008, Margueron and Reinberg, 2010). An elaborate and appropriate example of this is the deposition of the histone H3 variant CENP-A at specific sections of condensing chromosomes that ultimately define the centromere, a site upon which a key mitotic structure – the kinetochore – will be built (Sullivan, 2001, Van Hooser et al., 2001). Amazingly, histones, chromatin, and PTMs are highly conserved throughout evolution, showcasing the importance of studying histone function and chromatin structure.

In the G1 phase of the cell cycle, a multiprotein complex that coordinates the condensation of genetic material called condensin is distributed onto chromosomes to facilitate this process (Nasmyth and Haering, 2005). Chromosome condensation is an important facilitator of chromosome segregation during cell division and involves many different protein-protein or DNA-protein interactions (Hirano, 2005). Next, the replication of both the host DNA and activation of cohesin to maintain cohesion of replicated

chromosomes – called sister chromatids – occur during the synthesis (S-) phase of the cell cycle (Nasmyth and Haering, 2005). If the DNA is damaged prior to or during this replicative phase, specific molecular checkpoints inhibit progression until the damage is repaired or mitigated. The cell then enters a preparatory phase for cell division, G2, during which a period of rapid growth occurs and culminates in a cell cycle checkpoint that prevents cells from entering mitosis if problems with the replicated DNA are detected. Mitosis is the phase during which the duplicated DNA is actually parsed into nascent cells and is further partitioned into five sub-phases: prophase, prometaphase, metaphase, anaphase, and telophase.

Protein kinases as regulators of mitosis

Mitosis exists to accurately segregate condensed sister chromatids to their respective daughter nuclei. Therefore, it consists of many highly-regulated molecular processes. Controlling the intricacies of the cell cycle is an important task and requires the coordination of multiple cellular events. Protein kinases are recognized as guides that ensure the cell progresses through each phase correctly. The activity of cyclin-dependent kinases (CDKs), their binding partners, and the activity of downstream effectors oscillate temporally throughout the *C. elegans* cell cycle to ensure timely entry and exit from each phase (Boxem et al., 1999, Park and Krause, 1999, Boxem and van den Heuvel, 2001). Of particular importance are mitotic kinases, including those of the Aurora, Polo, and NIMA families (Nigg, 2001)

Cyclin-dependent kinases (CDKs) and cyclins

Cyclin-dependent kinases (CDKs) are small serine/threonine kinases that are activated by phosphorylation and binding to cyclin partner proteins. Association of one CDK with various cyclins can confer different regulatory functions upon the CDK. In *Saccharomyces cerevisiae*, there is a single CDK, p34CDC28, that acts in concert with different cyclins to promote progression through the various cell cycle phases (van den Heuvel, 2005). In mammals, there are several CDKs responsible for driving the cell cycle, including interphase-specific CDKs – CDK2, CDK4, and CDK6 - and the mitotic CDK, CDK1 (also known as cell division control protein 2 (CDC2), as well as ten cyclins that are grouped into four different classes – the A-, B-, D-, and E-type cyclins (Malumbres and Barbacid, 2009) – whose binding to the CDKs occurs in distinct cell cycle phases; for instance, CDK1 (*Ce*CDK-1/NCC-1) binding to cyclin B1 promotes mitotic entry and progression (Norbury and Nurse, 1991, Boxem et al., 1999, Jackman et al., 2003, van den Heuvel, 2005). In metazoa, both CDK4 or CDK6 complexed with cyclin D and CDK2 in complex with cyclin E are required for the G1-to-S transition; however, *C. elegans* has only one CDK4/CDK6 homologue, CDK-4, and one each of cyclin D (CYD-1) and cyclin E (CYE-1) (Park and Krause, 1999, Boxem and van den Heuvel, 2001, Kipreos, 2005). To further promote S-phase, CDK-4/CYD-1 phosphorylates the transcriptional repressor retinoblastoma protein (Rb) (*Ce*LIN-35), thus exhibiting the elaborate control and signaling potential of the CDKs (Kipreos, 2005). The activity of CDK1/cyclin B1 promotes mitotic entry, while the subsequent degradation of multiple cyclin B proteins after mitosis ensures the inactivation of this complex before the next cell cycle. Interestingly, in *C. elegans* and other organisms, the

maturation promoting factor (MPF) – a complex of CDK1 and cyclin B – is also necessary for oocyte maturation (Burrows et al., 2006).

Importantly, the CDKs are highly regulated, primarily by binding to their cyclin partners. However, complete activation of CDKs requires threonine phosphorylation by the CDK-Activating Kinase (CAK) and dephosphorylation of inhibitory phosphorylated residues by specific phosphatases (Coleman and Dunphy, 1994); the activated CDK-cyclin complexes can also be constrained by CDK inhibitory subunits (CKIs) or inhibitory phosphorylation of the CDK N-terminus (Morgan, 1997). The phosphorylation/ dephosphorylation crosstalk is intricately illustrated in the modulation of CDK1/cyclin B activity prior to and during mitosis. The inactive form of CDK1/cyclin B is present in interphase and is eventually phosphorylated at one site by CAK and at two adjacent sites by an inhibitory kinase, MYT1 (*Ce*WEE-1.3). At the G2-to-M transition, the dual-specificity phosphatase CDC25 dephosphorylates the inhibitory phosphorylation sites to allow mitotic entry via active CDK1/cyclin B (Burrows et al., 2006). The sophisticated coordination of these regulatory events allows for these protein complexes to accurately control the cell cycle.

Polo-like kinases

In a screen for *Drosophila melanogaster* mutants that fail to undergo normal mitoses, the laboratory of David Glover discovered a group of serine/threonine kinases required for normal spindle poles and faithful mitotic progression, which they christened as the Polo family of kinases (PLKs) (Sunkel and Glover, 1988, Llamazares et al., 1991). PLKs are necessary for mitotic entry, bipolar spindle formation, chromosome segregation, and

cytokinesis. They harbor an N-terminal catalytic domain and a hallmark C-terminal polo-box domain (PBD) that binds phosphorylated serines or threonines of target proteins (Barr et al., 2004). While *D. melanogaster* and yeast have one Polo kinase each, *Dm*Polo (Sunkel and Glover, 1988) and *Sc*Cdc5 (Kitada et al., 1993) /*Sp*Plo1p (Ohkura et al., 1995), respectively, vertebrates have several PLKs with PLK1 carrying out most of the functions of Polo, Cdc5, and Plo1p (Barr et al., 2004). *C. elegans* has multiple PLKs, and the PLK1 orthologue, PLK-1, is essential for the timing of M-phase entry (Budirahardja and Gonczy, 2008).

Polo plays an important role in the regulation of CDK1 (*Ce*NCC-1) by phosphorylation of the inhibitory MYT1 kinase to inactivate it, as well as phosphorylation of the CDC25 phosphatase to activate it, which, when taken together, activate CDK1 and promote mitotic entry (Chase et al., 2000, Budirahardja and Gonczy, 2008). Interestingly, in *C. elegans*, *plk-1(RNAi)* oocytes fail to undergo nuclear envelope breakdown, a phenotype reminiscent of *ncc-1(RNAi)* during early embryonic mitotic divisions (Boxem et al., 1999). The Pierre Gönczy group recently showed that after the first *C. elegans* asymmetric mitotic division, the amount of PLK-1 is greater in the anterior cell (AB) *vis-à-vis* the posterior cell (P1). This difference contributes to the decreased latency of mitotic entry in the AB cell compared to the P1 cell (Budirahardja and Gonczy, 2008).

PLK1 localizes to the centrosomes at the G2/M transition and allows for their maturation via phosphorylation of the ninein-like protein, NLP, which plays a role in γ-tubulin recruitment (Zhang et al., 2009). During prometaphase and metaphase, PLK1 is localized to the sister kinetochores via binding of the chromosomal passenger INCENP. CDK1 phosphorylates INCENP at two sites, creating a docking site for the PBD of PLK1

(Goto et al., 2006). INCENP then transports PLK1 to the kinetochore where it has important functions in chromosome separation. Impairment of PLK1 results in a delay of the metaphase-to-anaphase transition, most likely due to a failure to phosphorylate key APC/C substrates (Kotani et al., 1998, Kotani et al., 1999, Golan et al., 2002, Kraft et al., 2003); one of the many important substrates of Polo is cohesin, which must be phosphorylated by PLK1 in order to be cleaved by separase, allowing sister chromatids to separate (Alexandru et al., 2001). PLK1 also targets spindle assembly checkpoint proteins to the kinetochore prior to anaphase onset. The lack of tension resulting from microtubules incorrectly binding to kinetochores leads to the phosphorylation of BUBR1, and generates the epitope recognized by the 3F3/2 antibody, which has long been used as a marker of SAC activity (Wong and Fang, 2005, 2006, 2007). In mammalian cell culture, the 3F3/2 kinetochore phosphoepitope is correlated with the lack of tension created by treatment with the MT stabilizer taxol (Nigg and Raff, 2009); however, once tension is achieved through correct bipolar attachments, the 3F3/2 epitope is dephosphorylated and cells progress through anaphase. During anaphase and telophase, PLK1 relocates to the central spindle where it functions in cytokinesis. PLK1 also triggers the mitotic exit network before it is degraded in an APC/C-CDH1-dependent manner (Barr et al., 2004, Lindon and Pines, 2004)

Aurora kinases

Coincidently, the same screen that identified Polo as an important kinase for mitotic events also uncovered another important kinase, aurora (Sunkel and Glover, 1988, Glover et al., 1995). The *S. cerevisiae* aurora orthologue Increase-in-ploidy 1, Ipl1, was identified in a separate screen for mutants defective in chromosome segregation (Chan and Botstein, 1993).

Further study and characterization of *D. melanogaster* aurora and *S. cerevisiae* Ipl1 lead to the identification of aurora orthologues in other species, including two paralogous auroras in *Xenopus laevis,* AurA (Giet and Prigent, 2000) and AurB (Vagnarelli and Earnshaw, 2004); the two *C. elegans* Aurora-/Ipl1-related protein kinases AIR-1 (Aurora A) (Schumacher et al., 1998a) and AIR-2 (Aurora B) (Schumacher et al., 1998b); and three aurora paralogues in mammals, STK15 (Aurora A), STK12 (Aurora B), and STK13 (Aurora C) (Adams et al., 2001, Nigg, 2001)

Taken together, the aurora kinases comprise a family of conserved serine/threonine kinases required for both meiotic and mitotic processes. The aurora paralogues within species share a highly similar C-terminal kinase domain, while their N-termini harbor divergent sequences. However, overall they share a very high sequence similarity (Carmena and Earnshaw, 2003). Interestingly, overexpression of the Aurora kinases has been implicated in tumorigenesis and has been found in high levels in several human tumors and cancer cell lines, thus making them attractive drug targets for the development of new cancer therapies (Andrews, 2005).

Despite their homology, the Auroras have distinct functions and subcellular localizations. Aurora A is associated with centrosomes slightly prior to and throughout mitosis and is required for proper spindle assembly (Schumacher et al., 1998a, Hannak et al., 2001a). *C. elegans* AIR-1 is important for centrosome maturation via recruitment of γ-tubulin and the PCM components ZYG-9 and *Ce*Grip, as well as the maintenance of centrosome separation whilst the mitotic spindle is being assembled (Hannak et al., 2001b). While *air-1(RNAi)* embryos have bipolar spindles, they exhibit shorter microtubules than wild-type, as well as a terminal phenotype of severe aneuploidy propagated by incomplete

pronuclear migration, chromosome bridges during anaphase, and polyploid cells (Schumacher et al., 1998a). AIR-1 is also necessary for post-embryonic cell divisions and germline development (Furuta et al., 2002), suggesting that AIR-1/Aurora A is indispensable for mitosis throughout the lifetime of *C. elegans*.

Similarly, loss of AIR-2/Aurora B results in embryonic lethality with grotesque meiotic and mitotic defects. AIR-2 is initially associated with meiotic chromosomes in the prophase I-arrested oocytes prior to fertilization; after passing through the spermatheca, AIR-2 remains chromosome-associated throughout the subsequent meiotic divisions with the exception of anaphase when AIR-2 is localized between the separating chromosomes (Schumacher et al., 1998b). As mentioned previously, AIR-2 is the enzymatic crux of the highly conserved CPC whose activity is necessary in both meiosis and mitosis (Ruchaud et al., 2007). The *C. elegans* CPC is composed of AIR-2, ICP-1, BIR-1, and CSC-1. During mitosis, the CPC displays a well-defined localization pattern: in prophase, the CPC is found along the chromosome arms and begins to accumulate at the inner centromere between sister kinetochores during prometaphase; upon complete alignment at the metaphase plate, the CPC is spatially restricted from kinetochore targets due to tension (Liu et al., 2009); after chromosome separation during anaphase, the CPC relocates to the spindle midzone prior to concentrating at the cytokinesis midbody at telophase (Ruchaud et al., 2007) . The CPC is essential for cytokinesis: the cleavage furrow in *air-2* loss-of-function mutants initiates cytokinesis but is unable to complete the process and ultimately regresses (Severson et al., 2000); the same phenotype is observed when any of the other chromosomal passengers are depleted (Fraser et al., 1999, Kaitna et al., 2000, Romano et al., 2003).

Interestingly, RNAi knockdown of any CPC member delocalizes the entire complex and causes aberrant mitosis (Ruchaud et al., 2007), except in *C. elegans* where the non-enzymatic CPC units are not targeted in an AIR-2-dependent fashion (Romano et al., 2003). Importantly, Aurora B and the CPC are required for the mitotic phosphorylation of histone H3 (pH3), which coincides with DNA condensation during prophase and requires the AIR-2/Ipl1 kinase in *C. elegans*, *S. cerevisiae*, and in humans (Hsu et al., 2000). Additionally, AIR-2 is required for association of the condensin I and II subunits MIX-1 and SMC-4 with mitotic chromosomes (Hagstrom et al., 2002).

A mechanism that confers the spatial and functional differences of the Aurora kinases is their ability to bind to and be influenced by substrate activators. During G2, prior to mitosis, inactive Aurora A binds to and phosphorylates the LIM domain-containing protein AJUBA and becomes activated; this interaction is required for recruitment of CDK1-cyclin B to the centrosomes to promote mitotic entry (Hirota et al., 2003). Aurora A is further activated by the microtubule-associated protein TPX2. The *C. elegans* TPX2 homologue, *Ce*TPXL-1, is necessary to localize activated AIR-1 to mitotic spindles (Siller and Doe, 2009); this is also true in other organisms. Additionally, the protein kinase A (PKA) is also an *in vitro* activator of Aurora A (Walter et al., 2000), while the PP1 phosphatase negatively regulates both Aurora A and Aurora B (Schroer, 2004).

Because one Aurora B *modi operandi* is to correct erroneous K-MT attachments in early mitosis, the CPC is subject to precise regulation through a variety of means. Aurora B kinase activity is increased by Aurora B-dependent phosphorylation of the C-terminus of its fellow CPC protein INCENP (Bishop and Schumacher, 2002, Honda et al., 2003), by interacting with the CPC-associated protein TD-60 (Rosasco-Nitcher et al., 2008), through

local chromosomal clustering of the CPC (Kelly et al., 2007), and via phosphorylation of Borealin by the MPS1 kinase in mammals (Jelluma et al., 2008). Work from our lab also detailed the interaction of *C. elegans* AIR-2 with TLK-1, a substrate activator of AIR-2 (Han et al., 2005). The role of mitotic TLK-1 will be discussed in greater detail in a subsequent section.

The DNA damage checkpoint kinase, CHK1 phosphorylates Aurora B and increase its kinase activity *in vitro* (Zachos et al., 2007). As mentioned previously, Aurora B is also subordinate to negative regulation by the PP1 and PP2 phosphatases (Sugiyama et al., 2002, Emanuele et al., 2008), post-translational modifications of key substrates (Zhang et al., 2005, Rosasco-Nitcher et al., 2008), and CDH1-dependent proteosomal degradation via the APC/C pathway during telophase. Additionally, our group found that a *C. elegans* AFG2/SPAF-like AAA ATPase, CDC-48.3, binds to and inhibits the kinase activity of AIR-2, and regulates AIR-2 stability at mitotic exit (Heallen et al., 2008).

The exact mechanism of how cells translate the physical forces generated by K-MT attachments into centromeric signaling has yet to be elucidated. An attractive model is that the CPC must be relocated from the inner centromere to the central spindle in a timely fashion to disrupt the interaction between the CPC and its substrates at the kinetochore (Fuller et al., 2008). Recent experiments utilizing *in vivo* fluorescent sensors of Aurora B activity have illustrated an intracellular activity gradient that may impart signaling for the latter part of mitosis (Fuller et al., 2008), and have also revealed that constitutively tethering Aurora B at the kinetochore disrupts K-MT attachments and may cause persistent SAC activation; this problem is overcome by anaphase segregation of separated sister kinetochores, and thus CPC substrates, away from Aurora B (Liu et al., 2009). Regardless, it

is clear that Aurora B, the CPC, and their regulators play an intricate and integral role throughout mitosis; thus, understanding the consequences of their spatial and temporal localization is of significant importance to elucidating the molecular mechanisms governing mitosis.

Tousled-like kinases

The Tousled kinase (Tsl) was initially described in *Arabidopsis thaliana* as a mutation responsible for aberrant floral organ and leaf development. *Tsl* mutants exhibited flowering time defects and altered leaf morphology, implicating Tousled as a developmentally important gene (Roe et al., 1993, Roe et al., 1997). Tsl is a serine/threonine kinase with a C-terminal catalytic domain and an N-terminal regulatory domain, as well as two alpha helical segments that are necessary for oligomerization (Roe et al., 1997). Originally called PKUβ, human *Tlk1* was found in a screen of a bacteriophage expression library for novel protein kinases along with *Tlk2*, dubbed PKUα. TLK1 and TLK2 share 79% sequence identity; their catalytic domains share 94% identity (Yamakawa et al., 1997). In a subsequent study, database searches for Tsl homologues again revealed two human proteins with significant sequence similarity, TLK1 and TLK2 (Sillje et al., 1999). These kinases were shown to be nuclear proteins with their maximal activity tied to ongoing DNA replication during S-phase (Yamakawa et al., 1997, Sillje et al., 1999). Importantly, TLK1 is ubiquitously expressed and TLK1 protein levels remain consistent throughout the cell cycle.

TLK1 is capable of autophosphorylation and only the phosphoisoform of TLK1 is catalytically active (Yamakawa et al., 1997, Sillje et al., 1999). Very few substrates of TLK have been described with the most reported being the chromatin assembly factor ASF (Sillje

and Nigg, 2001, Carrera et al., 2003, Ehsan et al., 2004, Han et al., 2005, Pilyugin et al., 2009). Additional, albeit less reported, TLK substrates include histone H3 serine 10 (Li et al., 2001, Ehsan et al., 2004), the DEAD-box RNA helicase p68 (Kodym et al., 2005, Sunavala-Dossabhoy et al., 2005a), and the RAD9 DNA repair chaperone (Sunavala-Dossabhoy and De Benedetti, 2009).

Curiously, the kinase activity of TLK is inhibited in the presence of DNA double-stranded breaks, UV-induced DNA damage, and after blocking ongoing DNA replication (Sillje and Nigg, 2001, Groth et al., 2003, Krause et al., 2003). Direct phosphorylation of TLK by the DNA repair checkpoint kinase CHK1 results in TLK inhibition, and this phosphorylation is dependent on the upstream ATM checkpoint kinase rather than the canonical CHK1 activator, ATR (Groth et al., 2003). The Nijmegen Breakage Syndrome protein, NBS1, is also part of the signaling cascade leading to transient suppression of TLK activity in the presence of DSBs, blockage of DNA replication, or UV irradiation (Krause et al., 2003). Interestingly, overexpression of TLK1 both enhanced double-stranded break repair of UV-damaged DNA and bestowed resistance to ionizing radiation in a manner not requiring TLK1 kinase activity (Li et al., 2001, Sunavala-Dossabhoy et al., 2005b, Sen and De Benedetti, 2006, Sunavala-Dossabhoy and De Benedetti, 2009). Additionally, *At*Tsl is required for maintenance of transcriptional gene silencing in plants (Wang et al., 2007) and *C. elegans* TLK-1 is necessary for appropriate transcription elongation (Han et al., 2003). Post-translational modifications correlating with transcriptional elongation are markedly reduced in *tlk-1(RNAi)* embryos, including phosphorylation of RNA polymerase II (RNAPII) at serine 2 and methylation of histone H3 at lysine 36, providing evidence for an additional role of TLK-1 (Han et al., 2003).

The mammalian Tousled-like kinase is reported to be a histone H3 serine 10 kinase (H3S10), but studies in other organisms have suggested a non-direct mechanism of H3S10 phosphorylation. In *C. elegans*, TLK-1 does not directly phosphorylate H3S10, but instead acts as a substrate activator of AIR-2, a *bona fide* H3S10 kinase (Han et al., 2005). Our laboratory isolated TLK-1 in a yeast two-hybrid screen for AIR-2 interacting proteins. Utilizing a purified AIR-2/ICP-1 holoenzyme, we showed that AIR-2 phosphorylates TLK-1 at serine 634 [pTLK-1(S634)] and increases AIR-2 kinase activity *in vitro*. Furthermore, this activation is independent of TLK-1 kinase activity, which supports a novel non-catalytic function for TLK-1 (Riefler et al., 2008). This mechanism is reminiscent of the activation of AIR-2 by its chromosomal passenger partner, INCENP/ICP-1. Prior to mitosis TLK-1 is localized to the nucleus (Figure 6), while the AIR-2-phosphorylated TLK-1 phosphoisoform, pTLK-1(S634), as well as an AIR-2-independent TLK-1 phosphoisoform, pTLK-1(T610), are surprisingly different from that of nuclear-localized unmodified TLK-1 (Figure 7). Immunostaining experiments in *C. elegans* heterozygous for a *tlk-1* deletion allele (*tm2395*) combined with *tlk-1(RNAi)* further confirmed that the subcellular localization of AIR-2-mediated pTLK-1(S634) is specifically localized to the kinetochore. Indeed, the localization of pTLK-1(S634) in embryos from *tlk-1*+/Δ hermaphrodites was markedly reduced in a *tlk-1(RNAi)* background (Han et al., 2005).

Due to the interaction of TLK-1 with AIR-2 and the subsequent AIR-2-dependent phosphorylation of TLK-1 at serine 634 (Han et al., 2005), as well as the established role of AIR-2 in chromosome segregation, we hypothesized that TLK-1 may also influence this process. Several phenotypes were observed in the *tlk-1(RNAi)* embryos. My Master's thesis work showed that TLK-1-depleted cells exhibited a significant delay at prometaphase

concomitant with chromosome congression defects, severe chromosome segregation defects (*e.g.*, chromosome bridges at anaphase) (Figure 8), cells stalling at metaphase before transitioning to a pseudo-anaphase coupled with chromosome decondensation (*i.e.*, chromosomes do not segregate as they do in controls, but attempt to pull apart and begin the decondensation process while still in close proximity to one another) (Figure 9), and cells that appear to be arrested in interphase with polyploid and distended nuclei. Additionally, I found that TLK-1 is required for the timely completion of mitosis (Figure 10).

Consistent with these findings, TLKs have been shown to have mitotic functions in other systems. The *Trypanosoma brucei* homologue, *Tb*Tlk1, localized to centrosomes in an Aurora kinase-dependent fashion and loss of either Aurora or Tlk1 culminated in both chromosome segregation and cytokinesis problems (Li et al., 2007). Expression of catalytically-inactive Tlk1B in breast epithelial cells resulted in multiple mitotic spindles in a single cell, failure of chromosomes to attach to microtubules, and ultimately chromosome segregation defects (Sunavala-Dossabhoy et al., 2003). More recently, reduction of *tlk-1* expression in *Drosophila melanogaster* enhanced the chromosome segregation defects observed with the downregulation of a protein necessary for faithful chromosome segregation, *mars*, presumably due to an inability to correctly polymerize microtubules (Li et al., 2009).

Clearly, depletion of TLK-1 affects chromosome segregation and is necessary for faithful transmission of chromosomes to daughter cells. The mechanism by which TLK-1 affects chromosome segregation remains elusive. Further analysis of TLK-1 functions in upstream cellular events is necessary to determine the source of the chromosome segregation defects in the absence of TLK-1. In this dissertation, I will provide evidence for

an unexpected role for TLK-1 in the regulation of spatial and temporal centrosome positioning and movement, mitotic spindle positioning, and regulation of microtubule dynamics during the first asymmetric cell division in the *C. elegans* embryo.

Figure 6: TLK-1 exhibits nuclear localization.

Wild-type embryos were fixed and stained with an antibody against full-length, recombinant TLK-1 and counterstained with an α-tubulin antibody to visualize the mitotic spindle. TLK-1 was localized to the nucleus in prophase and telophase, as well as in interphase (multicellular panel). A faint halo can be seen in metaphase, and no specific staining is detected at anaphase. Scale bar = 5μm

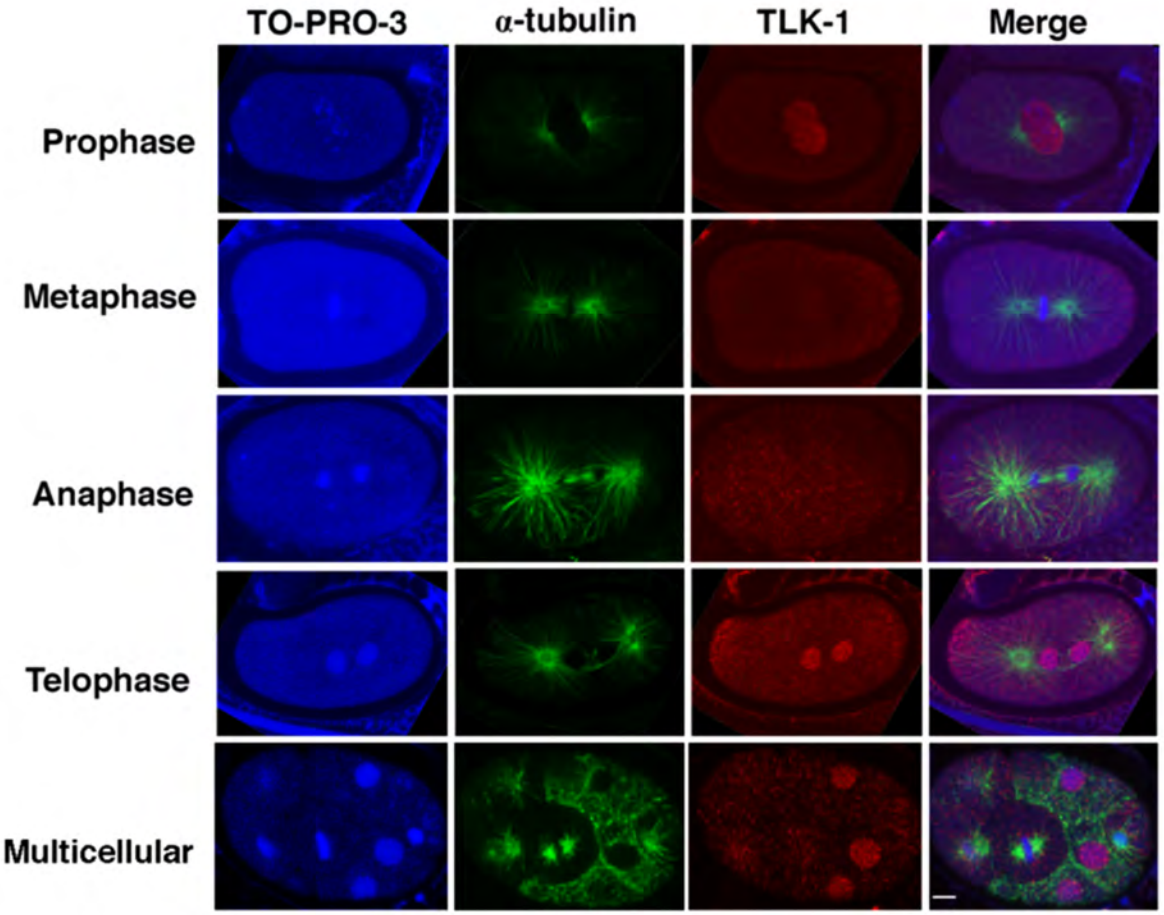
TO-PRO-3
α-tubulin
TLK-1
Merge
Prophase
Metaphase
Anaphase
Telophase
Multicellular

Figure 7: Localization of pTLK-1(S634).

Embryos were fixed and stained with antibodies against α-tubulin and pTLK-1(S634). pTLK-1(S634) is localized clearly to the kinetochore, spindle microtubules, and centrosomes at prophase and metaphase (Ford, 2009). Scale bar = 10μm.

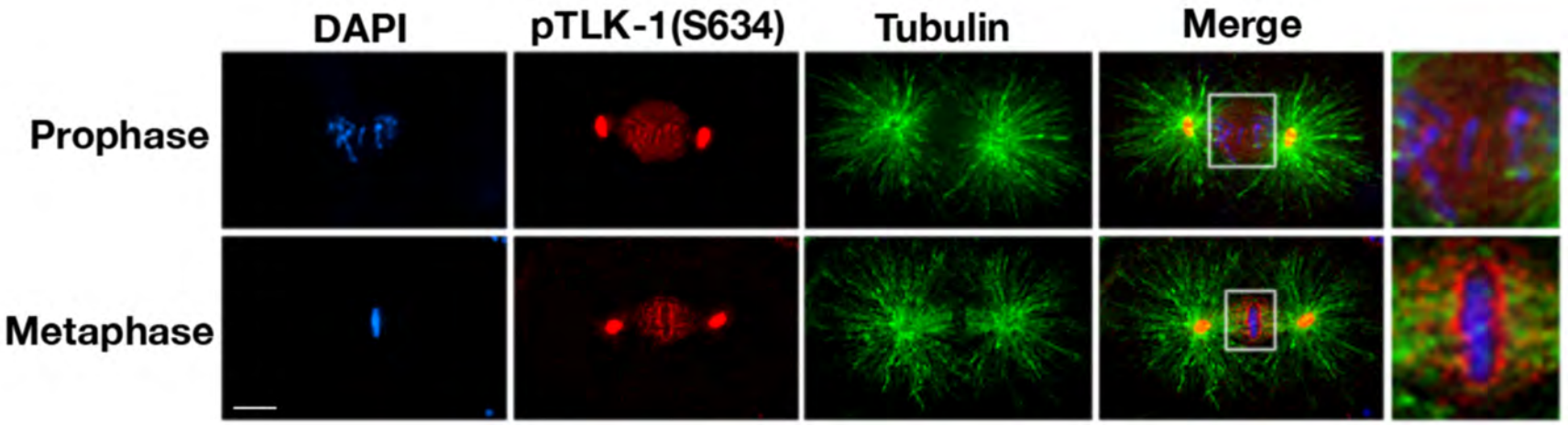
DAPI
pTLK-1(S634)
Tubulin
Merge
Prophase
Metaphase

Figure 8: TLK-1 is required for chromosome congression and segregation.

Live-cell imaging of embryos from a *tlk-1*Δ/+ hermaphrodite showed obvious mitotic defects when treated with *tlk-1(RNAi)*. Control embryos progressed normally through a timely mitosis, condensed chromosomes were more clearly defined than in *tlk-1(RNAi)* embryos (arrowheads). Wide metaphase plates were also observed in *tlk-1(RNAi)* embryos (arrows), as well as chromosome segregation defects in the form of anaphase bridges (open arrowheads) (Ford, 2009). Scale bar = 5μm.

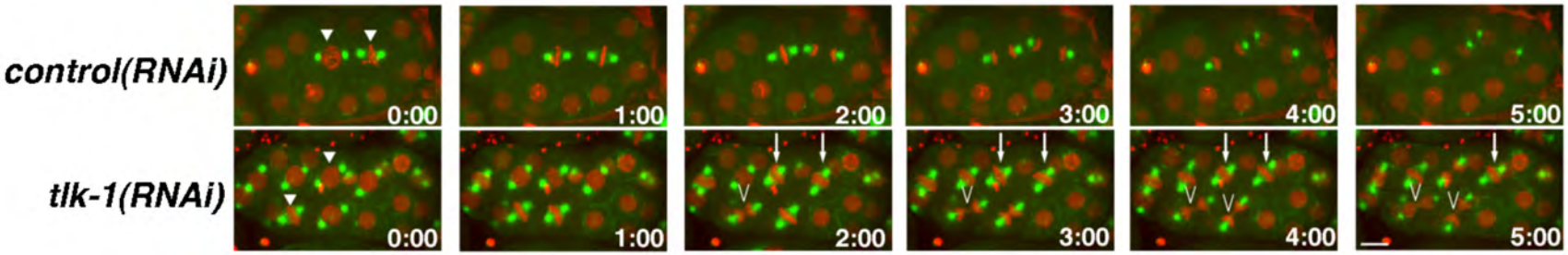
control(RNAi)
tlk-1(RNAi)
0:00
1:00
2:00
3:00
4:00
5:00
0:00
1:00
2:00
3:00
4:00
5:00

Figure 9: TLK-1 promotes timely and faithful chromosome segregation.

Live-cell imaging of metaphase alignment in embryos from *tlk-1*Δ/+ hermaphrodites subjected to *control* or *tlk-1(RNAi)* revealed that TLK-1 is required for timely and accurate chromosome segregation. Control embryos progressed normally through mitosis, and condensed chromosomes formed more clearly defined metaphase plates than in *tlk-1(RNAi)* embryos (arrowheads). Wide metaphase plates were consistently observed in late *tlk-1(RNAi)* embryos. Additionally, TLK-1-depleted embryos attempted chromosome segregation much later than controls, ultimately decondensing chromosomes before complete separation (Ford, 2009).

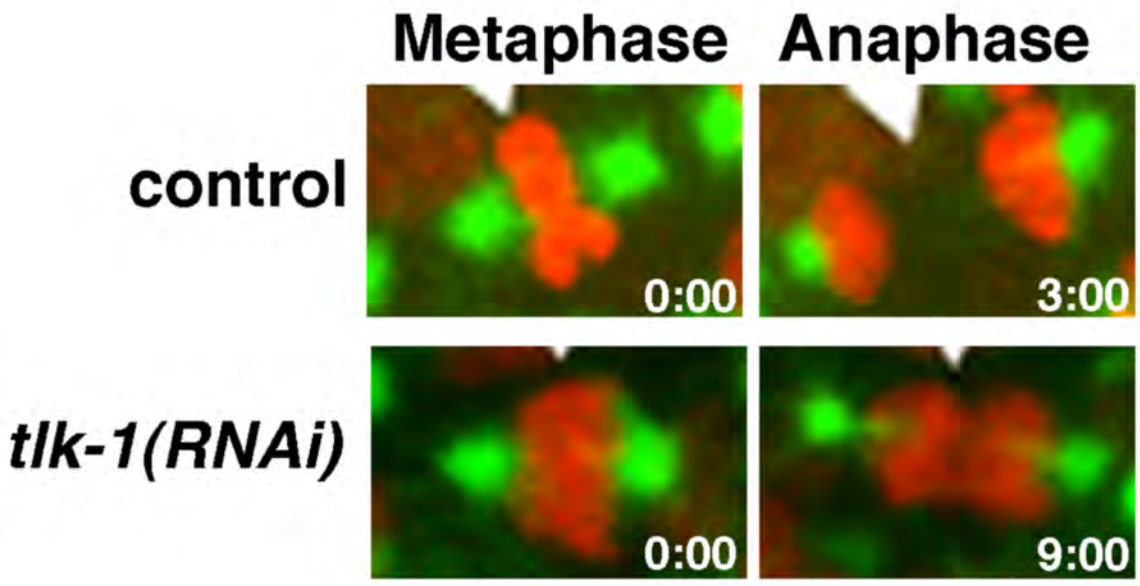
Metaphase
Anaphase
control
0:00
3:00
tlk-1(RNAi)
0:00
9:00

Figure 10: TLK-1 is required for timely mitotic progression.

Live-cell imaging of early embryos from *tlk-1*Δ/+ hermaphrodites subjected to *control* or *tlk-1(RNAi)* revealed that *tlk-1(RNAi)* embryos experience a significant delay from NEBD to metaphase versus controls, as evidenced here in both the anterior and the posterior cell (Ford, 2009). Scale bar = 10μm

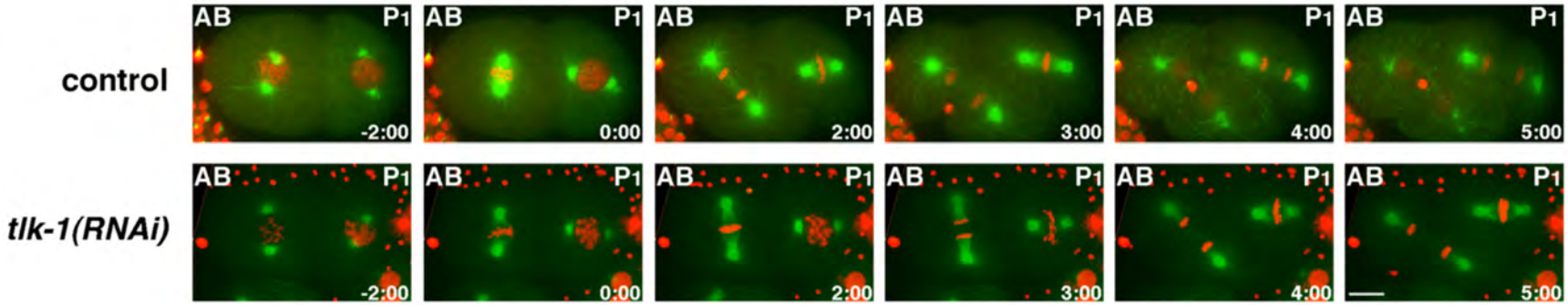
control
tlk-1(RNAi)
AB
P1
-2:00
0:00
2:00
3:00
4:00
5:00

Chapter II: Results

INTRODUCTION

Given that TLK-1 has pleiotropic effects during development, including roles in DNA replication (Krause, Jonnalagadda et al. 2003), DNA repair (Groth, Lukas et al. 2003), transcription (Han, Saam et al. 2003), chromatin assembly (Sillje and Nigg 2001) and condensation (Yeh, Yang et al. 2010), and chromosome segregation (Han, Riefler et al. 2005), I sought to further elucidate the precise contributions of TLK-1 to the cell cycle and embryogenesis in *C. elegans*. Depletion of TLK-1 by RNA interference (RNAi) leads to embryonic arrest at the 50-100 cell stage with large, distended nuclei and ultimately embryonic lethality. Prior to terminal arrest, TLK-1-depleted embryos undergo aberrant mitoses characterized by poor metaphase chromosome alignment, delayed mitotic progression, lagging chromosomes and chromosome bridging, and supernumerary centrosomes (our unpublished data). However, these striking *tlk-1(RNAi)* phenotypes are most obvious in late stage embryos, which makes the accurate comparison of affected cells between different embryos much more difficult. To unearth the contributions of TLK-1 during embryogenesis, I focused on the earliest observable phenotype in *Cænorhabditis elegans* embryos depleted of TLK-1 by RNA-interference.

RESULTS

Chromosome condensation does not require TLK-1 during the first mitotic prophase

TLK-1 is essential during embryogenesis and there are severe mitotic defects in TLK-1-depleted embryos. Therefore, to elucidate the effects of TLK-1 in the early *C. elegans* embryo,

I performed live-cell spinning disk confocal microscopy to monitor early mitotic events, including pronuclear migration, chromosome condensation, pronuclear meeting (PNM), nuclear envelope breakdown (NEBD), and NCC centration and rotation in developing single-cell *tlk-1(RNAi)* embryos expressing GFP::histone H2B and GFP::γ-tubulin (Maddox, Portier et al. 2006). Previous reports implicate TLK-1 in AB lineage-specific chromosome condensation (Yeh, Yang et al. 2010), which led to the hypothesis that TLK-1 was affecting the process of chromosome condensation during embryogenesis. Given the chromosome segregation defects observed in *tlk-1(RNAi)* embryos at later stages, I posited that early defects in correctly condensing chromosomes could be contributing to phenotypes observed in later-stage embryos. An inability for chromosomes to align well at prometaphase to metaphase due to inappropriate or incomplete condensation could be contributing to the perturbed kinetochore structure and severe chromosome segregation defects I previously observed (Ford 2009).

To quantitatively address whether TLK-1 affected chromosome condensation, I imaged GFP::H2B by live-cell confocal microscopy, collecting a *z*-series over time of the paternal pronucleus through the first mitotic prophase (from pronuclear migration to NEBD, Figure 11). I then generated maximum intensity projections for each time point, followed by analysis of a square region of interest inside of male pronucleus (Figure 12). In the sperm pronucleus, the chromatin is decondensed and replicated after fertilization, followed by subsequent condensation during the first mitotic prophase. This is strikingly different than the chromatin in the female pronucleus, which undergoes meiotic segregation twice prior to S-phase and the first mitotic division (Maddox et al. 2006). Thus, chromosome condensation was assessed in the male pronucleus to quantitate any differences in *control* and *tlk-1(RNAi)* embryos.

Figure 11: Examples of time-points measured to quantitate chromosome condensation. Live-cell spinning disk confocal imaging of GFP:H2B in the paternal pronucleus through the first mitotic prophase (from pronuclear migration through NEBD) was used to quantitatively assess the contribution of TLK-1 to chromosome condensation. Shown are representative images that were used to measure the level of chromosome condensation. Scale bar = 10μm

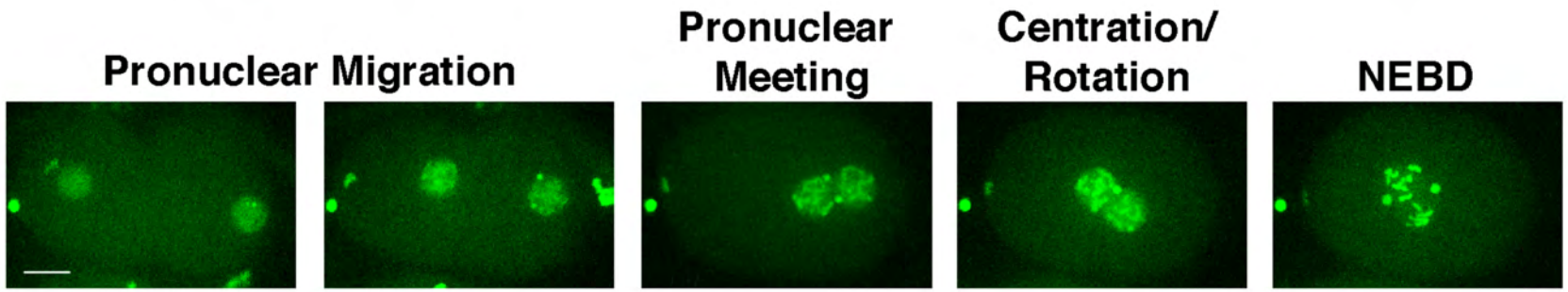
Pronuclear Migration
Pronuclear Meeting
Centration/ Rotation
NEBD

Figure 12: Chromosome condensation is not differentially affected by TLK-1 depletion during the first asymmetric division

(A) Live-cell spinning disk confocal imaging of GFP:H2B in the paternal pronucleus through the first mitotic prophase.

(B) Kinetic plots of the percentage of pixels below each threshold (the condensation parameter) as a function of time in *control* (*n*=10) and *tlk-1(RNAi)* (*n*=10) embryos. The *control(RNAi)* plot is overlaid on the *tlk-1(RNAi)* plot. *smc-4(RNAi)* was used as a control for aberrant chromosome condensation. Error bars are ± standard deviation.

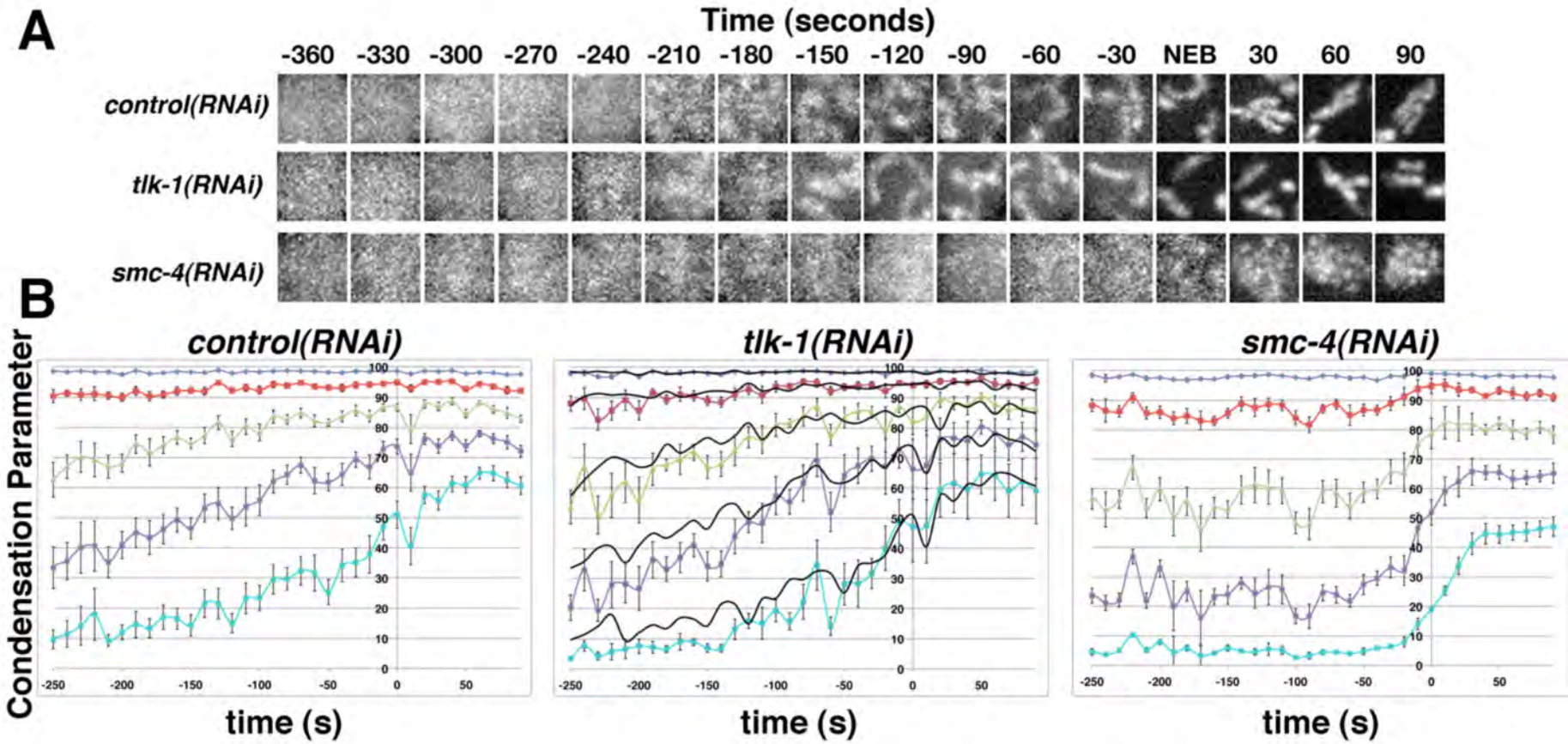
A
Time (seconds)
-360 -330 -300 -270 -240 -210 -180 -150 -120 -90 -60 -30 NEB 30 60 90
control(RNAi)
tlk-1(RNAi)
smc-4(RNAi)
B
Condensation Parameter
control(RNAi)
tlk-1(RNAi)
smc-4(RNAi)
time (s)
time (s)
time (s)

The images of the paternal chromatin were individually scaled from 0 to a maximum of 255 using custom macros (Maddox, Portier et al. 2006). *A priori*, fluctuations in the distribution of fluorescence intensity of the pronuclear GFP::H2B signal over time can serve as a read-out for chromosome condensation dynamics. When the chromatin is decondensed, the GFP::H2B signal is uniform throughout the pronucleus; however, the fluorescence signal shifts and accumulates to distinct areas of the pronucleus during chromosome condensation. This shift in fluorescence intensity over time was quantified as previously described by plotting the pixel flux at several intensity thresholds, specifically 80%, 65%, 50%, 35%, and 20% of the maximum intensity of the image (Maddox, Portier et al. 2006). Times were calculated with respect to NEBD, and for *control* and *tlk-1(RNAi)* the condensation parameters measured from time-aligned sequences of 10 different embryos were averaged and plotted (Figure 12). Depletion of SMC-4, a member of the condensin complexes necessary for chromosome condensation, was used as a negative control (Hagstrom, Holmes et al. 2002; Maddox, Portier et al. 2006; Csankovszki, Collette et al. 2009).

Quantitative analysis of chromosome condensation in TLK-1-depleted embryos did not reveal a significant difference in the flux of pixel intensity compared to control. Thus, I conclude from this experiment that TLK-1 under these conditions at this level of TLK-1 depletion is not differentially affecting chromosome condensation during the first mitotic prophase. However, another group using DAPI analysis did implicate TLK-1 in chromosome condensation in the AB lineage starting at the 16-32 cell cycle stage (Yeh, Yang et al. 2010). Thus, taken together these data imply two possibilities: that TLK-1 is required for condensation but was not depleted enough in these assays to cause a quantative

difference in chromosome condensation prior to the 16-32 cell stage, or that TLK-1 is not required for early chromosome condensation.

TLK-1 is required for timely mitotic spindle rotation in the one-cell C. elegans embryo

While analyzing 1-cell *tlk-1(RNAi)* embryos for chromosome condensation defects, strikingly, I found there was a significant delay in the rotation of the nuclear/centrosome complex (NCC) in approximately 50% of TLK-1-depleted embryos (Figure 13). Both *control* and *tlk-1(RNAi)* embryos proceeded through pronuclear migration, PNM, and centration in a timely fashion; there was no significant difference in the rate of maternal pronuclear migration or positioning (Figure 14). In addition, the timing of PNM relative to NEBD (Figure 14, asterisks) in *control* or *tlk-1(RNAi)* was not significantly different. However, in 47% of the *tlk-1(RNAi)* embryos analyzed (n=15), an obvious defect in spindle rotation was observed (Figure 13). Spindle rotation eventually occurred in these affected embryos after NEBD, whereas rotation in *control(RNAi)* embryos occurred prior to or during NEBD (Figure 13). Some embryos exhibiting the TLK-1-dependent aberrant rotation phenotype did undergo a slight rotation before NEBD; however, all *tlk-1(RNAi)* embryos completed rotation before anaphase onset.

To quantify this phenotype, videos of individual embryos were aligned with the anterior end on the left and spindle rotation occurring in a counterclockwise manner. These

Figure 13: TLK-1 promotes timely rotation of the nuclear/centrosome complex (NCC) in the one-cell *C. elegans* embryo.

One-cell embryos dissected from *control* and *tlk-1*(*RNAi*) treated adult hermaphrodites expressing GFP::histone H2B;GFP::γ-tubulin (TH32) were subjected to live imaging using spinning disk confocal microscopy. PNM: pronuclear meeting; NEBD: nuclear envelope breakdown. Anterior is to the left in each embryo. Time 0 = NEBD. Arrowheads and arrows point to the differences in spindle rotation in *control* vs. *tlk-1(RNAi)* embryos at NEBD and metaphase respectively. Scale Bar = 10μm

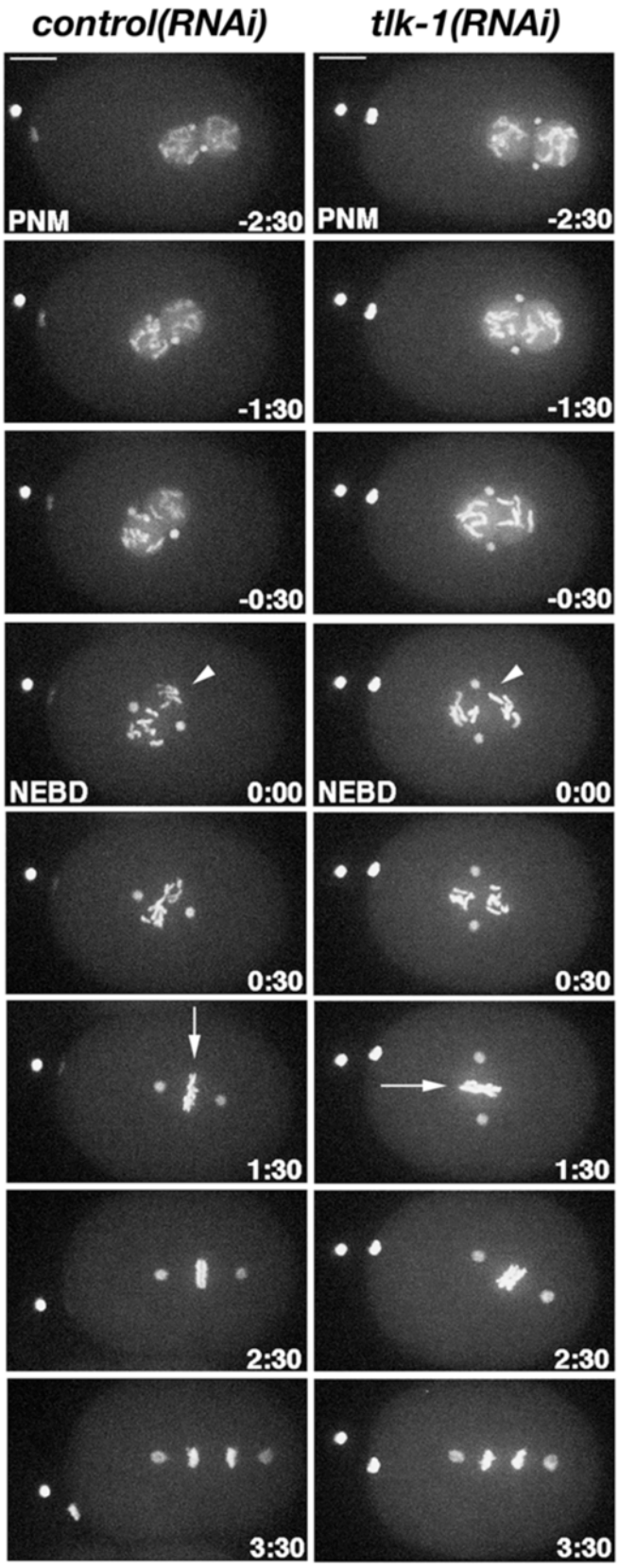
control(RNAi)
tlk-1(RNAi)
PNM
-2:30
PNM
-2:30
-1:30
-1:30
-0:30
-0:30
NEBD
0:00
NEBD
0:00
0:30
0:30
1:30
1:30
2:30
2:30
3:30
3:30

Figure 14: Pronuclear migration, pronuclear meeting, and centration occur normally in *tlk-1(RNAi)* embryos.

One-cell embryos dissected from *control* (*n*=9) and *tlk-1*(*RNAi*) (*n*=7) treated adult hermaphrodites expressing GFP::histone H2B;GFP::γ-tubulin (TH32) were subjected to live imaging using spinning disk confocal microscopy. A plot of the distance from the center of the maternal pronucleus to the posterior pole from pronuclear migration to NEBD is shown. The shaded area represents the centration event, where the NCC migrates towards the center of the embryo after PNM. Plot lines are average %EL ± SEM. * = average time PNM occurred for either *control* (t = -173.33 ± 16.41 seconds, *n*=9) or *tlk-1(RNAi)* (t = -158.57 ± 21.20 seconds, *n*=7) embryos.

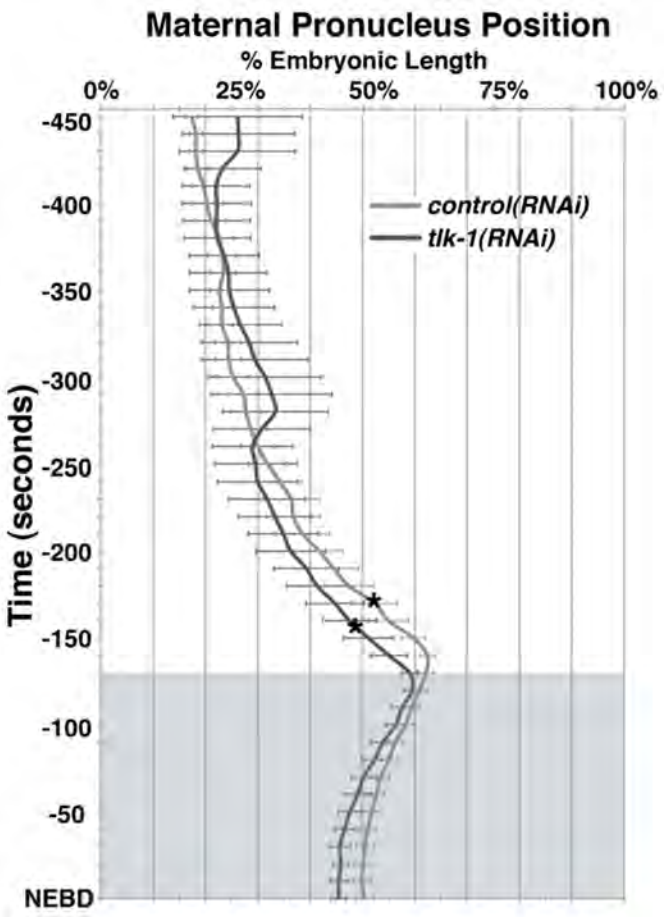
Maternal Pronucleus Position
% Embryonic Length
0%
25%
50%
75%
100%
-450
-400
-350
-300
-250
-200
-150
-100
-50
NEBD
Time (seconds)
control(RNAi)
tlk-1(RNAi)

embryos were temporally aligned with NEBD being time-zero. To measure the rate of rotation, the angle between the two centrosomes and the anteroposterior axis over time was determined (Figure 15A). The affected *tlk-1(RNAi)* embryos had a significant delay ($p < 0.05$) in NCC rotation compared to control embryos from 70 seconds prior to and after NEBD (Figure 15B). On average, NEBD occurred in *control* embryos when the NCC was at 149 ± 7.60° (degrees) relative to the AP axis, whereas in *tlk-1(RNAi)* embryos NEBD occurred when the NCC was at 114 ± 8.76° ($p < 0.03$) (Figure 15B). Calculation of the average times at which PNM and anaphase onset occurred relative to NEBD in each sample revealed that PNM occurred at -173.33 ± 16.41 seconds (s) in *control(RNAi)* and at -158.57 ± 21.20s in *tlk-1(RNAi)* embryos, while anaphase onset occurred at +152.50 ± 3.66s in *control(RNAi)* and at +157.14 ± 7.78s in *tlk-1(RNAi)* embryos, revealing that timing of these mitotic landmarks were not perturbed when TLK-1 was depleted (Table 1).

Table 1: Average times of PNM and Anaphase Onset relative to NEBD

	PNM	**Anaphase Onset**
control(RNAi)	-173.33 ± 16.41s	+152.50 ± 3.66s
tlk-1(RNAi)	-158.57 ± 21.20s	+157.14 ± 7.78s

In addition, the *control(RNAi)* embryos exhibit a significantly different rotation profile than the TLK-1-depleted embryos during the first mitotic division (Figure 15B). To quantitate the rate of spindle rotation for each sample set, the slopes between data points were calculated to provide the speed of rotation in degrees per second. During the interval from pronuclear meeting to NEBD (-150 seconds to 0), *control(RNAi)* embryos rotate significantly faster (2.5 fold) than *tlk-1(RNAi)* embryos (0.414 vs 0.163 degrees/second)

(Table 2, Figure 16), with control embryos averaging a 57.90 ± 5.45° rotation and *tlk-1(RNAi)* embryos averaging a 22.77 ± 6.05° rotation by NEBD (Figure 15B). However, during the interval from NEBD to anaphase onset (0 to 110 seconds), *tlk-1(RNAi)* embryos rotate twice as fast as *control(RNAi)* embryos (0.343 vs. 0.171 degrees/second) (Table 2, Figure 16**)**, with control embryos averaging a 18.84 ± 5.26° rotation and *tlk-1(RNAi)* embryos averaging a 37.77 ± 11.03° rotation by anaphase onset (Figure 15B). Embryos subjected to *tlk-1(RNAi)* did not exhibit a significant change in overall rotation rate compared to *control(RNAi)* embryos from PNM to anaphase onset. These overall comparable rates of spindle rotation in *control* versus *tlk-1(RNAi)* embryos are due to TLK-1-depleted embryos significantly speeding up rotation after NEBD in order to compensate for their significantly delayed rotation prior to NEBD, thus allowing *tlk-1(RNAi)* embryos to correctly align the mitotic spindle along the AP axis by anaphase onset (Figures 15 and 16).

Calculation of the instantaneous velocities between each individual data point in the two data sets revealed that *control(RNAi)* embryos move more quickly and smoothly in a constant direction than their *tlk-1(RNAi)* counterparts (Figure 17**)**. TLK-1-depleted embryos show a generally slower rate of rotation and reverse their rotation direction temporarily several times prior to NEBD (Figure 17, *tlk-1(RNAi*) at *t*=-100s, *t*=-60, and *t*=-10). Whereas *control(RNAi)* velocities start out fast and gradually slow down during the rotation event, *tlk-1(RNAi)* embryos speed up their rotation velocities in a lurching manner only after NEBD, when the control embryos are slowing down (Figure 17). This suggests that TLK-1 is required for maintenance of speed and direction of the NCC during rotation from PNM to anaphase onset.

Figure 15: NCC rotation is significantly delayed in *tlk-1(RNAi)* embryos.

(A) Schematic of spindle angle measurement over time. θ: angle between the centrosome complex and the anterior-posterior axis (A: anterior; P: posterior).

(B) Plot of spindle angle (θ) over time in embryos imaged as in Figure 13. Left and right grey shading represents the respective time frames in which PNM and anaphase onset occurred. Time 0 = NEBD. Error bars: ± standard error of the means (SEM). * $p < 0.05$, Student's *t*-test.

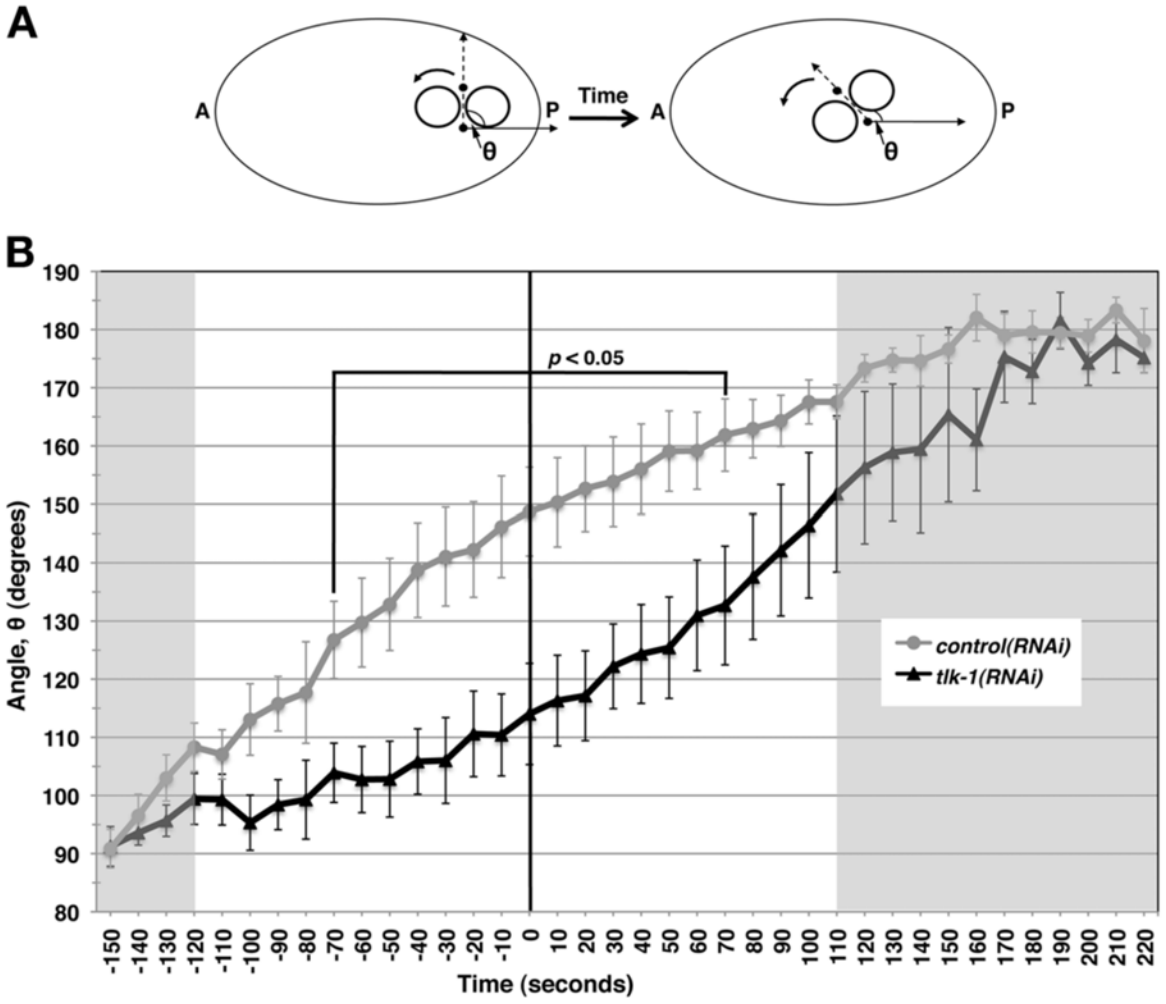
A
A
P
θ
Time
A
P
θ
B
Angle, θ (degrees)
Time (seconds)
p < 0.05
control(RNAi)
tlk-1(RNAi)

Figure 16: TLK-1 affects the rate of spindle rotation

(A) Quantitation of spindle rotation rates in *control* and *tlk-1(RNAi)* embryos. Rate of spindle rotation (degrees/second) from i) PNM to NEBD, ii) NEBD to anaphase onset, iii) PNM to anaphase onset. Error bars = ± SEM calculated from the individual slopes between each data point. * $p < 0.05$, Student's *t*-test.

(B) Plot of spindle angle (θ) over time in *control* and *tlk-1(RNAi)* embryos from Figure 15B with slope lines for distinct time periods drawn in for reference. Lines A (red) and D (orange) represent the slopes from PNM to NEBD in *control* and *tlk-1(RNAi)* embryos, respectively. Lines B (red) and E (orange) represent the slopes from NEBD to anaphase onset in *control* and *tlk-1(RNAi)* embryos, respectively. Lines C (red) and F (orange) represent the overall slopes from PNM to anaphase onset in *control* and *tlk-1(RNAi)* embryos, respectively.

(C) Table of the rates of NCC rotation (degrees/second) and the total amount of spindle rotation (degrees) from PNM to NEBD, NEBD to anaphase onset, or overall rotation (PNM to anaphase onset) as measured from (B).

A

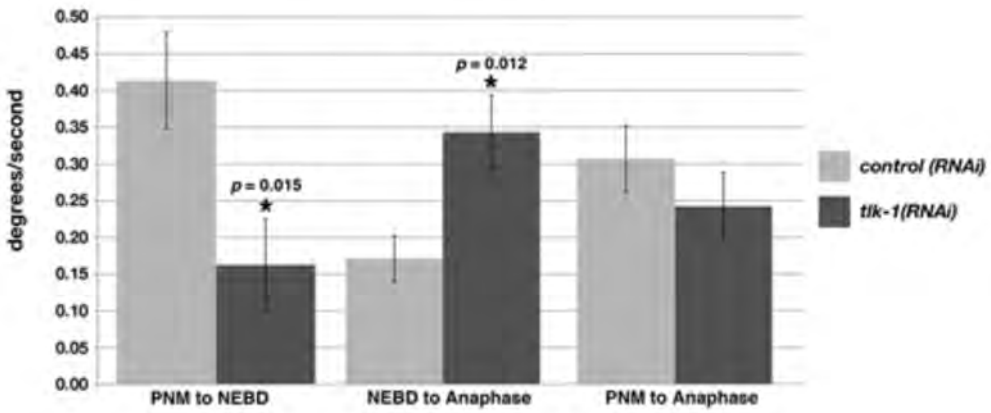

B

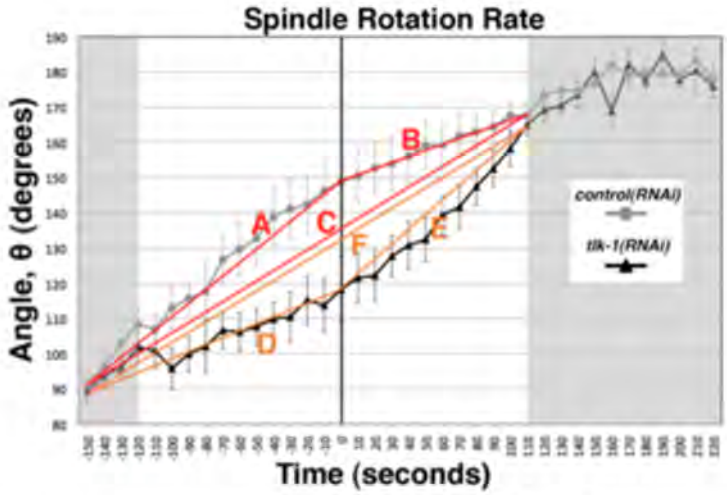

C

	Pronuclear Meeting → NEBD	Total rotation PNM → NEBD	NEBD → Anaphase Onset	Total rotation NEBD → Anaphase Onset	Pronuclear Meeting → Anaphase Onset
control(RNAi)	0.414 deg/sec (A)	57.90±5.45°	0.171 deg/sec (A)	18.90±5.26°	0.307 deg/sec (C)
tlk-1(RNAi)	0.163 deg/sec (D)	22.77±6.05°	0.343 deg/sec (D)	37.90±11.03°	0.242 deg/sec (F)
Difference (x = fold change)	0.39x	35.13±5.75°	2.00x	-18.93±8.15°	No significant difference

Figure 17: Instantaneous velocity of overall spindle rotation.

The velocity of rotation was calculated as the first derivative, or change in slope, between each data point for *control(RNAi)* and *tlk-1(RNAi)*. This parameter is a measure of the speed and direction of spindle rotation, and can thus be used to further visualize the difference in rotation rate between wild-type and TLK-1-depleted embryos. t = 0 is NEBD.

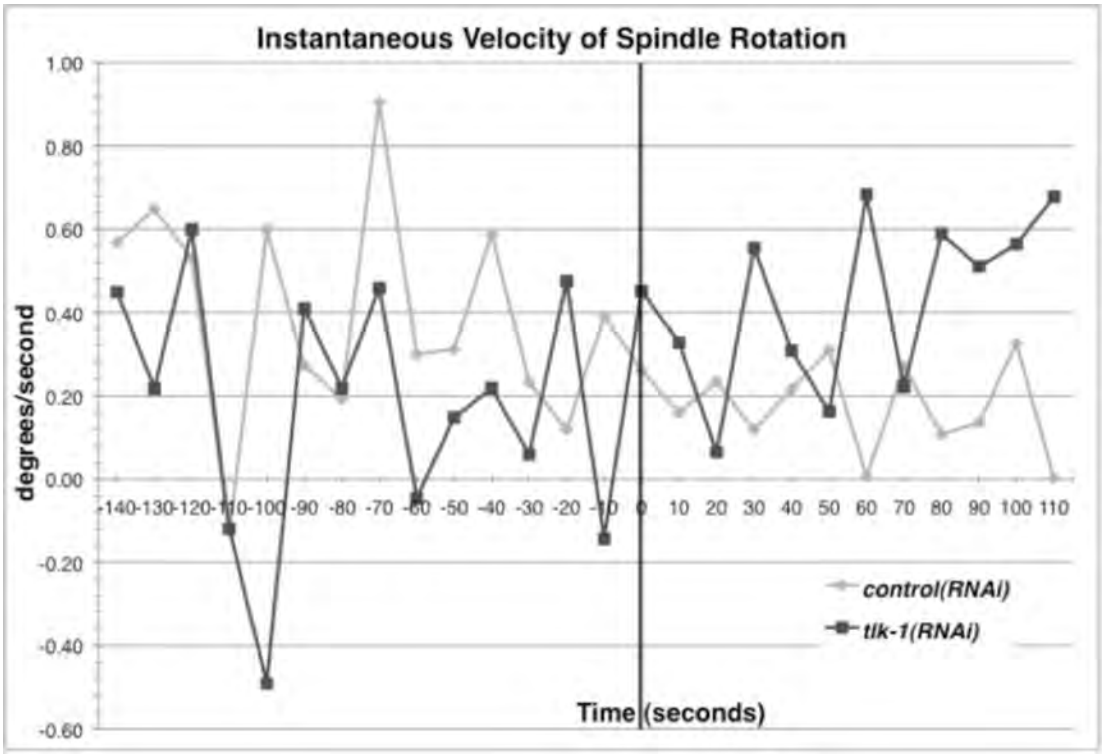
Instantaneous Velocity of Spindle Rotation
degrees/second
1.00
0.80
0.60
0.40
0.20
0.00
-0.20
-0.40
-0.60
-140 -130 -120 -110 -100 -90 -80 -70 -60 -50 -40 -30 -20 -10 0 10 20 30 40 50 60 70 80 90 100 110
Time (seconds)
control(RNAi)
tlk-1(RNAi)

TLK-1 impacts the trajectory of centrosome movement and their positioning in the one-cell embryo

Accurate spindle positioning depends on the interaction of astral microtubules with the cell cortex (Tsou, Hayashi et al. 2002; Nguyen-Ngoc, Afshar et al. 2007). Since astral microtubules are nucleated from centrosomes, precise centrosome positioning is critical for timely and correct execution of developmentally-programmed spindle rotation events. To assess the role of TLK-1 in centrosome positioning, GFP::H2B; GFP::γ-tubulin-expressing embryos were subjected to *control* or *tlk-1(RNAi)* and aligned temporally at NEBD. The distances from the anterior and posterior centrosomes to a single spot on the posterior end of each embryo were calculated over the duration of the first mitotic cycle (Figure 18A). Kymographs of these centrosome positions over time were then generated (Figure 18B).

Anterior displacement between the anterior and posterior centrosomes in *control(RNAi)* embryos initiates at approximately 140 seconds prior to NEBD, and is statistically significant by 50 seconds prior to NEBD. In TLK-1-depleted embryos, anterior displacement begins at approximately -80 seconds and is statistically significant by 70 seconds prior to NEBD. To determine whether the length of the mitotic spindle was altered in *control* versus *tlk-1(RNAi)* embryos, I calculated the physical distance between the anterior and posterior centrosomes in *control* and *tlk-1(RNAi)* embryos. There was no significant difference in the distance between the anterior and posterior centrosomes from PNM to cytokinesis (Figure 19). However, our data did show that the posterior centrosomes in TLK-1-depleted embryos undergo a statistically significant anterior displacement compared to controls during the time interval from 80 seconds to 20 seconds prior to NEBD.

Figure 18: TLK-1 impacts the positioning of posterior centrosomes

(A) Schematic of the measurements of centrosome positions over time. The distances from each centrosome to a point at the posterior end of the embryo were measured and calculated as a percentage of total embryo length from the anterior to the posterior. A: Anterior, 0%; P: Posterior, 100%.

(B) One-cell embryos dissected from *control*- and *tlk-1*(*RNAi*)-treated adult hermaphrodites expressing GFP::histone H2B;GFP::γ-tubulin (TH32) were subjected to live imaging using spinning disk confocal microscopy. The distance of each centrosome from the posterior was measured as in (A) and displayed as a kymograph of % embryo length over time. Time 0 = NEBD. Error bars: ± SEM, * $p < 0.05$, Student's *t*-test.

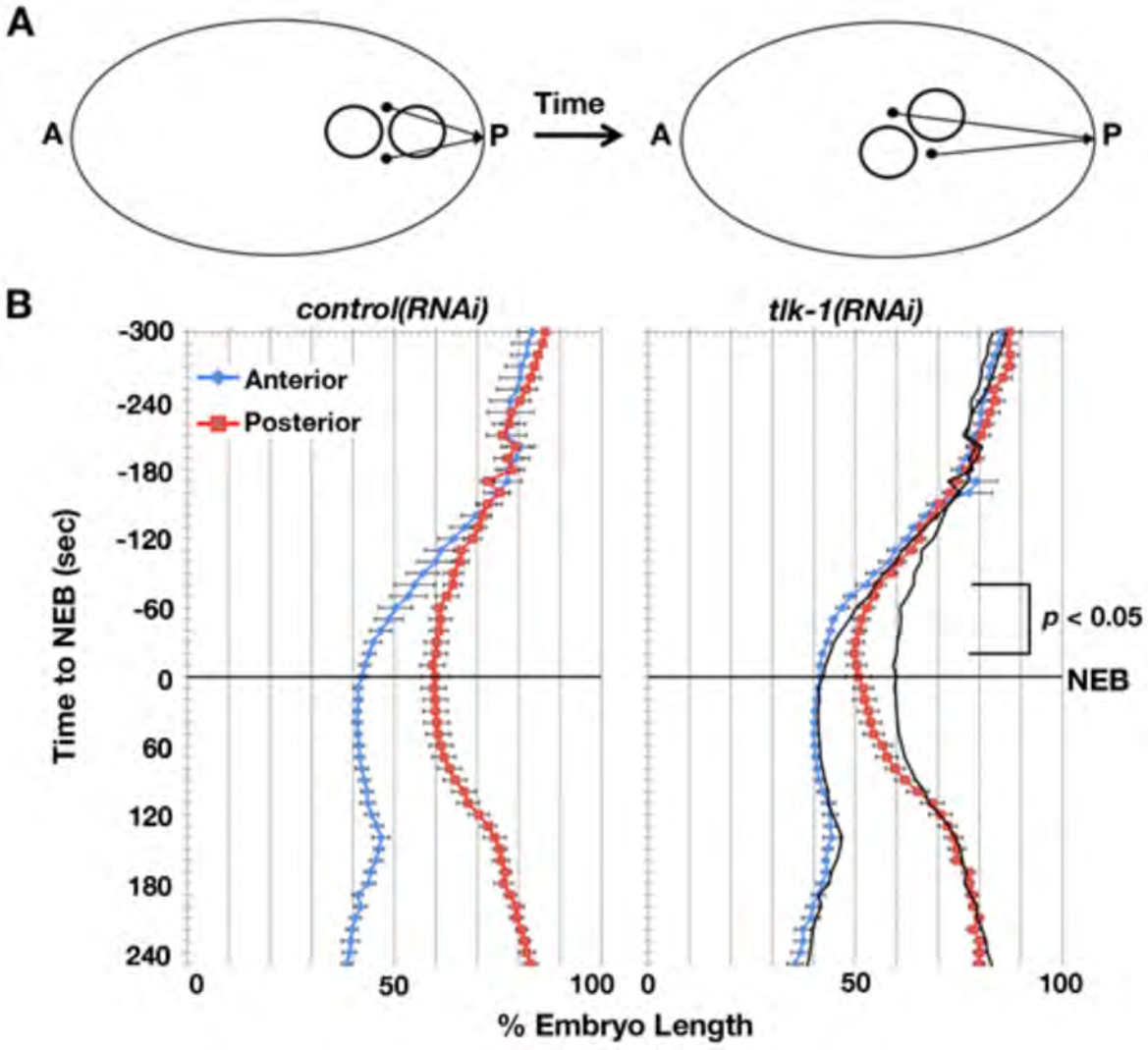
A
A
P
Time
A
P
B
control(RNAi)
tlk-1(RNAi)
Anterior
Posterior
-300
-240
-180
-120
-60
0
60
120
180
240
Time to NEB (sec)
0
50
100
0
50
100
% Embryo Length
p < 0.05
NEB

Table 2: Position of the Posterior Centrosomes in *control* and *tlk-1(RNAi) embryos*

Time before NEBD (sec)	Position of the Posterior Centrosome (%EL)		Δ%
	control(RNAi) *(n*=10)	***tlk-1(RNAi)*** (*n=5*)	
-80	64.1±2.17%	55.5±1.95%	8.6%
-70	62.7±2.80%	54.4±1.25%	8.3%
-60	60.8±1.62%	52.8±1.79%	8.0%
-50	61.1±2.62%	51.5±2.00%	9.6%
-40	60.7±2.72%	51.0±1.75%	9.7%
-30	60.1±2.82%	50.1±1.97%	10.0%
-20	60.0±2.70%	49.8±2.13%	10.2%
Average	**61.4±2.49%**	**52.2±1.83%**	**9.2%**

Figure 19: Spindle length is not altered during the aberrant NCC rotation in TLK-1-depleted embryos.

Plot of the distance between the anterior and posterior centrosomes through pronuclear migration, PNM, centration, and rotation. Plot lines are distance (μm) between centrosomes ± SEM (a readout of spindle length during the first asymmetric division (Jaensch, Decker et al. 2010)). There was no significant difference in spindle length between *control* and *tlk-1(RNAi)* embryos. * = average time of anaphase onset with respect to NEBD in *control* (*t* = +152.50 ± 3.66 seconds, *n*=9) or *tlk-1(RNAi)* (*t* = +157.14 ± 7.78 seconds, *n*=7) embryos.

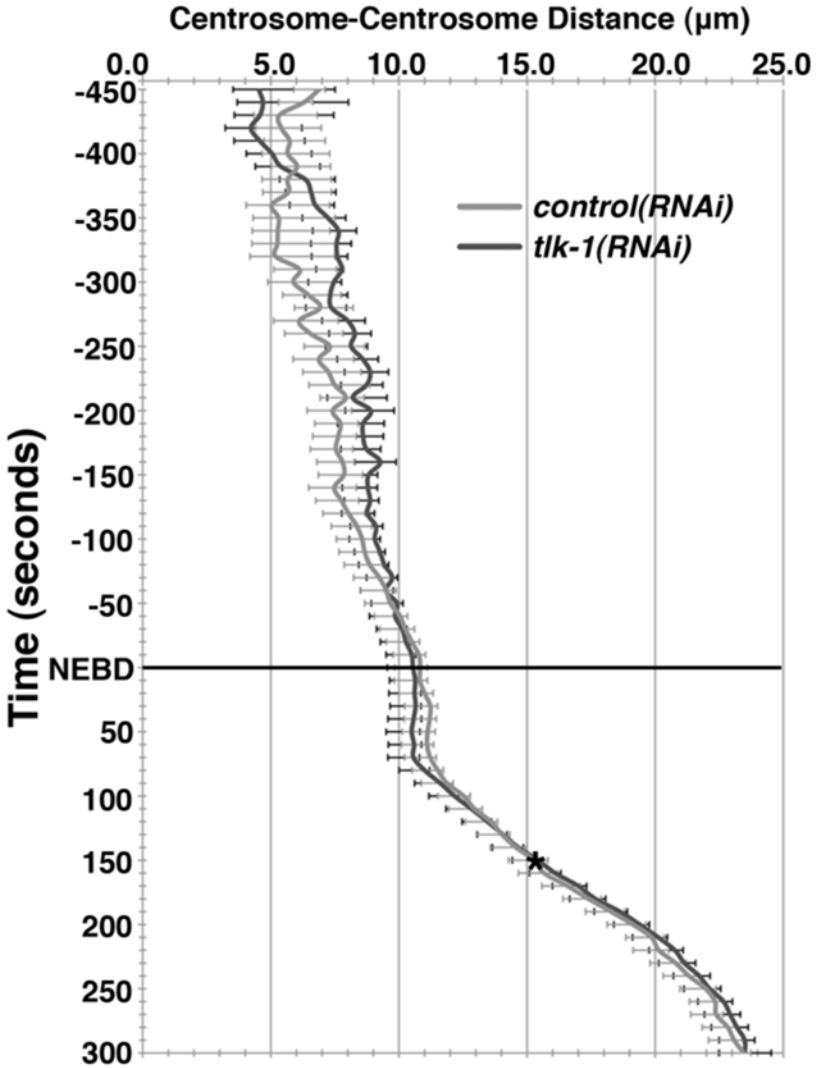
Centrosome-Centrosome Distance (μm)
0.0
5.0
10.0
15.0
20.0
25.0
Time (seconds)
-450
-400
-350
-300
-250
-200
-150
-100
-50
NEBD
50
100
150
200
250
300
control(RNAi)
tlk-1(RNAi)
*

Posterior centrosomes in *tlk-1(RNAi)* embryos are an average of 9.2% embryonic length more anteriorly displaced than control posterior centrosomes during this time period (Table 3). These results suggest that TLK-1 affects posterior centrosome positioning prior to nuclear envelope breakdown.

While these data allowed me to determine the movement of centrosomes with respect to one another and the anterior-posterior axis, I sought to assess centrosome behavior in three-dimensional space over time. Hence, four-dimensional live-cell spinning disk confocal microscopy was performed with *C. elegans* embryos co-expressing plasma membrane and centrosome markers (GFP::$PH^{PLC1\delta1}$ and GFP:: γ-tubulin) (Toya, Iida et al. 2010). Videos of *control* and *tlk-1(RNAi)* embryos were taken from pronuclear migration through completion of the first mitotic division. All videos were temporally aligned using anaphase onset as a reference point; this time point was chosen since it was not possible to reliably demarcate the precise time at which NEBD occurred.

Five *control* and five affected *tlk-1(RNAi)* embryos (*i.e.*, those exhibiting aberrant spindle rotation) were subjected to imaging and analysis as described in Materials and Methods. Initial centrosome positions at approximately PNM (Figure 20), while somewhat stochastic prior to centration, were more tightly organized overall in *control* versus *tlk-1(RNAi)* embryos, as observed in both top-down and side-on views. The positions of centrosomes in anaphase (Figure 20) were also less spatially organized in *tlk-1(RNAi)* embryos but less so than at PNM. The paths of centrosomes movement were traced over time in Imaris to generate individual tracks for the anterior and posterior centrosomes in *control* (n=5) and *tlk-1(RNAi)* (n=5) embryos. The paths of five anterior and five posterior centrosomes were then overlaid. During the first asymmetric division, the positioning

Figure 20: TLK-1 affects the spatial positioning of centrosomes during NCC rotation. Centrosome positions at PNM (-300 seconds from anaphase) and anaphase onset (*t*=0, as assessed by posterior spindle displacement) in *control* (n = 5) and *tlk-1(RNAi)* (n = 5) embryos. Top panels are a top-down view and bottom panels are a side-on view. Anterior is to the left and NCC rotation occurred in a counter-clockwise manner. Anterior and posterior centrosomes from the same embryo are the same color. Scale bar = 10μm

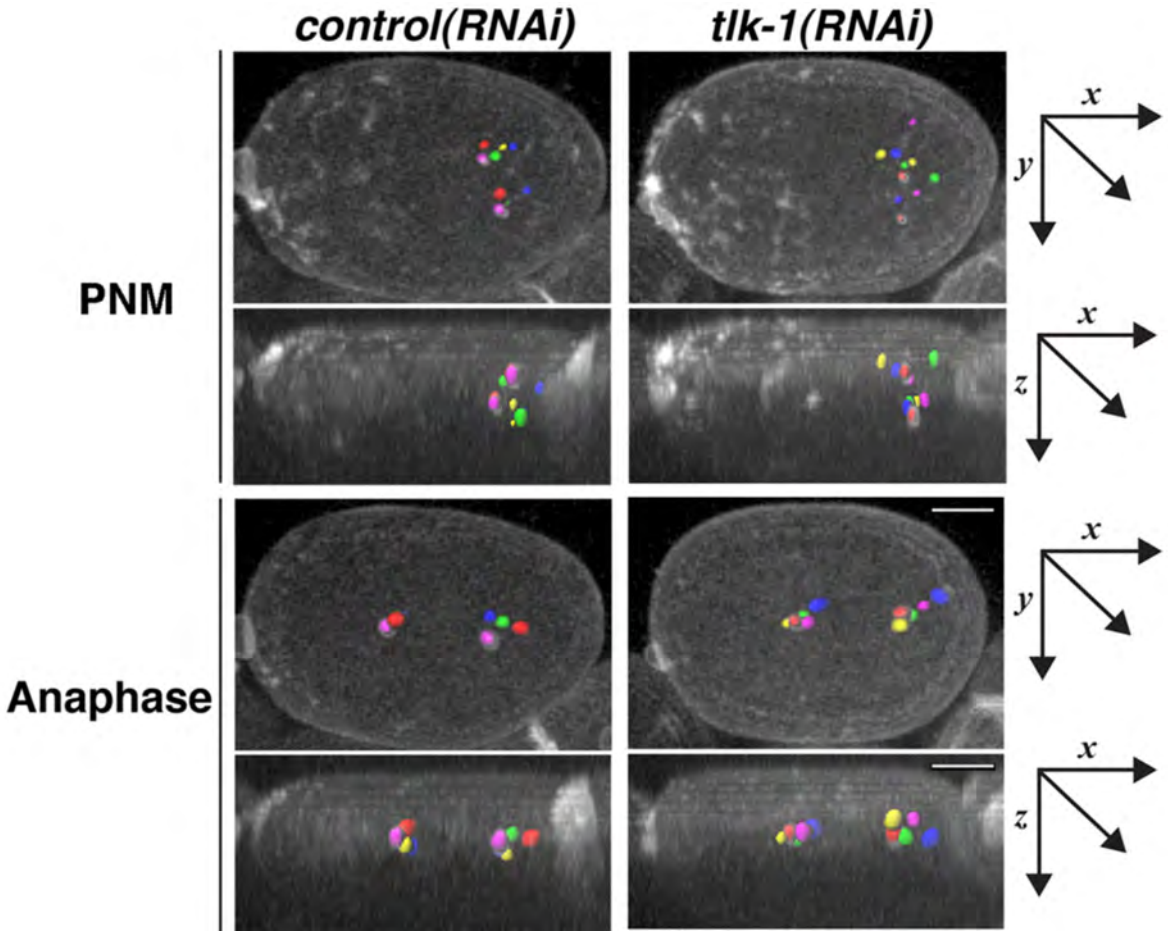
control(RNAi)
tlk-1(RNAi)
PNM
Anaphase
x
y
z

and movement of centrosomes from TLK-1-depleted embryos were radically different than *control(RNAi)* centrosomes. The paths traveled by the anterior centrosomes in *control(RNAi)* embryos (Figure 21) follow a similar path in a characteristic smooth arcing pattern. The anterior tracks of *tlk-1(RNAi)* embryos also follow an arcing pattern, but these traces do not overlap as in controls. The posterior centrosome tracks (Figure 21) in *tlk-1(RNAi)* embryos typically extend farther anteriorly than control embryos, following markedly different, chaotic paths. When all anterior and posterior tracks are overlaid onto a single embryo, the smooth, stereotypical overall rotation paths are clearly different for *control* versus *tlk-1(RNAi)* embryos, with the *tlk-1(RNAi)* rotation paths being extremely disorganized and stochastic in all dimensions (Figure 21). These results suggest that TLK-1 regulates centrosome movement and positioning spatially and temporally in the early *C. elegans* embryo.

Polarity is established normally and does not contribute to aberrant TLK-1-dependent spindle rotation

A priori, the NCC rotation phenotype and disrupted spindle positioning seen in *tlk-1(RNAi)* embryos could result, in part, from defects in polarity establishment. To assess polarity, I performed live-cell spinning disk microscopy on *control* and *tlk-1(RNAi)* embryos expressing either GFP::PAR-6, which demarcates the anterior cortex, or GFP::PAR-2, which demarcates the posterior cortex. Neither GFP::PAR-6- nor GFP::PAR-2-expressing *control* or *tlk-1(RNAi)* embryos showed any obvious defects in polarity establishment from pseudocleavage through cytokinesis (Figure 22). GFP::PAR-6 was more intense in

Figure 21: TLK-1 affects the spatial movement of centrosomes during NCC rotation.

Tracking of the paths the anterior and posterior centrosomes (from (A)) followed during NCC rotation in *control* and *tlk-1(RNAi)* embryos. Track colors correspond to analogously-colored centrosome pairs in (A). Top panels are a top-down view and bottom panels are a side-on view. Scale bar = 10μm

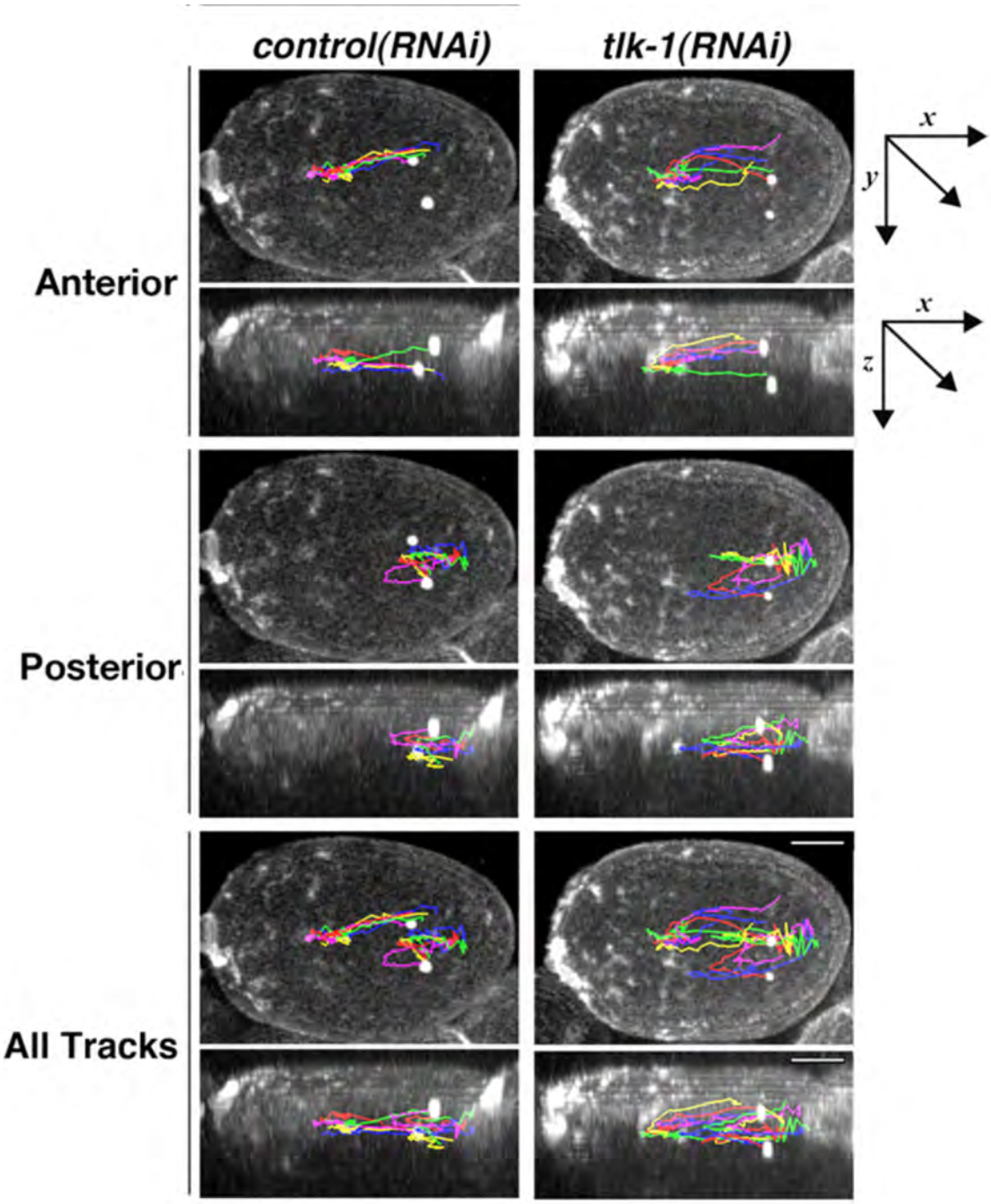
control(RNAi)
tlk-1(RNAi)
Anterior
Posterior
All Tracks
x
y
x
z

tlk-1(RNAi) embryos along the anterior cortex than in controls, but otherwise was in a similar distribution in both samples from PNM through cytokinesis and formation of the cleavage furrow (Figure 22). Posterior polarity as determined by GFP::PAR-2 localization also appeared normal in TLK-1-depleted embryos compared to controls (Figure 22). Although, PAR-2 was more intense in *tlk-1(RNAi)* embryos. While the cortical localizations of both GFP::PAR-2 and GFP::PAR-6 in *tlk-1(RNAi)* embryos were normal, there was a visual difference in intensity between TLK-1-depleted embryos and controls. The live-cell imaging presented here precludes quantitative analysis of GFP::PAR-2/6 proteins levels in *tlk-1(RNAi)* embryos, but the disparity in intensity when TLK-1 is depleted could be biologically significant since members of the polarity-establishment pathway are also cortical force determinants (Tsou, Hayashi et al. 2002; Severson and Bowerman 2003; Tsou, Hayashi et al. 2003; Nguyen-Ngoc, Afshar et al. 2007). Depletion of TLK-1 could have affected the GFP::PAR-2/6 transgenes in the same manner, although such a difference is not observed with other transgenes such as GFP::β-tubulin. To assess this difference in intensity, antibody staining against the PAR-2 and PAR-6 proteins can be performed and their protein levels quantitated, and other cortical proteins (*i.e.*, PAR-1//3, GPR-1/2) can be assessed as well.

Figure 22: Normal anterior polarity is established in TLK-1-depleted embryos.

(A) Still images from live-cell videos of *control* (*n*=4) and *tlk-1(RNAi)* (*n*=3) embryos expressing GFP::PAR-6. Anterior localization of GFP::PAR-6 at pseudocleavage, PNM, and cytokinesis is similar between *control* and *tlk-1(RNAi)* embryos. Scale bar = 10μm

(B) Still images from live-cell videos of *control* (*n*=4) and *tlk-1(RNAi)* (*n*=3) embryos expressing GFP::PAR-2. There is no discernible difference in posterior localization of GFP::PAR-2 immediately before cleavage furrow ingression or at cytokinesis between *control* and *tlk-1(RNAi)* embryos. Scale bar = 10μm

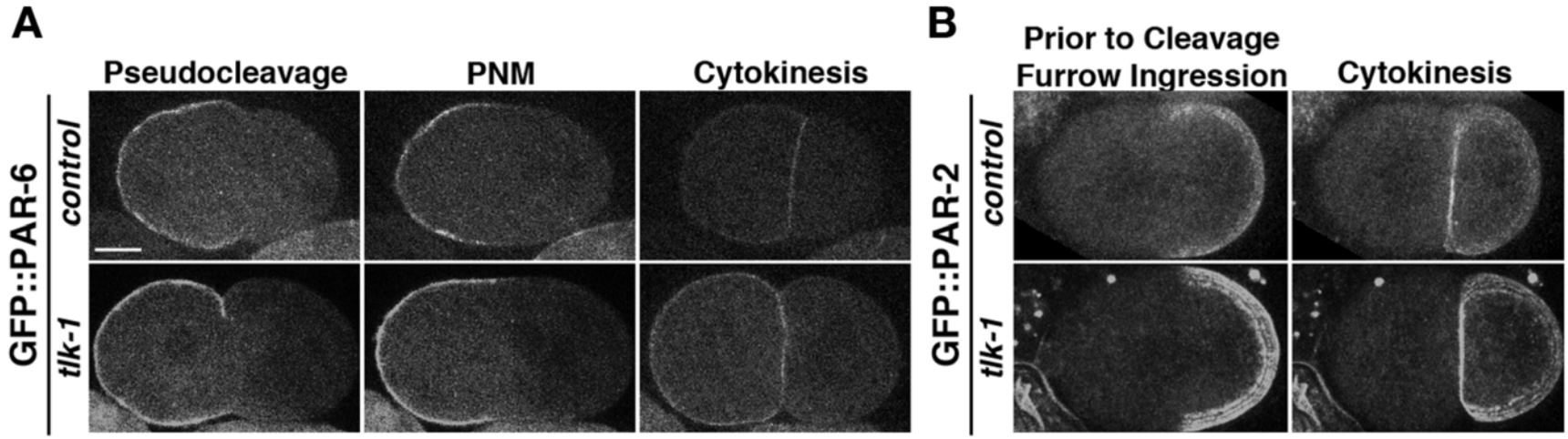
A
Pseudocleavage
PNM
Cytokinesis
GFP::PAR-6
control
tlk-1
B
Prior to Cleavage
Furrow Ingression
Cytokinesis
GFP::PAR-2
control
tlk-1

TLK-1 is required for LET-99 localization and restriction to the posterior-lateral cortical domain

Differential pulling forces emanating from defined regions of the cell cortex are responsible for spindle rotation during centration (Siller and Doe 2009). Stronger pulling from the anterior cortex centrate the NCC while diminished forces from the lateral posterior domain allow astral microtubule attachments at the anterior and posterior cortices to rotate the NCC as it moves anteriorly. Inhibition of the cortical pulling forces at the lateral posterior domain by LET-99 is essential for NCC rotation to occur in a timely manner to align the mitotic spindle along the AP axis prior to chromosome segregation (Tsou, Hayashi et al. 2002). Therefore, I sought to determine if LET-99 was differentially localized in *tlk-1(RNAi)* embryos.

Using live-cell spinning disk microscopy, I imaged RL238 YFP::LET-99-expressing embryos subjected to *control* and *tlk-1(RNAi)* undergoing the first mitotic division. Embryos were temporally aligned at NEBD, which was defined as the first frame in which a distinct influx of cytoplasmic YFP::LET-99 into the former pronuclear space could be reliably observed. In both *control* and *tlk-1(RNAi)* embryos, there was an intense YFP::LET-99 signal at the polar bodies, hence for the purposes of assessing the cortical localization of YFP::LET-99, I masked the polar bodies on the anterior and disregarded the strong YFP::LET-99 signal emanating from the polar bodies. Control embryos exhibited YFP::LET-99 maxima around 45%-75% embryonic length during NCC rotation, increasing in intensity and spreading toward the posterior to around 80% EL after NEBD and up until

Figure 23: LET-99 is differentially distributed throughout the cell cortex TLK-1-depleted embryos.

Still images from videos of RL238 (*let-99(dd17);*YFP::LET-99) *control* or *tlk-1(RNAi)* embryos from 180 seconds prior to and 60 seconds after NEBD. The polar bodies were masked in these panels due to their brightness. Depletion of TLK-1 results in a more intense and broader cortical accumulation of YFP::LET-99 from PNM through NCC. Scale bar = 8μm

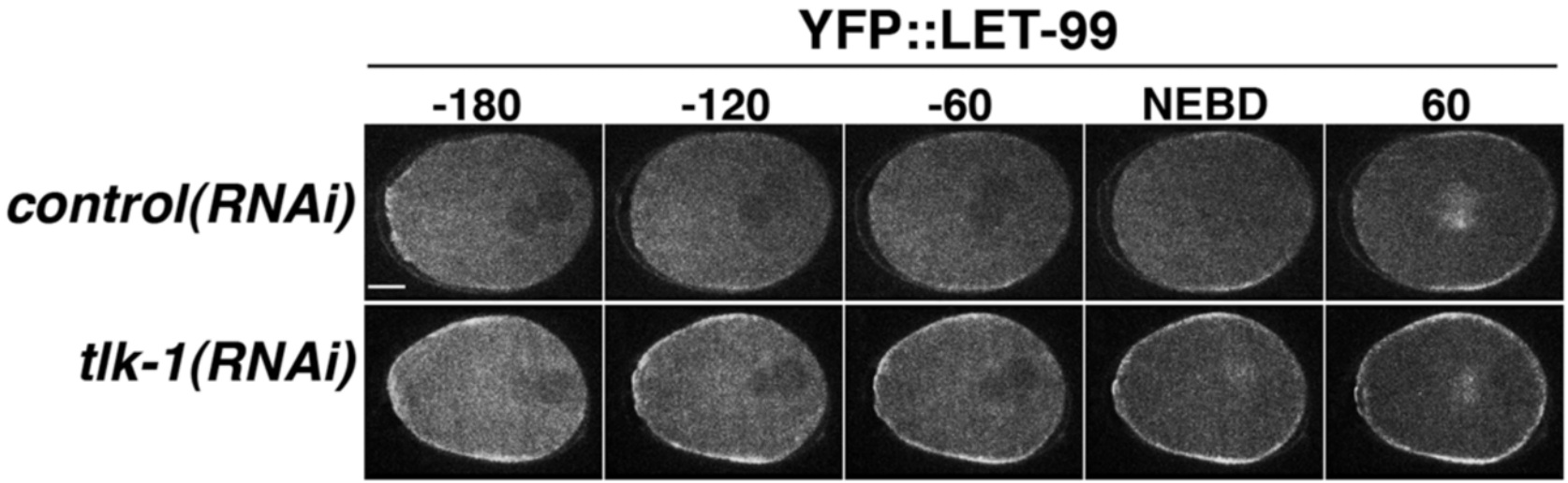
YFP::LET-99
-180
-120
-60
NEBD
60
control(RNAi)
tlk-1(RNAi)

metaphase (Figure 23, *n*=4). However, *tlk-1(RNAi)* embryos showed a strikingly higher intensity of YFP::LET-99 throughout the entire cortex from PNM through metaphase, especially localizing more anteriorly than in controls (Figure 23, *n*=4).

Recognizing the limitations of quantifying protein levels using live-cell imaging, I performed fixed-cell immunofluorescence of TH73 (YFP::LET-99) embryos subjected to *control* or *tlk-1(RNAi*) in order to more precisely quantitate the aberrant YFP::LET-99 localization and intensities from PNM through NCC rotation. Previous *in situ* immunolocalization showed maximal LET-99 protein localization from approximately 50-75% embryonic length at PNM (Tsou, Hayashi et al. 2002). I found that intensity of YFP::LET-99 was significantly higher in *tlk-1(RNAi)* embryos versus controls at or shortly after PNM from 32% to 52% embryonic length, with YFP::LET-99 being ≥1.5x brighter in TLK-1-depleted embryos over this range (Figures 24 and 25). These data suggest that there is an increase in and less cortical restriction of YFP::LET-99 protein levels at PNM in TLK-1-depleted embryos (Figures 24 and 25).

I also analyzed *tlk-1(RNAi)* embryos post-PNM that were undergoing NCC rotation and found that levels of YFP::LET-99 were significantly higher throughout the anterior cortex (0% EL) to the posterior lateral cortical domain (75% EL). From the anterior cortex to about 44% EL, YFP::LET-99 was between 2.0-2.5x brighter in TLK-1-depleted embryos compared to controls (Figure 26 and 27). A sharp increase of YFP::LET-99 in *tlk-1(RNAi)* embryos was observed after 44% EL, which was anterior of the YFP::LET-99 domain in control embryos, beginning at approximately 53% EL. YFP::LET-99 levels peaked in both control and *tlk-1(RNAi)* embryos at 60% EL, but YFP::LET-99 was 2.8x brighter in TLK-1-depleted embryos (Figures 26 and 27). Taken together, these data indicate that TLK-1

affects the amount and cortical position of LET-99 from PNM through centration and NCC rotation. Thus, I conclude that TLK-1 plays an unexpected role in regulating LET-99-positioning during the first asymmetric division.

Because LET-99 is known to inhibit cortical pulling forces in the posterior-lateral domain of the embryo, I next assessed how microtubule dynamics and attachments were differentially affected when TLK-1 was depleted. Quantitative analysis of embryos stained with anti-α-tubulin revealed that *tlk-1(RNAi)* embryos had significantly fewer microtubules reaching within 2μm of the cell cortex during NCC rotation (Figure 28A). This implies that less cortical force is being generated overall in TLK-1-depleted embryos due to attenuation of these astral microtubule attachments. Additionally, I performed live-cell spinning disk confocal imaging of GFP::EBP-2 (end-binding protein 2), which is localized to the plus-ends of microtubules being nucleated from the centrosomes and can be used as a readout of microtubule polymerization (Srayko, Kaya et al. 2005). Tracking of GFP::EBP-2 particles after NEBD in *control* and *tlk-1(RNAi)* embryos revealed that control microtubules nucleate to consistent, distinct areas of the cell cortex during rotation with microtubule attachments appearing to be generally more "end-on". No discernible pattern for the directionality of microtubule nucleation in *tlk-1(RNAi)* microtubules was observed except that more microtubules appear to be nucleating toward the inhibitory posterior-lateral cortex than in controls (Figure 28B (red domain)); however, generally the GFP::EBP-2 comets displayed a chaotic distribution throughout the cell and aberrant localization to the cell cortex. Microtubules in TLK-1-depleted embryos also appeared to slide along the cortex more than in control embryos (Figure 28B). Together, these data show that TLK-1 is necessary for

regulating the direction of microtubule nucleation during NCC rotation, as well as efficient nucleation of microtubules and their attachment to the cell cortex.

Figure 24: TLK-1 affects the level and cortical position of LET-99 during NCC rotation.

Fixed-cell quantitation of TH73 (YFP::LET-99) *control* (*n*=9) and *tlk-1(RNAi)* (*n*=8) at PNM. Raw data were normalized from 0 to 1 with respect to the minimum and maximum raw intensities for (B) and (C). Example embryos are shown in the right panels. The polar bodies were not considered part of the embryo. Graph represents average cortical intensities ± SEM. Shaded area = $p < 0.05$, Student's *t*-test. Scale bar = 8μm

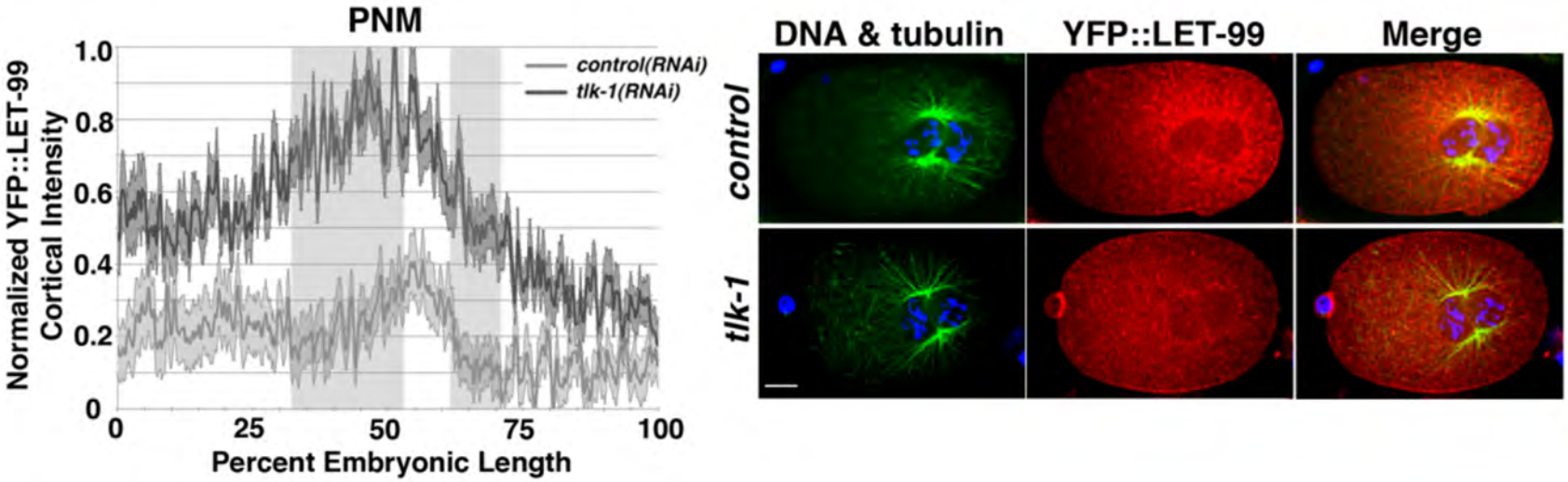
PNM
Normalized YFP::LET-99 Cortical Intensity
1.0
0.8
0.6
0.4
0.2
0
0
25
50
75
100
Percent Embryonic Length
control(RNAi)
tlk-1(RNAi)
DNA & tubulin
YFP::LET-99
Merge
control
tlk-1

Figure 25: Quantified raw intensities of YFP::LET-99 levels at PNM.

Raw, non-normalized fixed-cell quantitation data of TH73 (YFP::LET-99) *control* (*n*=9 embryos, 18 cortices) and *tlk-1(RNAi)* (*n*=8 embryos, 16 cortices) at PNM. The polar bodies were not considered part of the embryo. Graph represents average raw cortical intensities ± SEM. Shaded area = $p < 0.05$, Student's *t*-test.

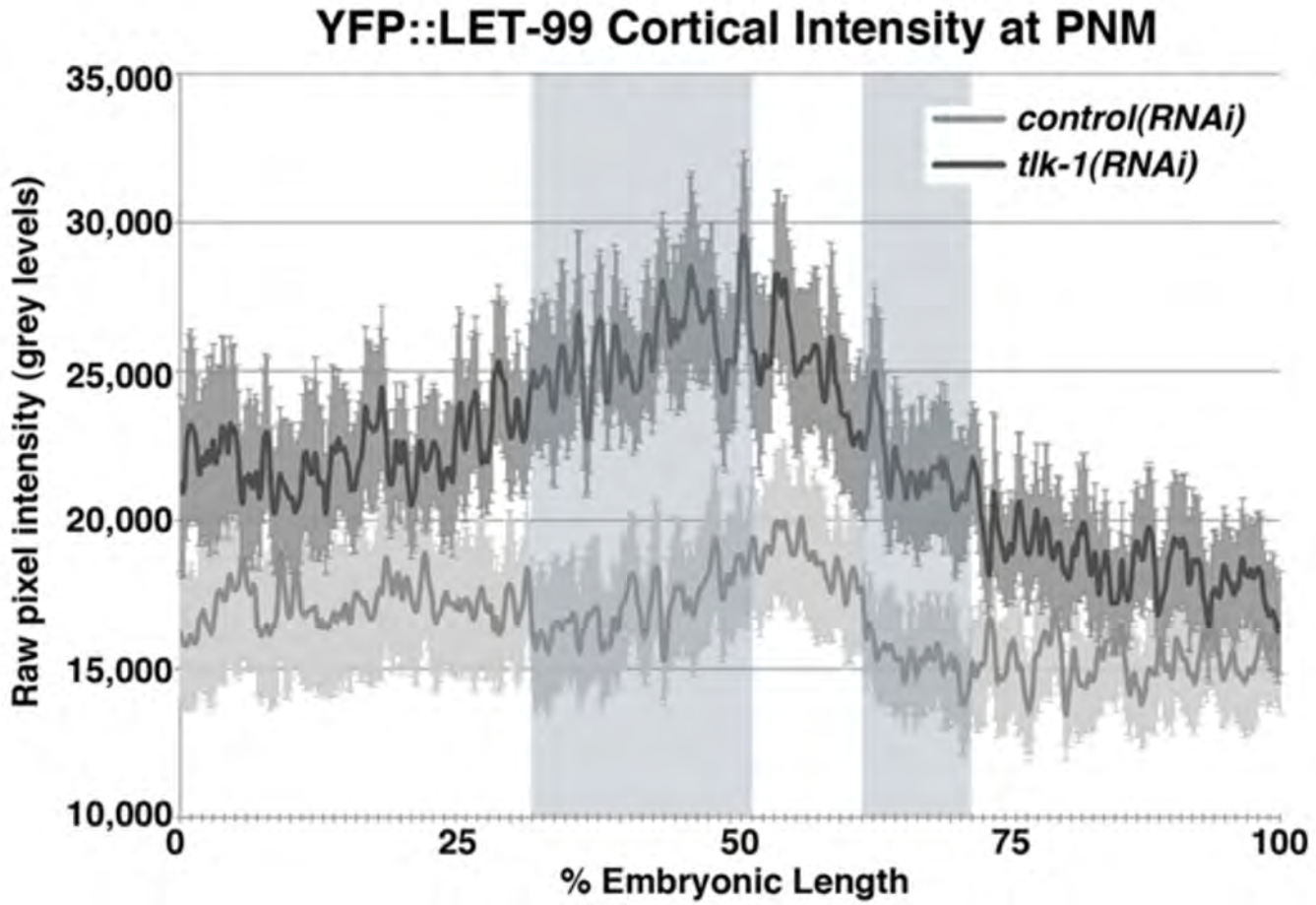
YFP::LET-99 Cortical Intensity at PNM
control(RNAi)
tlk-1(RNAi)
Raw pixel intensity (grey levels)
35,000
30,000
25,000
20,000
15,000
10,000
0
25
50
75
100
% Embryonic Length

Figure 26: TLK-1 affects the level and cortical position of LET-99 during NCC rotation.

Fixed-cell quantitation of TH73 (YFP::LET-99) *control* (*n=5*) and *tlk-1(RNAi)* (*n*=5) having undergone NEBD. Raw data were normalized as in Figure 24. Example embryos are shown in the right panels. Graph represents average cortical intensities ± SEM. Shaded area = $p < 0.05$, Student's *t*-test. Scale bar = 8μm

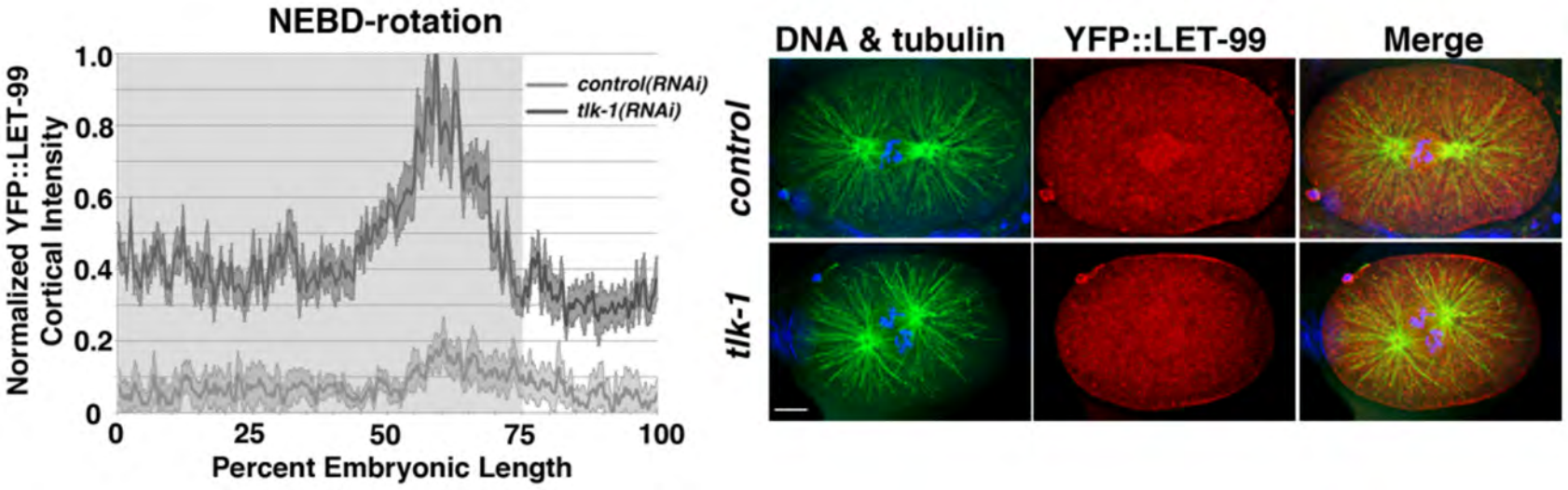
NEBD-rotation
Normalized YFP::LET-99 Cortical Intensity
1.0
0.8
0.6
0.4
0.2
0
0
25
50
75
100
Percent Embryonic Length
control(RNAi)
tlk-1(RNAi)
DNA & tubulin
YFP::LET-99
Merge
control
tlk-1

Figure 27: Quantified raw intensities of YFP::LET-99 levels at NEBD-rotation

Raw, non-normalized fixed-cell quantitation data of TH73 (YFP::LET-99) *control* (*n*=5 embryos, 10 cortices) and *tlk-1(RNAi)* (*n*=5 embryos, 10 cortices) at NEBD-rotation. The polar bodies were not considered part of the embryo. Graph represents average raw cortical intensities ± SEM. Shaded area = $p < 0.05$, Student's *t*-test.

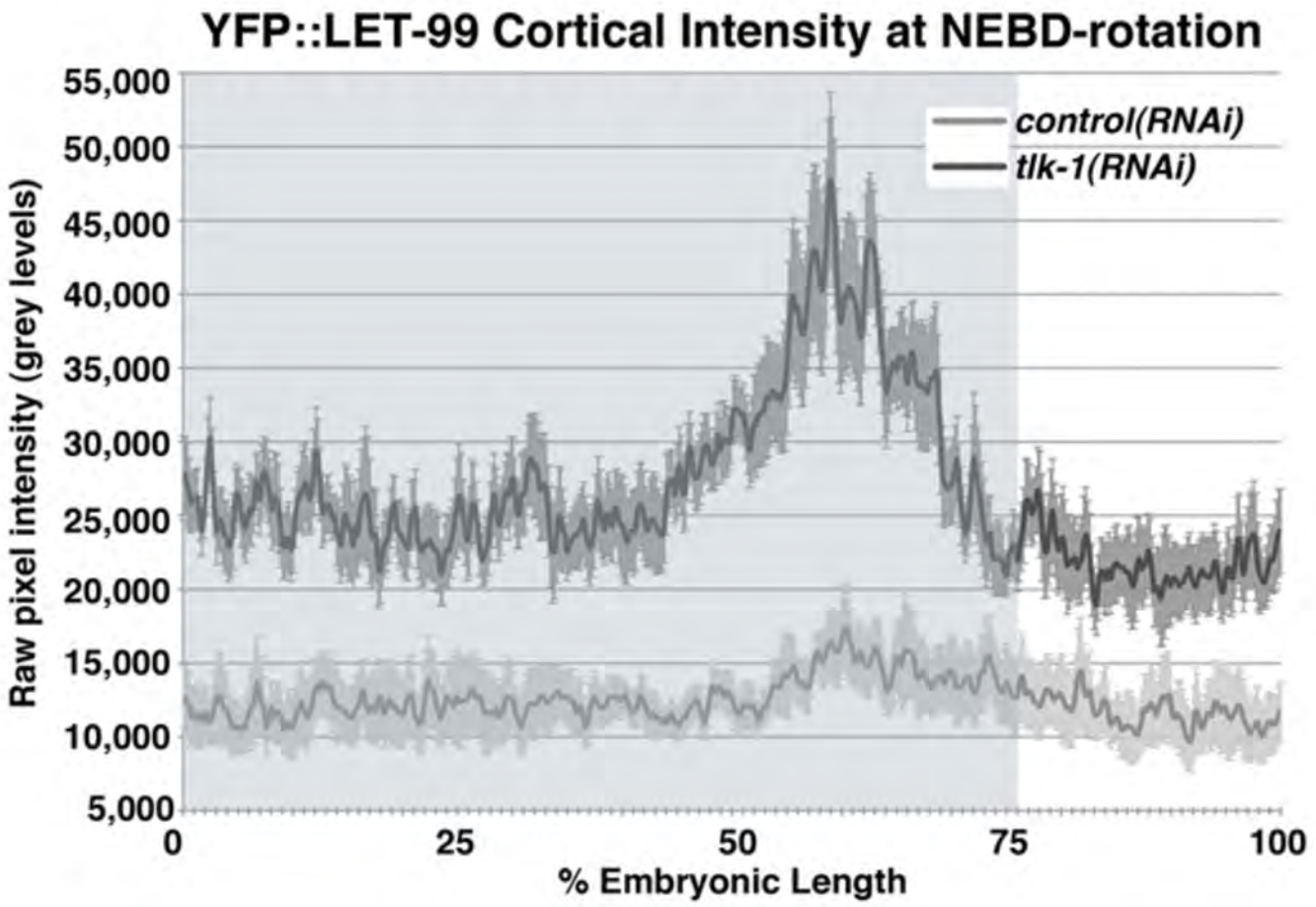
YFP::LET-99 Cortical Intensity at NEBD-rotation
Raw pixel intensity (grey levels)
55,000
50,000
45,000
40,000
35,000
30,000
25,000
20,000
15,000
10,000
5,000
0
25
50
75
100
% Embryonic Length
control(RNAi)
tlk-1(RNAi)

‘

Figure 28: Quantitation of astral microtubule at the cell cortex.

(A) Immunofluorescent analysis of astral microtubules in *tlk-1(RNAi)* embryos. TLK-1-depleted embryos exhibit fewer microtubules reaching to within 2μm of the cell cortices, suggesting that less microtubule attachments may also be contributing to the aberrant NCC rotation phenotype (n=5 for both conditions). Error bars = ± SEM. * = $p < 0.05$, Student's t-test.

(B) Tracking of GFP::EBP-2 particles after NEBD in *control* and *tlk-1(RNAi)* embryos. Control microtubules nucleate to consistent, distinct areas of the cell cortex during rotation with microtubule attachments appearing to be generally more "end-on". No discernible pattern for the directionality of microtubule nucleation in *tlk-1(RNAi)* microtubules was observed, with the GFP::EBP-2 comets displaying a chaotic distribution throughout the cell and aberrant localization to the cell cortex. Microtubules in TLK-1-depleted embryos also appeared to slide more when they reached the cortex than control embryos. Cortical domains are indicated in their respective colors. Images represent a 40s time from PNM through rotation. Arrow = "end on" microtubule attachments in *control(RNAi)*; arrowheads = microtubule cortical sliding in *tlk-1(RNAi)*

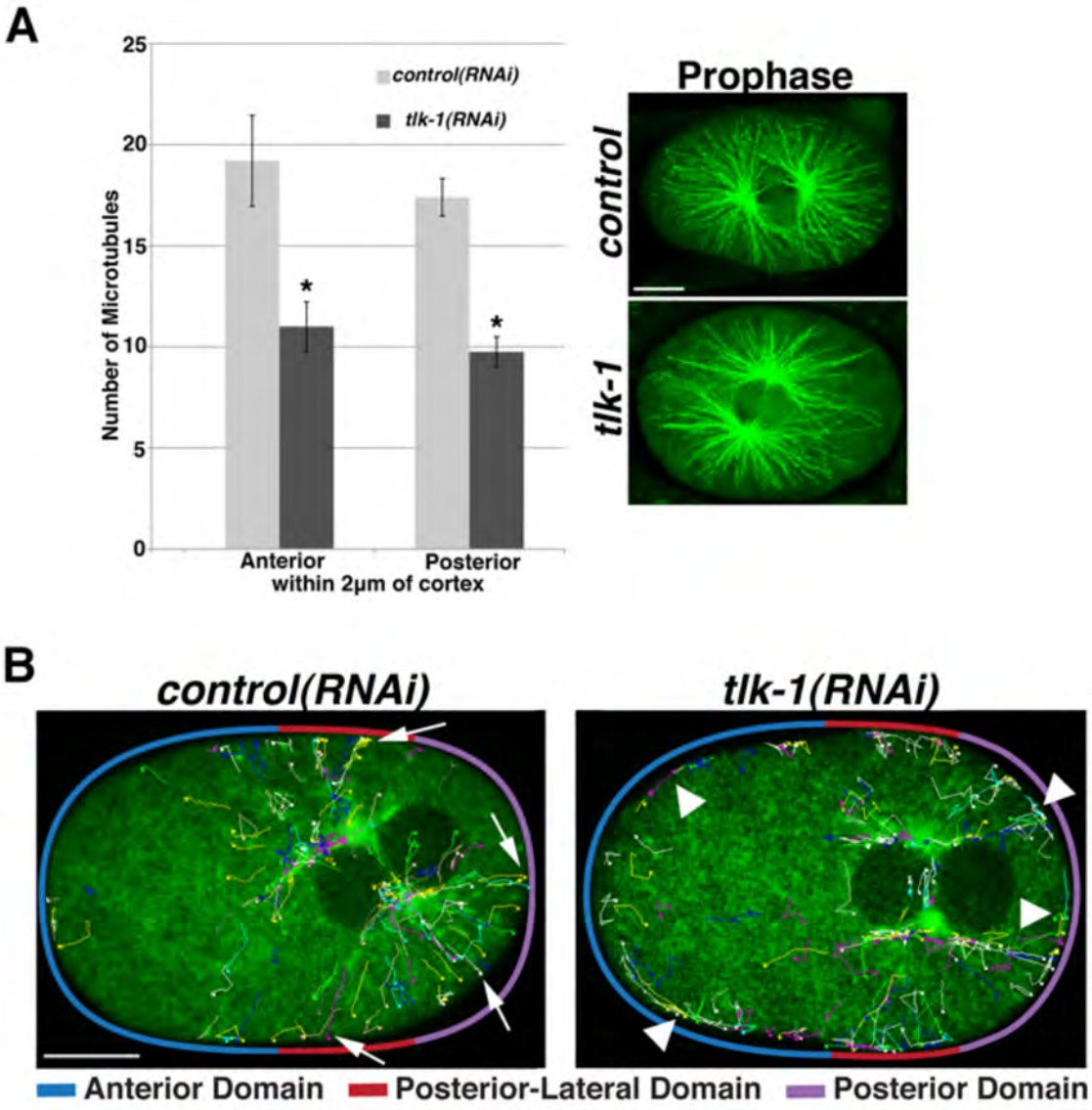
A
25
20
15
10
5
0
Number of Microtubules
control(RNAi)
tlk-1(RNAi)
*
*
Anterior
Posterior
within 2µm of cortex
Prophase
control
tlk-1
B
control(RNAi)
tlk-1(RNAi)
Anterior Domain
Posterior-Lateral Domain
Posterior Domain

CHAPTER III: DISCUSSION AND SIGNIFICANCE

DISCUSSION

Here I report that the *C. elegans* TLK-1 kinase has a role in the timing of nuclear core complex rotation, centrosome movement, mitotic spindle positioning and microtubule dynamics during the first asymmetric cell division. This is the first report demonstrating a critical role for a Tousled-like kinase in spindle dynamics in any organism. Human Tlks were initially described as functioning in S-phase, with implied roles in DNA replication (Krause et al. 2003), DNA repair (Groth et al. 2003), and chromatin assembly (Sillje and Nigg 2001). Work from our laboratory and others have also demonstrated a role for TLKs during mitosis, including chromosome condensation (Yeh et al. 2010) and chromosome segregation (Han et al. 2005). Tlks in humans and other organisms are necessary for survival and to maintain ploidy, and my work implicating TLK-1 in directly influencing microtubule-spindle dynamics suggests additional mechanisms through which Tlks are likely contributing to cellular maintenance.

During the asymmetric division of the early one-cell embryo, AP polarity is established and maintained by cues from the asymmetrically-localized PAR proteins. These polarity cues regulate cortical pulling forces on astral microtubule attachments at the cell cortex and are required for NCC rotation, posterior spindle displacement, and anaphase separation (Galli and van den Heuvel 2008). We show that depletion of TLK-1 does not affect establishment of polarity as represented by correct localization of PAR-6 to the anterior cortex and PAR-2 to the posterior cortex. Therefore, the aberrant spindle positioning and rotation observed in *tlk-1(RNAi)* embryos is not likely due to perturbed polarity. However, non-muscle myosin II (NMY-2) is necessary both for centration and for limiting PAR-3 to the anterior cortex during polarity establishment (Severson and Bowerman 2003), and is dynamically influenced by Gα proteins and LET-99 (Goulding et al. 2007); importantly, a regulatory subunit of non-muscle

myosin II has been reported to be a substrate of mammalian Tlk1 (Hashimoto et al. 2008). Therefore, it is possible that TLK-1 is indirectly affecting polarity establishment and downstream cortical force generation through regulation of NMY-2, but future analyses will be needed to determine what, if any, effects TLK-1 has on NMY-2 localization and function.

Attachment of astral microtubules to the cell cortex are necessary for generating the stability and forces necessary to drive spindle movement and rotation. Hence, a reduction in the amount of astral microtubules able to reach the cortex would result in less force and defects in spindle rotation. Accurate localization of LET-99 to the posterior-lateral cortex is also required for the inhibition of cortical pulling in this domain, thus allowing cortical pulling from the anterior and posterior domains to successfully rotate the NCC complex in a timely manner (Figure 29) (Krueger et al. 2010; Tsou et al. 2002). Thus, I posit that the striking increase of LET-99 protein levels and its broader distribution in *tlk-1(RNAi)* embryos is causing ectopic inhibition of cortical pulling during centration, which leads to delayed NCC rotation. In TLK-1-depleted embryos at PNM, I found significantly increased levels of LET-99 spreading into the anterior cortical domain of the embryo. Attenuation of cortical pulling in this area could explain why centration occurs in a timely manner without concomitant NCC rotation in *tlk-1(RNAi)* embryos: sufficient pulling enables the anterior cortex to centrate the NCC anteriorly, but there are insufficient forces emanating from the lateral anterior cortex to create the necessary rotational torque to rotate the NCC to lie along the AP axis. One model predicts that centrosome positions relative to the LET-99 band at PNM, when the centrosomes are positioned transversely to the AP axis, are key to determining the directionality of astral microtubules specifically towards the anterior, thus resulting in a greater net pulling force on that centrosome from the anterior (with a similar net posterior force acting on the other

centrosome), driving timely NCC rotation (Tsou et al. 2002). This model is consistent with our centrosome tracking experiments showing that TLK-1 is required for accurate spatial and temporal centrosome positioning during the first mitotic division.

One puzzling aspect of the TLK-1-dependent delayed NCC rotation is that the spindle eventually "catches up" to fully rotate along the AP axis by anaphase onset. By our model, this would suggest that the cortical force attenuation by aberrant LET-99 localization to the anterior cortex is eventually resolved, yet we observed significantly increased levels of LET-99 in *tlk-1(RNAi)* embryos compared to controls through the anterior domain during and after NEBD, as well as during the late rotation (Figures 26 and 27). However, in the TLK-1-depleted embryos, we also noticed a steep decrease in LET-99 intensity after a peak in the posterior-lateral domain. LET-99 intensity reaches its maximum at similar points in both *control* and *tlk-1(RNAi)*, but LET-99 intensity in *control(RNAi)* embryos decreases approximately 6.7x more gradually than *tlk-1(RNAi)* embryos. There was little significant difference in LET-99 levels between *control* and *tlk-1(RNAi)* embryos in the absolute posterior domain, suggesting that TLK-1 is not necessarily regulating LET-99 localization there. These data imply that the rapid reduction of LET-99 levels in TLK-1-depleted embryos observed at the posterior-lateral domain satisfy a putative LET-99 threshold, whereby once achieved the level of LET-99 force attenuation from the posterior-lateral domain is less than the remaining cortical pulling from the absolute posterior cortex (*i.e.*, LET-99 is no longer counteracting pulling forces at the posterior-lateral domain to sufficiently compete with posterior cortical pulling), resulting in the significantly faster posterior centrosome rotation observed during the aberrant NCC rotation phenotype in *tlk-1(RNAi)* embryos (Figure 29, bottom).

Another possibility for the ability of TLK-1-depleted embryos to eventually properly align spindles to the AP axis, as well as why I do not observe severe chromosome segregation phenotypes in early *tlk-1(RNAi)* embryos, is that *tlk-1(RNAi)* is not fully penetrant in the early embryo, suggesting that different thresholds of TLK-1 are required for different cellular functions (*e.g.*, chromosome condensation and/or segregation). Thus, it remains possible that residual TLK-1 protein persists in the early embryo and aiding in the correction of the delayed NCC rotation. Unfortunately, homozygous *tlk-1(tm2395*) hermaphrodites are sterile, which precludes analyzing the first asymmetric division in the total absence of TLK-1. It could also be that TLK-1 is not required until later stages of development, or that it is functioning redundantly with other factors during early embryogenesis to allow for initial stages of development without generating aneuploidy.

A second mechanism through which TLK-1 could be affecting spindle rotation is a functional relationship with the CLASP family of microtubule regulatory proteins. Our lab has discovered that TLK-1 is associated with the outer kinetochore and is required for the kinetochore association of both CLASP-2 (CLS-2) and LIS-1 (De Orbeta and Schumacher, manuscript in preparation), a component of the dynein complex that is also required for spindle rotation (Cockell et al. 2004; Siller and Doe 2008). Interestingly, Espiritu and Kreuger *et al.* demonstrated that in addition to regulating kinetochore microtubule attachments, CLS-2 functions redundantly with the other two *C. elegans* CLASP proteins to regulate mitotic spindle positioning during the first asymmetric division (Espiritu et al. 2012). Co-depletion of CLS-2 with either CLS-1 or CLS-3 resulted in a significantly delayed spindle rotation strikingly similar to the TLK-1-dependent aberrant NCC rotation I describe here. Strikingly, data from our laboratory indicates that TLK-1 is required for CLS-2 localization to the kinetochore, and

we also find that co-depletion of TLK-1 and CLS-2 displays significant chromosome congression and segregation errors in the early embryo (De Orbeta and Schumacher, manuscript in preparation). We posit that TLK-1 and CLS-2 may also be acting in concert to regulate astral microtubule dynamics by influencing downstream regulators of astral microtubule attachments to the cell cortex. One such regulatory complex is the dynein-dynactin complex, a well-established driver of early embryonic dynamics, including pronuclear migration, NCC rotation, and spindle positioning (Nguyen-Ngoc et al. 2007; Severson and Bowerman 2003; Skop and White 1998). Additionally, LIS-1, a component of the dynein complex, is also necessary for NCC rotation and interacts with GPR-1/2 and LIN-5, proteins which promote the presence of dynein at the cell cortex (Nguyen-Ngoc et al. 2007; Siller and Doe 2008). Thus, TLK-1 and LIS-1 may also be functioning together to promote timely NCC rotation. Furthermore, a recent large-scale project utilizing combined functional genomics, proteomics, and chemical biology approaches to determine interactions between mitotic proteins (Hutchins et al. 2010; Neumann et al. 2010) revealed that human orthologues of TLK-1 (Tlk1 and Tlk2) co-purified with multiple subunits of the dynein complex and other known microtubule-associated proteins, further corroborating our hypothesis that TLK-1 is influencing cortical force generation and regulation during asymmetric cell division.

Altogether, I provide evidence for an unexpected role for TLK-1 in regulating spindle positioning in mitosis. That TLK-1 depletion does not mimic all defects often associated with impaired microtubule-based mitotic processes (*i.e.,* reduction of dynein activity or impaired astral microtubule cortical attachments) (Galli and van den Heuvel 2008; Nguyen-Ngoc et al. 2007; Skop and White 1998; Tsou et al. 2002), including pronuclear migration, centration, and posterior spindle displacement at anaphase onset, likely reflects a specific requirement for

TLK-1 in the microtubule regulatory hierarchy. One simple explanation for this hypothesis is that TLK-1 could phosphorylate key cortical force generators, including non-muscle myosin II (Hashimoto et al. 2008), components of the dynein/dynactin complex such as LIS-1, or regulators of these forces (*e.g.*, CLS-2). Since fewer astral microtubules reach the cell cortex when TLK-1 is depleted, TLK-1 may regulate microtubule polymerization or the overall stability and rigidity of the astral microtubule lattice. Interestingly, CLS-2 regulates microtubule polymerization (Cheeseman et al. 2005), thus corroborating this hypothesis. Since Tlks appear to have kinase-independent scaffolding functions (De Benedetti 2010; Riefler et al. 2008b), perhaps TLK-1 acts as a scaffold at the kinetochore and/or centrosomes that organizes loading of the dynein/dynactin cargo that is necessary for wild-type microtubule dynamics. Additionally, Gary Deyter from our lab showed that cyclin B3, CYB-3, is a dynein regulator that also binds TLK-1 (Deyter et al. 2010), thus providing another potential mechanistic link through which TLK-1 could be functioning to regulate mitotic microtubule dynamics. Further biochemical and genetic analyses to address potential substrates and/or functions of TLK-1 that may affect cortical forces and microtubule dynamics in the early embryo are important considerations for future investigations.

SIGNIFICANCE

The research I presented in this Dissertation offers insight into a novel function of a Tousled-like kinase during the cell cycle. Tlks have primarily been implicated as S-phase kinases, but work from our lab has untousled a mitotic role for TLK-1 (Han et al. 2005). That I found TLK-1 to be influencing cytoskeletal processes is intriging, as defects in spindle-nuclear positioning, failures in spindle rotation, or aberrant centrosome positioning and mutations can

lead to disruptions in embryonic development leading to embryonic lethality, tumor formation, and diseases such as cancer, microcephaly, or lissencephaly in humans (Basto et al. 2008; Basto et al. 2006; Bond et al. 2002; Castellanos et al. 2008; Kumar et al. 2009; Lingle et al. 2002; Nigg and Raff 2009; Pihan et al. 1998; Tsai et al. 2007). In humans, Tlks are rapidly and transiently inhibited following the generation of DNA double-stranded breaks during S- phase; this is cell cycle checkpoint- and ATM-pathway dependent, and appears to regulate processes involved in chromatin assembly, most likely by phosphorylating the chromatin assembly factor ASF1. Tlks also protect cells from ionizing radiation by facilitating the repair of double stranded DNA breaks. Additionally, Tlks are overexpressed in triple negative breast cancer (J. Schumacher, unpublished), a group of neoplasms that are not candidates for current, target-specific therapies making patients' only option systemic chemotherapy (Flowers et al. 2009). Thus, elucidating the mechanisms by which Tlks regulate the cell cycle and accurate cellular division is vital for the generation of new treatments and therapies for patients in whom Tlk expression and/or function is perturbed. Through my research, I have provided exciting new insight into understanding TLK-1 function in cellular dynamics, thus generating new hypotheses to be tested in the future about how TLK-1-dependent spindle positioning, centrosome movements, and cytoskeletal dynamics contribute to aneuploidy, chromosome missegregation, and the ultimate demise of cells.

Figure 29: Model for TLK-1-dependent aberrant NCC rotation.

Cortical forces are tightly regulated to ensure timely and accurate spindle positioning. LET-99-dependent attenuation of forces at the posterior-lateral domain of the one-cell embryo allow for forces emanating from the anterior and posterior poles to rotate the NCC complex to align with the AP axis, an important step in generating the asymmetry needed for development. TLK-1 is necessary for restriction of LET-99 to the posterior-lateral domain, and may result in counter-acting forces that inhibit NCC rotation. Additionally, loss of TLK-1 results in fewer astral microtubules reaching the cell cortex during the time when NCC rotation should occur, which also could contribute to the disruption of cortical pulling throughout the entire cortex. Eventually, correct cortical forces are resolved in *tlk-1(RNAi)* embryos, allowing the NCC to rotate rapidly and align along the AP axis.

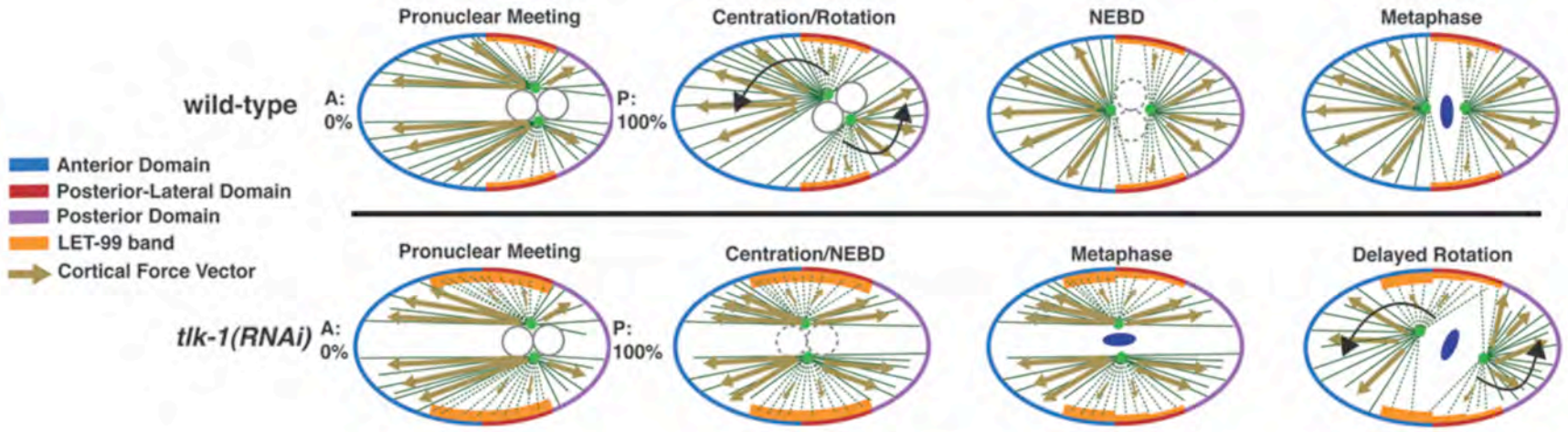
Pronuclear Meeting
Centration/Rotation
NEBD
Metaphase
wild-type
A:
0%
P:
100%
Anterior Domain
Posterior-Lateral Domain
Posterior Domain
LET-99 band
Cortical Force Vector
Pronuclear Meeting
Centration/NEBD
Metaphase
Delayed Rotation
tlk-1(RNAi)
A:
0%
P:
100%

CHAPTER IV: MATERIALS AND METHODS

Worm strains and growth

C. elegans strains were grown using standard techniques as previously described (Brenner 1974). The following strains were used: N2 [wild-type, Bristol]; JS604 *dpy-17(e164) tlk-1(tm2395)* III/*hT2 [qIs48]* (I, III); JS857 *dpy-17(e164) tlk-1(tm2385)* III/*hT2 [qIs48]* (I, III); *gfp::tba-21;mCherry::his-58;* TH32 (provided by the *Cænorhabditis* Genetics Center, University of Minnesota) *ddIs6[tbg-1::gfp unc-119(+)] ruIs32[unc-119(+) Ppie-1::gfp::his-58]* (Maddox et al. 2006); SA164 (provided by A. Sugimoto, Tōhoku University, Sendai, Japan) *ltIs38 [pAA1; Ppie-1::gfp::PH$^{PLC\delta1}$ unc-119(+)] ddIs6[tbg-1::gfp::unc-119(+)]* (Toya et al. 2010); TH73 (provided by L. Rose, University of California, Davis, David, CA, and H. Bringmann, Max Planck Institute for Biophysical Chemistry, Göttingen, Germany) *unc-119(ed3)III; ddIs64[Ppie-1::yfp::let-99(genomic);unc-119(+)]* (Bringmann et al. 2007); RL238 (unpublished, a gift from L. Rose, University of California, Davis, David, CA) *unc-22(e66) let-99(dd17); unc-119(ed3)III; ddIs64[Ppie-1::yfp::let-99(genomic);unc-119(+)]*; TH66 *unc-119(ed3); ddIs14[Ppie-1::ebp-2::gfp]* (Srayko et al. 2005); JH1380 *axEx1094 [pMW1.03 Ppie-1::par-2::gfp pRF4]* (Wallenfang and Seydoux 2000); TH25 *pddIs8[gfp::par-6(cDNA); unc-119(+)]* (Schonegg and Hyman 2006) (TH25, TH66, and JH1380 were provided by A. Hyman, Max Planck Institute for Molecular Cell Biology and Genetics, Dresden, Germany). N2 and JS604 were maintained at 20°C and GFP or YFP transgenic strains were maintained at 25°C to optimize transgene expression.

The JS604 strain was generated from the FX2395 strain containing *tlk-1(tm2395)* allele (Gengyo-Ando and Mitani 2000). *tm2395* contains a 678bp deletion from exon 5 to 6 and was detected using the primers 5'-GGATCCAATCAAGGATCACCGAAGAGG-3', 5'-

TCTCAAGTGCTCCCTGCGCAG-3', and 5'-CTCGAGTTACTTATCGATAAGTAATCGC-3'. Heterozygous *tm2395* was crossed in with *dpy17 unc32/++* males, and from heterozygous *tm2395/dpy17 unc32* recombinants were isolated, then backcrossed twice and balanced with *hT2[qIs48]*. Homozygous *tm2395* hermaphrodites are sterile, so the strain is maintained as heterozygotes. The strain was created by Tokiko Furuta.

Table 3: *C. elegans* strains used in this study

Name	Genotype
N2	wild-type
JS604	*dpy-17(e164) tlk-1(tm2395)* III/*hT2 [qIs48]* (I, III)
JS857	*dpy-17(e164) tlk-1(tm2385)* III/*hT2 [qIs48]* (I, III); *gfp::tba-21;mCherry::his-58*
SA164	*ltIs38 [pAA1; Ppie-1::gfp::PH$^{PLC\delta1}$ unc-119(+)] ddIs6[tbg-1::gfp::unc-119(+)]*
TH73	*unc-119(ed3)III; ddIs64[Ppie-1::yfp::let-99(genomic);unc-119(+)]*
RL238	*unc-22(e66) let-99(dd17); unc-119(ed3)III; ddIs64[Ppie-1::yfp::let-99(genomic);unc-119(+)]*
TH66	*unc-119(ed3); ddIs14[Ppie-1::ebp-2::gfp]*
JH1380	*axEx1094 [pMW1.03 Ppie-1::par-2::gfp pRF4]*
TH25	*pddIs8[gfp::par-6(cDNA); unc-119(+)]*

RNA interference

The feeding method of RNAi delivery was used to inhibit TLK-1 expression (Timmons and Fire 1998). L4440 vector alone or full-length *tlk-1* cDNA/L4440 constructs were transformed into HT115 (DE3) chemically competent *E. coli* bacteria, and grown in 5 mL LB media supplemented with 100 μg/μl ampicillin at 37°C with shaking overnight. These cultures were diluted 1:100 in 50 mL LB/amp and grown for six hours before being spread onto nematode growth (NG) plates supplemented with 100 μg/μl ampicillin and 20% β-lactose and placed at 25°C for 72 hours. The plates were then seeded with L4-stage hermaphrodites and incubated at

25°C for 24 hours (Arur et al. 2009). The L4440 RNAi vector alone was used as a control (*control(RNAi)*).

Live-cell imaging and quantification

For live-cell spinning disk confocal microscopy, embryos were dissected from control- and RNAi-treated *C. elegans* hermaphrodites into 10µl PBS on a 22mm^2 1.5 coverslip, placed onto a 2% agarose pad on a 22x40cm glass slide, and then sealed. Embryos were imaged using an Ultraview spinning disk confocal (Perkin Elmer, Waltham, MA) attached to a Nikon TE2000U inverted microscope. Images were acquired using an ORCA-ER digital camera (Hamamatsu, Bridgewater, NJ). A 60x 1.45 NA Plan Apo VC oil immersion lens was used for all experiments, except that a 60x 1.2 NA Plan Apo water immersion lens was used for imaging the centrosome tracking experiments (Figures 20 and 21). An additional 1.5x auxiliary magnification was used for imaging the TH32 strain. The confocal microscope and camera were controlled by Ultraview software (Perkin Elmer). Images were processed using Adobe Photoshop.

Chromosome Condensation Assay

Embryos from TH32 were subjected to live-cell spinning disk confocal microscopy as described above, using a 60x 1.45 NA Plan Apo VC oil immersion lens and additional 1.5x auxiliary magnification. Images were captured as 15 x 1 µm *z*-sections at 250 ms exposure over 10-second intervals through the first mitotic division and then exported using Ultraview (Perkin Elmer) as 16-bit raw projections of the *z*-plane. These images were then imported into MetaMorph and subjected to custom macros (provided by Dr. Paul Maddox, University of

Montreal, Montreal, Canada) to calculate the condensation parameter as previously described (Maddox et al. 2006). Data was exported to MS Excel for analysis, and kinetic plots of the condensation parameters were generated.

Spindle Rotation and Centrosome Positioning Measurements

For quantification of spindle movement and rotation and centrosome positions (Figures 14-19), images were captured as 15 x 1 μm *z*-sections at 250 ms exposure over 10-second intervals through the first mitotic division. The Angle Tool in ImageJ was used to measure the angle between the centrosomes and the anteroposterior axis over time. The Line Tool was used to measure the distance of each centrosome to a single point on the posterior end of the embryo. Data were exported from ImageJ and kymographs, standard error of the means (SEM), and significance were generated in MS Excel. For TH25 (GFP::PAR-6), images were captured as 15 x 1 μm *z*-sections at 250 ms exposure over 10-second intervals; for JH1380 (GFP::PAR-2), images were captured as 7 x 1 μm *z*-sections at 800 ms exposure over 10-second intervals. For RL238 (*let-99(dd17)*;YFP::LET-99), images were captured as 5 x 1μm *z*-sections at 350 ms exposure over 10-second intervals. All live-cell spinning disk confocal experiments utilized 2 x 2 binning.

Centrosome Tracking

For the centrosome tracking experiment in Figures 20 and 21, SA164 embryos were prepared and mounted as above. To capture the entire embryo, 36 x 1 μm *z*-sections were imaged at 150 ms exposure over 10-second intervals. Acquisitions from each time-point and *z*-slice were exported as 16-bit raw TIFF images in Ultraview software (Perkin Elmer) and imported into

Imaris (Bitplane) as a time-lapse series. Embryos were oriented spatially so that the anterior was always to the left and spindle rotation occurred in a counter-clockwise manner. To view the image series in four-dimensions, the voxel size based on acquisition (0.226 μm x 0.226 μm x 1.0 μm) was entered into Imaris, and embryos were cropped to be the same size as one another. The bottom leftmost (*x,y,z*) position of each cropped embryo in the workspace was normalized to (0,0,0). Isosurfaces were built over the ellipsoid centrosome pairs of each embryo and their paths were traced over time using the Surface and Track tools, respectively. Centrosome isosurfaces and tracks from *control* and *tlk-1(RNAi)* embryos were exported as Matlab objects using the Object Manager interface and then their paths overlayed in a single *control* or *tlk-1(RNAi)* embryo for comparison. Anterior and posterior tracks were parsed separately using the Track Duration module.

Immunostaining and image acquisition

TH73 (YFP::LET-99) L4 hermaphrodites were seeded onto *control* or *tlk-1(RNAi)* plates and incubated at 25°C for 24 hours. The following day, nematodes were picked onto a 10 μL spot of egg buffer on a Poly-L-Lysine coated glass slide (Sigma, St Louis, MO). A 22x40 mm coverslip was placed over the animals and light pressure was applied to free the embryos from the hermaphrodites. Slides were placed on an aluminum sheet over dry ice for 60 minutes, and coverslips were snapped off to crack the embryo cuticle. Specimens were then fixed briefly in -20°C methanol followed by paraformaldehyde, as described previously (Seydoux and Dunn 1997) and then washed in PBS with 0.1% Triton and 0.1% BSA (PBSTb). Samples were incubated overnight with primary antibody diluted in PBSTb at 4°C (anti-GFP [1:100] (rabbit polyclonal, Invitrogen, Eugene, OR) and anti-α-tubulin [1:1,000] (mouse monoclonal DM1α,

Sigma). Samples were then washed with PBSTb and secondary antibodies were applied (goat-anti-mouse IgG AlexaFluor 488 [1:1,000] and goat-anti-rabbit IgG AlexaFluor 555 [1:1,000] (Invitrogen) for 60 minutes at 25°C. Specimens were washed and then mounted in Prolong Gold with DAPI (Invitrogen). Immunofluorescent images were acquired on a Nikon 2000U inverted microscope equipped with a Photometrics Coolsnap HQ camera controlled by Metamorph software using a 60x 1.49NA Plan Apo oil immersion objective.

YFP::LET-99 quantitation

Images from fixed TH73 embryos were acquired on a Nikon 2000U inverted microscope equipped with a Photometrics Coolsnap HQ camera with all functions controlled by Metamorph software. For all TH73 embryos, three channel images were acquired as 11 z-sections at 0.2-µm steps centered at a mid-embryo focal plane with a 60x 1.2 NA water immersion objective. For quantification of YFP::LET-99, all images were acquired on the same day using the same below-saturation exposure parameters. All *z*-stacks were imported into Autodeblur (Autoquant Media Cybernetics, Bethesda MD) and deconvolved for 10 iterations. Raw deconvolved files were then imported into Metamorph, and sum projections of all 11 *z*-planes were created using the Stack Arithmetic function. Projected 16-bit images were then aligned along the anteroposterior axis using the polar body as a landmark for the anterior.

Metamorph software was used to quantify YFP::LET-99 cortical fluorescence intensity as previously described (Bringmann et al. 2007). Manually-drawn region-of-interests were traced along both the upper and lower cortices of each embryo, starting at the anterior pole and ending at the posterior pole (the polar body was excluded). A linescan width of nine pixels was produced and the maximum intensity was measured for all points in the ROI, with the first

point at 0% and the last point at 100% embryonic length (%EL). Maximum intensity profiles for all embryo cortices were exported to MS Excel. For both *control* and *tlk-1(RNAi)* conditions, the upper and lower cortical measurements corresponding to the same %EL of each embryo were averaged together and plotted along with their respective SEM for each data point. The data were then normalized with the maximum raw intensity set to 1.0 and the minimum raw intensity set to 0.0 using the formula $x_{norm} = (x_i - X_{min}) / (X_{max} - X_{min})$; SEMs were normalized by dividing by the maximum raw intensity of the data set. For Figures 24 and 25 [fixed-cell quantitation of YFP::LET-99 at PNM], nine *control* (18 cortices) and eight *tlk-1(RNAi)* embryos (16 cortices) were averaged; for Figures 26 and 27 (rotation-NEBD) five embryos (ten cortices) of each condition were averaged. The average YFP::LET-99 intensities from all cortices are shown ± SEM.

To quantitate the number of astral microtubules within close proximity of the cell cortex in *control* and *tlk-1(RNAi)* embryos, the λ:488 nm metadata (corresponding to the α-tubulin signal) from the TH73 image acquisition used in Figures 26 and 27 described above were imported into Metamorph. Two regions-of-interest (RoI) were drawn at 1 μm and 2 μm away from the cell cortex throughout and within the embryos, and the histogram/LUT for each embryo was adjusted manually so that microtubules could be reliably visualized. Microtubules crossing the 1 μm or 2μm RoI were manually counted and scored depending on from which centrosome they had clearly emanated. Data were entered into MS Excel for graphing and statistical analysis.

GFP::EBP-2 imaging and tracking

To image GFP::EBP-2, embryos were prepared and mounted as above, and imaged via spinning disk confocal microscopy using a 60x 1.45NA Plan Apo oil immersion lens. Embryos were exposed to 488 wavelength for 400 ms at a single focal plane during the first mitotic division. Videos of the acquisitions were produced in Ultraview as AVIs and imported into ImageJ for analysis. The MOSAIC particle tracker (ETH, Zurich) (Sbalzarini and Koumoutsakos 2005) was used to detect GFP::EBP-2 comets and then divided into 40 second intervals relative to NEBD for analysis. Maximum *z*-projections of GFP::EBP-2 comets over 100 frames (40s) were generated in ImageJ.

BIBLIOGRAPHY

Adams RR, Carmena M, Earnshaw WC. 2001. Chromosomal passengers and the (aurora) ABCs of mitosis. Trends in cell biology 11(2):49-54.

Ahringer J, Kimble J. 1991. Control of the sperm-oocyte switch in Caenorhabditis elegans hermaphrodites by the fem-3 3' untranslated region. Nature 349(6307):346-348.

Albertson DG. 1984. Formation of the first cleavage spindle in nematode embryos. Dev Biol 101(1):61-72.

Albertson DG, Rose AM, Villeneuve AM. 1997. Chromosome Organization, Mitosis, and Meiosis. In: Riddle DL, Blumenthal T, Meyer BJ, Priess JR, editors. C elegans II. 2nd ed. Cold Spring Harbor (NY).

Alexandru G, Uhlmann F, Mechtler K, Poupart MA, Nasmyth K. 2001. Phosphorylation of the cohesin subunit Scc1 by Polo/Cdc5 kinase regulates sister chromatid separation in yeast. Cell 105(4):459-472.

Altun ZFaH, D. H. 2002-2006. WormAtlas.

Andrews PD. 2005. Aurora kinases: shining lights on the therapeutic horizon? Oncogene 24(32):5005-5015.

Arur S, Ohmachi M, Berkseth M, Nayak S, Hansen D, Zarkower D, Schedl T. 2011. MPK-1 ERK controls membrane organization in C. elegans oogenesis via a sex-determination module. Developmental cell 20(5):677-688.

Arur S, Ohmachi M, Nayak S, Hayes M, Miranda A, Hay A, Golden A, Schedl T. 2009. Multiple ERK substrates execute single biological processes in Caenorhabditis elegans

germ-line development. Proceedings of the National Academy of Sciences of the United States of America 106(12):4776-4781.

Bachorik JL, Kimble J. 2005. Redundant control of the Caenorhabditis elegans sperm/oocyte switch by PUF-8 and FBF-1, two distinct PUF RNA-binding proteins. Proceedings of the National Academy of Sciences of the United States of America 102(31):10893-10897.

Barr FA, Sillje HH, Nigg EA. 2004. Polo-like kinases and the orchestration of cell division. Nat Rev Mol Cell Biol 5(6):429-440.

Basto R, Brunk K, Vinadogrova T, Peel N, Franz A, Khodjakov A, Raff JW. 2008. Centrosome amplification can initiate tumorigenesis in flies. Cell 133(6):1032-1042.

Basto R, Lau J, Vinogradova T, Gardiol A, Woods CG, Khodjakov A, Raff JW. 2006. Flies without centrioles. Cell 125(7):1375-1386.

Beitel GJ, Clark SG, Horvitz HR. 1990. Caenorhabditis elegans ras gene let-60 acts as a switch in the pathway of vulval induction. Nature 348(6301):503-509.

Berger SL, Kouzarides T, Shiekhattar R, Shilatifard A. 2009. An operational definition of epigenetics. Genes & development 23(7):781-783.

Betschinger J, Knoblich JA. 2004. Dare to be different: asymmetric cell division in Drosophila, C. elegans and vertebrates. Current biology : CB 14(16):R674-685.

Bishop JD, Schumacher JM. 2002. Phosphorylation of the carboxyl terminus of inner centromere protein (INCENP) by the Aurora B Kinase stimulates Aurora B kinase activity. J Biol Chem 277(31):27577-27580.

Bond J, Roberts E, Mochida GH, Hampshire DJ, Scott S, Askham JM, Springell K, Mahadevan M, Crow YJ, Markham AF, Walsh CA, Woods CG. 2002. ASPM is a major determinant of cerebral cortical size. Nature genetics 32(2):316-320.

Boxem M, Srinivasan DG, van den Heuvel S. 1999. The Caenorhabditis elegans gene ncc-1 encodes a cdc2-related kinase required for M phase in meiotic and mitotic cell divisions, but not for S phase. Development 126(10):2227-2239.

Boxem M, van den Heuvel S. 2001. lin-35 Rb and cki-1 Cip/Kip cooperate in developmental regulation of G1 progression in C. elegans. Development 128(21):4349-4359.

Brenner S. 1974. The genetics of Caenorhabditis elegans. Genetics 77(1):71-94.

Bringmann H, Cowan CR, Kong J, Hyman AA. 2007. LET-99, GOA-1/GPA-16, and GPR-1/2 are required for aster-positioned cytokinesis. Current biology : CB 17(2):185-191.

Budirahardja Y, Gonczy P. 2008. PLK-1 asymmetry contributes to asynchronous cell division of C. elegans embryos. Development 135(7):1303-1313.

Burrows AE, Sceurman BK, Kosinski ME, Richie CT, Sadler PL, Schumacher JM, Golden A. 2006. The C. elegans Myt1 ortholog is required for the proper timing of oocyte maturation. Development 133(4):697-709.

Carmena M, Earnshaw WC. 2003. The cellular geography of aurora kinases. Nature reviews Molecular cell biology 4(11):842-854.

Carrera P, Moshkin YM, Gronke S, Sillje HH, Nigg EA, Jackle H, Karch F. 2003. Tousled-like kinase functions with the chromatin assembly pathway regulating nuclear divisions. Genes Dev 17(20):2578-2590.

Castellanos E, Dominguez P, Gonzalez C. 2008. Centrosome dysfunction in Drosophila neural stem cells causes tumors that are not due to genome instability. Current biology : CB 18(16):1209-1214.

Chan CS, Botstein D. 1993. Isolation and characterization of chromosome-gain and increase-in-ploidy mutants in yeast. Genetics 135(3):677-691.

Chase D, Serafinas C, Ashcroft N, Kosinski M, Longo D, Ferris DK, Golden A. 2000. The polo-like kinase PLK-1 is required for nuclear envelope breakdown and the completion of meiosis in Caenorhabditis elegans. Genesis 26(1):26-41.

Cheeseman IM, Desai A. 2008. Molecular architecture of the kinetochore-microtubule interface. Nat Rev Mol Cell Biol 9(1):33-46.

Cheeseman IM, MacLeod I, Yates JR, 3rd, Oegema K, Desai A. 2005. The CENP-F-like proteins HCP-1 and HCP-2 target CLASP to kinetochores to mediate chromosome segregation. Curr Biol 15(8):771-777.

Cheeseman IM, Niessen S, Anderson S, Hyndman F, Yates JR, 3rd, Oegema K, Desai A. 2004. A conserved protein network controls assembly of the outer kinetochore and its ability to sustain tension. Genes Dev 18(18):2255-2268.

Cheng NN, Kirby CM, Kemphues KJ. 1995. Control of cleavage spindle orientation in Caenorhabditis elegans: the role of the genes par-2 and par-3. Genetics 139(2):549-559.

Church DL, Guan KL, Lambie EJ. 1995. Three genes of the MAP kinase cascade, mek-2, mpk-1/sur-1 and let-60 ras, are required for meiotic cell cycle progression in Caenorhabditis elegans. Development 121(8):2525-2535.

Cockell MM, Baumer K, Gonczy P. 2004. lis-1 is required for dynein-dependent cell division processes in C. elegans embryos. J Cell Sci 117(Pt 19):4571-4582.

Coleman TR, Dunphy WG. 1994. Cdc2 regulatory factors. Current opinion in cell biology 6(6):877-882.

Colombo K, Grill SW, Kimple RJ, Willard FS, Siderovski DP, Gonczy P. 2003. Translation of polarity cues into asymmetric spindle positioning in Caenorhabditis elegans embryos. Science 300(5627):1957-1961.

Cowan CR, Hyman AA. 2004. Centrosomes direct cell polarity independently of microtubule assembly in C. elegans embryos. Nature 431(7004):92-96.

Crittenden SL, Bernstein DS, Bachorik JL, Thompson BE, Gallegos M, Petcherski AG, Moulder G, Barstead R, Wickens M, Kimble J. 2002. A conserved RNA-binding protein controls germline stem cells in Caenorhabditis elegans. Nature 417(6889):660-663.

Csankovszki G, Collette K, Spahl K, Carey J, Snyder M, Petty E, Patel U, Tabuchi T, Liu H, McLeod I, Thompson J, Sarkeshik A, Yates J, Meyer BJ, Hagstrom K. 2009. Three distinct condensin complexes control C. elegans chromosome dynamics. Curr Biol 19(1):9-19.

Cuenca AA, Schetter A, Aceto D, Kemphues K, Seydoux G. 2003. Polarization of the C. elegans zygote proceeds via distinct establishment and maintenance phases. Development 130(7):1255-1265.

De Benedetti A. 2010. Tousled kinase TLK1B mediates chromatin assembly in conjunction with Asf1 regardless of its kinase activity. BMC Res Notes 3:68.

Dernburg AF. 2001. Here, there, and everywhere: kinetochore function on holocentric chromosomes. J Cell Biol 153(6):F33-38.

Desai A, Mitchison TJ. 1997. Microtubule polymerization dynamics. Annual review of cell and developmental biology 13:83-117.

Deyter GM, Furuta T, Kurasawa Y, Schumacher JM. 2010. Caenorhabditis elegans cyclin B3 is required for multiple mitotic processes including alleviation of a spindle checkpoint-dependent block in anaphase chromosome segregation. PLoS Genet 6(11):e1001218.

Eckmann CR, Crittenden SL, Suh N, Kimble J. 2004. GLD-3 and control of the mitosis/meiosis decision in the germline of Caenorhabditis elegans. Genetics 168(1):147-160.

Ehsan H, Reichheld JP, Durfee T, Roe JL. 2004. TOUSLED kinase activity oscillates during the cell cycle and interacts with chromatin regulators. Plant Physiol 134(4):1488-1499.

Eitoku M, Sato L, Senda T, Horikoshi M. 2008. Histone chaperones: 30 years from isolation to elucidation of the mechanisms of nucleosome assembly and disassembly. Cellular and molecular life sciences : CMLS 65(3):414-444.

Emanuele MJ, Lan W, Jwa M, Miller SA, Chan CS, Stukenberg PT. 2008. Aurora B kinase and protein phosphatase 1 have opposing roles in modulating kinetochore assembly. The Journal of cell biology 181(2):241-254.

Encalada SE, Willis J, Lyczak R, Bowerman B. 2005. A spindle checkpoint functions during mitosis in the early Caenorhabditis elegans embryo. Mol Biol Cell 16(3):1056-1070.

Espiritu EB, Krueger LE, Ye A, Rose LS. 2012. CLASPs function redundantly to regulate astral microtubules in the C. elegans embryo. Developmental biology.

Flowers A, Chu QD, Panu L, Meschonat C, Caldito G, Lowery-Nordberg M, Li BD. 2009. Eukaryotic initiation factor 4E overexpression in triple-negative breast cancer predicts a worse outcome. Surgery 146(2):220-226.

Ford JR. 2009. Identifying the role of the Tousled-like kinase during the cell cycle. UT GSBS Dissertations and Theses:112.

Ford JR, Schumacher JM. 2009. Chromosome dynamics: the case of the missing condensin. Curr Biol 19(3):R127-129.

Fraser AG, James C, Evan GI, Hengartner MO. 1999. Caenorhabditis elegans inhibitor of apoptosis protein (IAP) homologue BIR-1 plays a conserved role in cytokinesis. Curr Biol 9(6):292-301.

Frokjaer-Jensen C, Davis MW, Hopkins CE, Newman BJ, Thummel JM, Olesen SP, Grunnet M, Jorgensen EM. 2008. Single-copy insertion of transgenes in Caenorhabditis elegans. Nat Genet 40(11):1375-1383.

Fuller BG, Lampson MA, Foley EA, Rosasco-Nitcher S, Le KV, Tobelmann P, Brautigan DL, Stukenberg PT, Kapoor TM. 2008. Midzone activation of aurora B in anaphase produces an intracellular phosphorylation gradient. Nature 453(7198):1132-1136.

Furuta T, Baillie DL, Schumacher JM (Caenorhabditis elegans Aurora A kinase AIR-1 is required for postembryonic cell divisions and germline development. Genesis 34:244-250.2002).

Galli M, van den Heuvel S. 2008. Determination of the cleavage plane in early C. elegans embryos. Annual review of genetics 42:389-411.

Garner EC, Campbell CS, Mullins RD. 2004. Dynamic instability in a DNA-segregating prokaryotic actin homolog. Science 306(5698):1021-1025.

Gassmann R, Vagnarelli P, Hudson D, Earnshaw WC. 2004. Mitotic chromosome formation and the condensin paradox. Exp Cell Res 296(1):35-42.

Gengyo-Ando K, Mitani S. 2000. Characterization of mutations induced by ethyl methanesulfonate, UV, and trimethylpsoralen in the nematode Caenorhabditis elegans. Biochemical and biophysical research communications 269(1):64-69.

Giet R, Prigent C. 2000. The Xenopus laevis aurora/Ip11p-related kinase pEg2 participates in the stability of the bipolar mitotic spindle. Exp Cell Res 258(1):145-151.

Glotzer M. 2005. The molecular requirements for cytokinesis. Science 307(5716):1735-1739.

Glover DM, Leibowitz MH, McLean DA, Parry H. 1995. Mutations in aurora prevent centrosome separation leading to the formation of monopolar spindles. Cell 81(1):95-105.

Golan A, Yudkovsky Y, Hershko A. 2002. The cyclin-ubiquitin ligase activity of cyclosome/APC is jointly activated by protein kinases Cdk1-cyclin B and Plk. J Biol Chem 277(18):15552-15557.

Goldstein B, Hird SN. 1996. Specification of the anteroposterior axis in Caenorhabditis elegans. Development 122(5):1467-1474.

Goldstein B, Hird SN, White JG. 1993. Cell polarity in early C. elegans development. Development:279-287.

Goldstein P. 1982. The synaptonemal complexes of Caenorhabditis elegans: pachytene karyotype analysis of male and hermaphrodite wild-type and him mutants. Chromosoma 86(4):577-593.

Goldstein P, Slaton DE. 1982. The synaptonemal complexes of caenorhabditis elegans: comparison of wild-type and mutant strains and pachytene karyotype analysis of wild-type. Chromosoma 84(4):585-597.

Gonczy P. 2008. Mechanisms of asymmetric cell division: flies and worms pave the way. Nature reviews Molecular cell biology 9(5):355-366.

Gonczy P, Echeverri C, Oegema K, Coulson A, Jones SJ, Copley RR, Duperon J, Oegema J, Brehm M, Cassin E, Hannak E, Kirkham M, Pichler S, Flohrs K, Goessen A, Leidel S, Alleaume AM, Martin C, Ozlu N, Bork P, Hyman AA. 2000. Functional genomic analysis of cell division in C. elegans using RNAi of genes on chromosome III. Nature 408(6810):331-336.

Gonczy P, Pichler S, Kirkham M, Hyman AA. 1999. Cytoplasmic dynein is required for distinct aspects of MTOC positioning, including centrosome separation, in the one cell stage Caenorhabditis elegans embryo. The Journal of cell biology 147(1):135-150.

Gonczy P, Rose LS. 2005. Asymmetric cell division and axis formation in the embryo. WormBook : the online review of C elegans biology:1-20.

Goto H, Kiyono T, Tomono Y, Kawajiri A, Urano T, Furukawa K, Nigg EA, Inagaki M. 2006. Complex formation of Plk1 and INCENP required for metaphase-anaphase transition. Nature cell biology 8(2):180-187.

Gotta M, Ahringer J. 2001. Distinct roles for Galpha and Gbetagamma in regulating spindle position and orientation in Caenorhabditis elegans embryos. Nature cell biology 3(3):297-300.

Gotta M, Dong Y, Peterson YK, Lanier SM, Ahringer J. 2003. Asymmetrically distributed C. elegans homologs of AGS3/PINS control spindle position in the early embryo. Current biology : CB 13(12):1029-1037.

Goulding MB, Canman JC, Senning EN, Marcus AH, Bowerman B. 2007. Control of nuclear centration in the C. elegans zygote by receptor-independent Galpha signaling and myosin II. The Journal of cell biology 178(7):1177-1191.

Green RA, Kao HL, Audhya A, Arur S, Mayers JR, Fridolfsson HN, Schulman M, Schloissnig S, Niessen S, Laband K, Wang S, Starr DA, Hyman AA, Schedl T, Desai A, Piano F, Gunsalus KC, Oegema K. 2011. A high-resolution C. elegans essential gene network based on phenotypic profiling of a complex tissue. Cell 145(3):470-482.

Greenstein D. 2005. Control of oocyte meiotic maturation and fertilization. WormBook:1-12.

Grill SW, Gonczy P, Stelzer EH, Hyman AA. 2001. Polarity controls forces governing asymmetric spindle positioning in the Caenorhabditis elegans embryo. Nature 409(6820):630-633.

Groth A, Lukas J, Nigg EA, Sillje HH, Wernstedt C, Bartek J, Hansen K. 2003. Human Tousled like kinases are targeted by an ATM- and Chk1-dependent DNA damage checkpoint. The EMBO journal 22(7):1676-1687.

Hagan IM, Jones N, Carr AM. 2001. New insights into development from mitosis of a unicellular yeast. Dev Cell 1(2):158-160.

Hagstrom KA, Holmes VF, Cozzarelli NR, Meyer BJ. 2002. C. elegans condensin promotes mitotic chromosome architecture, centromere organization, and sister chromatid segregation during mitosis and meiosis. Genes & development 16(6):729-742.

Hamill DR, Severson AF, Carter JC, Bowerman B. 2002. Centrosome maturation and mitotic spindle assembly in C. elegans require SPD-5, a protein with multiple coiled-coil domains. Dev Cell 3(5):673-684.

Han Z, Riefler GM, Saam JR, Mango SE, Schumacher JM. 2005. The C. elegans Tousled-like kinase contributes to chromosome segregation as a substrate and regulator of the Aurora B kinase. Current biology : CB 15(10):894-904.

Han Z, Saam JR, Adams HP, Mango SE, Schumacher JM. 2003. The C. elegans Tousled-like kinase (TLK-1) has an essential role in transcription. Curr Biol 13(22):1921-1929.

Hannak E, Kirkham M, Hyman AA, Oegema K. 2001. Aurora-A kinase is required for centrosome maturation in Caenorhabditis elegans. J Cell Biol 155(7):1109-1116.

Hannak E, Oegema K, Kirkham M, Gonczy P, Habermann B, Hyman AA. 2002. The kinetically dominant assembly pathway for centrosomal asters in Caenorhabditis elegans is gamma-tubulin dependent. J Cell Biol 157(4):591-602.

Hansen D, Hubbard EJ, Schedl T. 2004a. Multi-pathway control of the proliferation versus meiotic development decision in the Caenorhabditis elegans germline. Developmental biology 268(2):342-357.

Hansen D, Wilson-Berry L, Dang T, Schedl T. 2004b. Control of the proliferation versus meiotic development decision in the C. elegans germline through regulation of GLD-1 protein accumulation. Development 131(1):93-104.

Hashimoto M, Matsui T, Iwabuchi K, Date T. 2008. PKU-beta/TLK1 regulates myosin II activities, and is required for accurate equaled chromosome segregation. Mutation research 657(1):63-67.

Hauf S, Waizenegger IC, Peters JM. 2001. Cohesin cleavage by separase required for anaphase and cytokinesis in human cells. Science 293(5533):1320-1323.

Heallen TR, Adams HP, Furuta T, Verbrugghe KJ, Schumacher JM. 2008. An Afg2/Spaf-related Cdc48-like AAA ATPase regulates the stability and activity of the C. elegans Aurora B kinase AIR-2. Dev Cell 15(4):603-616.

Hillier LW, Coulson A, Murray JI, Bao Z, Sulston JE, Waterston RH. 2005. Genomics in C. elegans: so many genes, such a little worm. Genome Res 15(12):1651-1660.

Hirano T. 2005. Condensins: organizing and segregating the genome. Curr Biol 15(7):R265-275.

Hird SN, White JG. 1993. Cortical and cytoplasmic flow polarity in early embryonic cells of Caenorhabditis elegans. The Journal of cell biology 121(6):1343-1355.

Hirota T, Kunitoku N, Sasayama T, Marumoto T, Zhang D, Nitta M, Hatakeyama K, Saya H. 2003. Aurora-A and an interacting activator, the LIM protein Ajuba, are required for mitotic commitment in human cells. Cell 114(5):585-598.

Honda R, Korner R, Nigg EA. 2003. Exploring the functional interactions between Aurora B, INCENP, and survivin in mitosis. Mol Biol Cell 14(8):3325-3341.

Howard J. 2001. Mechanics of Motor Proteins and the Cytoskeleton. Trends in cell biology 11(11):452-453.

Hsu JY, Sun ZW, Li X, Reuben M, Tatchell K, Bishop DK, Grushcow JM, Brame CJ, Caldwell JA, Hunt DF, Lin R, Smith MM, Allis CD. 2000. Mitotic phosphorylation of histone H3 is governed by Ipl1/aurora kinase and Glc7/PP1 phosphatase in budding yeast and nematodes. Cell 102(3):279-291.

Hsu V, Zobel CL, Lambie EJ, Schedl T, Kornfeld K. 2002. Caenorhabditis elegans lin-45 raf is essential for larval viability, fertility and the induction of vulval cell fates. Genetics 160(2):481-492.

Hubbard EJ, Greenstein D. 2005. Introduction to the germ line. WormBook : the online review of C elegans biology:1-4.

Hutchins JR, Toyoda Y, Hegemann B, Poser I, Heriche JK, Sykora MM, Augsburg M, Hudecz O, Buschhorn BA, Bulkescher J, Conrad C, Comartin D, Schleiffer A, Sarov M, Pozniakovsky A, Slabicki MM, Schloissnig S, Steinmacher I, Leuschner M, Ssykor A, Lawo S, Pelletier L, Stark H, Nasmyth K, Ellenberg J, Durbin R, Buchholz F, Mechtler K, Hyman AA, Peters JM. 2010. Systematic analysis of human protein complexes identifies chromosome segregation proteins. Science 328(5978):593-599.

Hyman AA, White JG. 1987. Determination of cell division axes in the early embryogenesis of Caenorhabditis elegans. The Journal of cell biology 105(5):2123-2135.

Jackman M, Lindon C, Nigg EA, Pines J. 2003. Active cyclin B1-Cdk1 first appears on centrosomes in prophase. Nat Cell Biol 5(2):143-148.

Jaensch S, Decker M, Hyman AA, Myers EW. 2010. Automated tracking and analysis of centrosomes in early Caenorhabditis elegans embryos. Bioinformatics 26(12):i13-20.

Jantsch-Plunger V, Gonczy P, Romano A, Schnabel H, Hamill D, Schnabel R, Hyman AA, Glotzer M. 2000. CYK-4: A Rho family gtpase activating protein (GAP) required for central spindle formation and cytokinesis. J Cell Biol 149(7):1391-1404.

Jelluma N, Brenkman AB, van den Broek NJ, Cruijsen CW, van Osch MH, Lens SM, Medema RH, Kops GJ. 2008. Mps1 phosphorylates Borealin to control Aurora B activity and chromosome alignment. Cell 132(2):233-246.

Jorgensen EM, Mango SE. 2002. The art and design of genetic screens: caenorhabditis elegans. Nature reviews Genetics 3(5):356-369.

Kadyk LC, Kimble J. 1998. Genetic regulation of entry into meiosis in Caenorhabditis elegans. Development 125(10):1803-1813.

Kaitna S, Mendoza M, Jantsch-Plunger V, Glotzer M. 2000. Incenp and an aurora-like kinase form a complex essential for chromosome segregation and efficient completion of cytokinesis. Curr Biol 10(19):1172-1181.

Karashima T, Sugimoto A, Yamamoto M. 2000. Caenorhabditis elegans homologue of the human azoospermia factor DAZ is required for oogenesis but not for spermatogenesis. Development 127(5):1069-1079.

Kelly AE, Sampath SC, Maniar TA, Woo EM, Chait BT, Funabiki H. 2007. Chromosomal enrichment and activation of the aurora B pathway are coupled to spatially regulate spindle assembly. Developmental cell 12(1):31-43.

Kemp CA, Kopish KR, Zipperlen P, Ahringer J, O'Connell KF. 2004. Centrosome maturation and duplication in C. elegans require the coiled-coil protein SPD-2. Dev Cell 6(4):511-523.

Kemphues KJ, Priess JR, Morton DG, Cheng NS. 1988. Identification of genes required for cytoplasmic localization in early C. elegans embryos. Cell 52(3):311-320.

Kemphues KJ, Strome S. 1997. Fertilization and Establishment of Polarity in the Embryo. In: Riddle DL, Blumenthal T, Meyer BJ, Priess JR, editors. C elegans II. 2nd ed. Cold Spring Harbor (NY).

Kimura A, Onami S. 2005. Computer simulations and image processing reveal length-dependent pulling force as the primary mechanism for C. elegans male pronuclear migration. Dev Cell 8(5):765-775.

Kipreos ET. 2005. C. elegans cell cycles: invariance and stem cell divisions. Nat Rev Mol Cell Biol 6(10):766-776.

Kitada K, Johnson AL, Johnston LH, Sugino A. 1993. A multicopy suppressor gene of the Saccharomyces cerevisiae G1 cell cycle mutant gene dbf4 encodes a protein kinase and is identified as CDC5. Molecular and cellular biology 13(7):4445-4457.

Kitagawa R. 2009. Key players in chromosome segregation in Caenorhabditis elegans. Front Biosci 14:1529-1557.

Kodym R, Henockl C, Furweger C. 2005. Identification of the human DEAD-box protein p68 as a substrate of Tlk1. Biochemical and biophysical research communications 333(2):411-417.

Kotani S, Tanaka H, Yasuda H, Todokoro K. 1999. Regulation of APC activity by phosphorylation and regulatory factors. J Cell Biol 146(4):791-800.

Kotani S, Tugendreich S, Fujii M, Jorgensen PM, Watanabe N, Hoog C, Hieter P, Todokoro K. 1998. PKA and MPF-activated polo-like kinase regulate anaphase-promoting complex activity and mitosis progression. Mol Cell 1(3):371-380.

Kraemer B, Crittenden S, Gallegos M, Moulder G, Barstead R, Kimble J, Wickens M. 1999. NANOS-3 and FBF proteins physically interact to control the sperm-oocyte switch in Caenorhabditis elegans. Current biology : CB 9(18):1009-1018.

Kraft C, Herzog F, Gieffers C, Mechtler K, Hagting A, Pines J, Peters JM. 2003. Mitotic regulation of the human anaphase-promoting complex by phosphorylation. EMBO J 22(24):6598-6609.

Krause DR, Jonnalagadda JC, Gatei MH, Sillje HH, Zhou BB, Nigg EA, Khanna K. 2003. Suppression of Tousled-like kinase activity after DNA damage or replication block requires ATM, NBS1 and Chk1. Oncogene 22(38):5927-5937.

Krueger LE, Wu JC, Tsou MF, Rose LS. 2010. LET-99 inhibits lateral posterior pulling forces during asymmetric spindle elongation in C. elegans embryos. The Journal of cell biology 189(3):481-495.

Kumar A, Girimaji SC, Duvvari MR, Blanton SH. 2009. Mutations in STIL, encoding a pericentriolar and centrosomal protein, cause primary microcephaly. American journal of human genetics 84(2):286-290.

Kuwabara PE. 1998. Gametogenesis: keeping the male element under control. Current biology : CB 8(8):R278-281.

Labbe JC, McCarthy EK, Goldstein B. 2004. The forces that position a mitotic spindle asymmetrically are tethered until after the time of spindle assembly. J Cell Biol 167(2):245-256.

Lewellyn L, Carvalho A, Desai A, Maddox AS, Oegema K. 2011. The chromosomal passenger complex and centralspindlin independently contribute to contractile ring assembly. The Journal of cell biology 193(1):155-169.

Li HH, Chiang CS, Huang HY, Liaw GJ. 2009. mars and tousled-like kinase act in parallel to ensure chromosome fidelity in Drosophila. J Biomed Sci 16:51.

Li Y, DeFatta R, Anthony C, Sunavala G, De Benedetti A. 2001. A translationally regulated Tousled kinase phosphorylates histone H3 and confers radioresistance when overexpressed. Oncogene 20(6):726-738.

Li Z, Gourguechon S, Wang CC. 2007. Tousled-like kinase in a microbial eukaryote regulates spindle assembly and S-phase progression by interacting with Aurora kinase and chromatin assembly factors. J Cell Sci 120(Pt 21):3883-3894.

Lindon C, Pines J. 2004. Ordered proteolysis in anaphase inactivates Plk1 to contribute to proper mitotic exit in human cells. The Journal of cell biology 164(2):233-241.

Lingle WL, Barrett SL, Negron VC, D'Assoro AB, Boeneman K, Liu W, Whitehead CM, Reynolds C, Salisbury JL. 2002. Centrosome amplification drives chromosomal instability in breast tumor development. Proceedings of the National Academy of Sciences of the United States of America 99(4):1978-1983.

Liu D, Vader G, Vromans MJ, Lampson MA, Lens SM. 2009. Sensing chromosome bi-orientation by spatial separation of aurora B kinase from kinetochore substrates. Science 323(5919):1350-1353.

Llamazares S, Moreira A, Tavares A, Girdham C, Spruce BA, Gonzalez C, Karess RE, Glover DM, Sunkel CE. 1991. polo encodes a protein kinase homolog required for mitosis in Drosophila. Genes Dev 5(12A):2153-2165.

Maddox PS, Oegema K, Desai A, Cheeseman IM. 2004. "Holo"er than thou: chromosome segregation and kinetochore function in C. elegans. Chromosome Res 12(6):641-653.

Maddox PS, Portier N, Desai A, Oegema K. 2006. Molecular analysis of mitotic chromosome condensation using a quantitative time-resolved fluorescence microscopy assay. Proc Natl Acad Sci U S A 103(41):15097-15102.

Malone CJ, Misner L, Le Bot N, Tsai MC, Campbell JM, Ahringer J, White JG. 2003. The C. elegans hook protein, ZYG-12, mediates the essential attachment between the centrosome and nucleus. Cell 115(7):825-836.

Malumbres M, Barbacid M. 2009. Cell cycle, CDKs and cancer: a changing paradigm. Nat Rev Cancer 9(3):153-166.

Margueron R, Reinberg D. 2010. Chromatin structure and the inheritance of epigenetic information. Nature reviews Genetics 11(4):285-296.

Mishima M, Kaitna S, Glotzer M. 2002. Central spindle assembly and cytokinesis require a kinesin-like protein/RhoGAP complex with microtubule bundling activity. Dev Cell 2(1):41-54.

Mito Y, Sugimoto A, Yamamoto M. 2003. Distinct developmental function of two Caenorhabditis elegans homologs of the cohesin subunit Scc1/Rad21. Molecular biology of the cell 14(6):2399-2409.

Morgan DO. 1997. Cyclin-dependent kinases: engines, clocks, and microprocessors. Annu Rev Cell Dev Biol 13:261-291.

Musacchio A, Salmon ED. 2007. The spindle-assembly checkpoint in space and time. Nat Rev Mol Cell Biol 8(5):379-393.

Nasmyth K, Haering CH. 2005. The structure and function of SMC and kleisin complexes. Annu Rev Biochem 74:595-648.

Nayak S, Santiago FE, Jin H, Lin D, Schedl T, Kipreos ET. 2002. The Caenorhabditis elegans Skp1-related gene family: diverse functions in cell proliferation, morphogenesis, and meiosis. Current biology : CB 12(4):277-287.

Nedelec F, Foethke D. 2007. Collective Langevin dynamics of flexible cytoskeletal fibers. New Journal of Physics 9.

Neumann B, Walter T, Heriche JK, Bulkescher J, Erfle H, Conrad C, Rogers P, Poser I, Held M, Liebel U, Cetin C, Sieckmann F, Pau G, Kabbe R, Wunsche A, Satagopam V,

Schmitz MH, Chapuis C, Gerlich DW, Schneider R, Eils R, Huber W, Peters JM, Hyman AA, Durbin R, Pepperkok R, Ellenberg J. 2010. Phenotypic profiling of the human genome by time-lapse microscopy reveals cell division genes. Nature 464(7289):721-727.

Nguyen-Ngoc T, Afshar K, Gonczy P. 2007. Coupling of cortical dynein and G alpha proteins mediates spindle positioning in Caenorhabditis elegans. Nature cell biology 9(11):1294-1302.

Nigg EA. 2001. Mitotic kinases as regulators of cell division and its checkpoints. Nature reviews Molecular cell biology 2(1):21-32.

Nigg EA, Raff JW. 2009. Centrioles, centrosomes, and cilia in health and disease. Cell 139(4):663-678.

Norbury C, Nurse P. 1991. Cyclins and cell cycle control. Curr Biol 1(1):23-24.

O'Connell CB, Wang YL. 2000. Mammalian spindle orientation and position respond to changes in cell shape in a dynein-dependent fashion. Mol Biol Cell 11(5):1765-1774.

O'Connell KF. 2000. The centrosome of the early C. elegans embryo: inheritance, assembly, replication, and developmental roles. Curr Top Dev Biol 49:365-384.

O'Connell KF, Maxwell KN, White JG. 2000. The spd-2 gene is required for polarization of the anteroposterior axis and formation of the sperm asters in the Caenorhabditis elegans zygote. Dev Biol 222(1):55-70.

Oegema K, Desai A, Rybina S, Kirkham M, Hyman AA. 2001. Functional analysis of kinetochore assembly in Caenorhabditis elegans. J Cell Biol 153(6):1209-1226.

Oegema K, Hyman AA. 2006. Cell division. WormBook:1-40.

Ohkura H, Hagan IM, Glover DM. 1995. The conserved Schizosaccharomyces pombe kinase plo1, required to form a bipolar spindle, the actin ring, and septum, can drive septum formation in G1 and G2 cells. Genes & development 9(9):1059-1073.

Park DH, Rose LS. 2008. Dynamic localization of LIN-5 and GPR-1/2 to cortical force generation domains during spindle positioning. Developmental biology 315(1):42-54.

Park M, Krause MW. 1999. Regulation of postembryonic G(1) cell cycle progression in Caenorhabditis elegans by a cyclin D/CDK-like complex. Development 126(21):4849-4860.

Pearson CG, Yeh E, Gardner M, Odde D, Salmon ED, Bloom K. 2004. Stable kinetochore-microtubule attachment constrains centromere positioning in metaphase. Current biology : CB 14(21):1962-1967.

Pelletier L, O'Toole E, Schwager A, Hyman AA, Muller-Reichert T. 2006. Centriole assembly in Caenorhabditis elegans. Nature 444(7119):619-623.

Pelletier L, Ozlu N, Hannak E, Cowan C, Habermann B, Ruer M, Muller-Reichert T, Hyman AA. 2004. The Caenorhabditis elegans centrosomal protein SPD-2 is required for both pericentriolar material recruitment and centriole duplication. Curr Biol 14(10):863-873.

Pellettieri J, Seydoux G. 2002. Anterior-posterior polarity in C. elegans and Drosophila--PARallels and differences. Science 298(5600):1946-1950.

Piano F, Schetter AJ, Mangone M, Stein L, Kemphues KJ. 2000. RNAi analysis of genes expressed in the ovary of Caenorhabditis elegans. Curr Biol 10(24):1619-1622.

Pihan GA, Purohit A, Wallace J, Knecht H, Woda B, Quesenberry P, Doxsey SJ. 1998. Centrosome defects and genetic instability in malignant tumors. Cancer research 58(17):3974-3985.

Pilyugin M, Demmers J, Verrijzer CP, Karch F, Moshkin YM. 2009. Phosphorylation-mediated control of histone chaperone ASF1 levels by Tousled-like kinases. PLoS One 4(12):e8328.

Poulin G, Nandakumar R, Ahringer J. 2004. Genome-wide RNAi screens in Caenorhabditis elegans: impact on cancer research. Oncogene 23(51):8340-8345.

Powers J, Bossinger O, Rose D, Strome S, Saxton W. 1998. A nematode kinesin required for cleavage furrow advancement. Curr Biol 8(20):1133-1136.

Praitis V, Casey E, Collar D, Austin J. 2001. Creation of low-copy integrated transgenic lines in Caenorhabditis elegans. Genetics 157(3):1217-1226.

Raich WB, Moran AN, Rothman JH, Hardin J. 1998. Cytokinesis and midzone microtubule organization in Caenorhabditis elegans require the kinesin-like protein ZEN-4. Mol Biol Cell 9(8):2037-2049.

Riefler GM, Dent SY, Schumacher JM. 2008a. Tousled-mediated activation of Aurora B kinase does not require Tousled kinase activity in vivo. The Journal of biological chemistry 283(19):12763-12768.

Riefler GM, Dent SY, Schumacher JM. 2008b. Tousled-mediated activation of Aurora B kinase does not require Tousled kinase activity in vivo. J Biol Chem 283(19):12763-12768.

Roe JL, Nemhauser JL, Zambryski PC. 1997. TOUSLED participates in apical tissue formation during gynoecium development in Arabidopsis. Plant Cell 9(3):335-353.

Roe JL, Rivin CJ, Sessions RA, Feldmann KA, Zambryski PC. 1993. The Tousled gene in A. thaliana encodes a protein kinase homolog that is required for leaf and flower development. Cell 75(5):939-950.

Romano A, Guse A, Krascenicova I, Schnabel H, Schnabel R, Glotzer M. 2003. CSC-1: a subunit of the Aurora B kinase complex that binds to the survivin-like protein BIR-1 and the incenp-like protein ICP-1. J Cell Biol 161(2):229-236.

Rosasco-Nitcher SE, Lan W, Khorasanizadeh S, Stukenberg PT. 2008. Centromeric Aurora-B activation requires TD-60, microtubules, and substrate priming phosphorylation. Science 319(5862):469-472.

Ruchaud S, Carmena M, Earnshaw WC. 2007. Chromosomal passengers: conducting cell division. Nat Rev Mol Cell Biol 8(10):798-812.

Sbalzarini IF, Koumoutsakos P. 2005. Feature point tracking and trajectory analysis for video imaging in cell biology. Journal of structural biology 151(2):182-195.

Schmidt DJ, Rose DJ, Saxton WM, Strome S. 2005. Functional analysis of cytoplasmic dynein heavy chain in Caenorhabditis elegans with fast-acting temperature-sensitive mutations. Mol Biol Cell 16(3):1200-1212.

Schneider SQ, Bowerman B. 2003. Cell polarity and the cytoskeleton in the Caenorhabditis elegans zygote. Annual review of genetics 37:221-249.

Schonegg S, Hyman AA. 2006. CDC-42 and RHO-1 coordinate acto-myosin contractility and PAR protein localization during polarity establishment in C. elegans embryos. Development 133(18):3507-3516.

Schroer TA. 2004. Dynactin. Annual review of cell and developmental biology 20:759-779.

Schumacher JM, Ashcroft N, Donovan PJ, Golden A. 1998a. A highly conserved centrosomal kinase, AIR-1, is required for accurate cell cycle progression and segregation of developmental factors in Caenorhabditis elegans embryos. Development 125(22):4391-4402.

Schumacher JM, Golden A, Donovan PJ. 1998b. AIR-2: An Aurora/Ipl1-related protein kinase associated with chromosomes and midbody microtubules is required for polar body extrusion and cytokinesis in Caenorhabditis elegans embryos. J Cell Biol 143(6):1635-1646.

Sen SP, De Benedetti A. 2006. TLK1B promotes repair of UV-damaged DNA through chromatin remodeling by Asf1. BMC Mol Biol 7:37.

Severson AF, Bowerman B. 2003. Myosin and the PAR proteins polarize microfilament-dependent forces that shape and position mitotic spindles in Caenorhabditis elegans. The Journal of cell biology 161(1):21-26.

Severson AF, Hamill DR, Carter JC, Schumacher J, Bowerman B. 2000. The aurora-related kinase AIR-2 recruits ZEN-4/CeMKLP1 to the mitotic spindle at metaphase and is required for cytokinesis. Curr Biol 10(19):1162-1171.

Seydoux G, Dunn MA. 1997. Transcriptionally repressed germ cells lack a subpopulation of phosphorylated RNA polymerase II in early embryos of Caenorhabditis elegans and Drosophila melanogaster. Development 124(11):2191-2201.

Siller KH, Doe CQ. 2008. Lis1/dynactin regulates metaphase spindle orientation in Drosophila neuroblasts. Developmental biology 319(1):1-9.

Siller KH, Doe CQ. 2009. Spindle orientation during asymmetric cell division. Nature cell biology 11(4):365-374.

Sillje HH, Nigg EA. 2001. Identification of human Asf1 chromatin assembly factors as substrates of Tousled-like kinases. Current biology : CB 11(13):1068-1073.

Sillje HH, Takahashi K, Tanaka K, Van Houwe G, Nigg EA. 1999. Mammalian homologues of the plant Tousled gene code for cell-cycle-regulated kinases with maximal activities linked to ongoing DNA replication. Embo J 18(20):5691-5702.

Singson A. 2001. Every sperm is sacred: fertilization in Caenorhabditis elegans. Dev Biol 230(2):101-109.

Skop AR, White JG. 1998. The dynactin complex is required for cleavage plane specification in early Caenorhabditis elegans embryos. Current biology : CB 8(20):1110-1116.

Sonnichsen B, Koski LB, Walsh A, Marschall P, Neumann B, Brehm M, Alleaume AM, Artelt J, Bettencourt P, Cassin E, Hewitson M, Holz C, Khan M, Lazik S, Martin C, Nitzsche B, Ruer M, Stamford J, Winzi M, Heinkel R, Roder M, Finell J, Hantsch H, Jones SJ, Jones M, Piano F, Gunsalus KC, Oegema K, Gonczy P, Coulson A, Hyman AA, Echeverri CJ. 2005. Full-genome RNAi profiling of early embryogenesis in Caenorhabditis elegans. Nature 434(7032):462-469.

Speliotes EK, Uren A, Vaux D, Horvitz HR. 2000. The survivin-like C. elegans BIR-1 protein acts with the Aurora-like kinase AIR-2 to affect chromosomes and the spindle midzone. Mol Cell 6(2):211-223.

Srayko M, Kaya A, Stamford J, Hyman AA. 2005. Identification and characterization of factors required for microtubule growth and nucleation in the early C. elegans embryo. Developmental cell 9(2):223-236.

Srinivasan DG, Fisk RM, Xu H, van den Heuvel S. 2003. A complex of LIN-5 and GPR proteins regulates G protein signaling and spindle function in C elegans. Genes & development 17(10):1225-1239.

Strome S, Wood WB. 1983. Generation of asymmetry and segregation of germ-line granules in early C. elegans embryos. Cell 35(1):15-25.

Sugiyama K, Sugiura K, Hara T, Sugimoto K, Shima H, Honda K, Furukawa K, Yamashita S, Urano T. 2002. Aurora-B associated protein phosphatases as negative regulators of kinase activation. Oncogene 21(20):3103-3111.

Sullivan KF. 2001. A solid foundation: functional specialization of centromeric chromatin. Current opinion in genetics & development 11(2):182-188.

Sun Y, Kucej M, Fan HY, Yu H, Sun QY, Zou H. 2009. Separase is recruited to mitotic chromosomes to dissolve sister chromatid cohesion in a DNA-dependent manner. Cell 137(1):123-132.

Sunavala-Dossabhoy G, Balakrishnan SK, Sen S, Nuthalapaty S, De Benedetti A. 2005. The radioresistance kinase TLK1B protects the cells by promoting repair of double strand breaks. BMC molecular biology 6:19.

Sunavala-Dossabhoy G, De Benedetti A. 2009. Tousled homolog, TLK1, binds and phosphorylates Rad9; TLK1 acts as a molecular chaperone in DNA repair. DNA repair 8(1):87-102.

Sunavala-Dossabhoy G, Li Y, Williams B, De Benedetti A. 2003. A dominant negative mutant of TLK1 causes chromosome missegregation and aneuploidy in normal breast epithelial cells. BMC Cell Biol 4:16.

Sunkel CE, Glover DM. 1988. polo, a mitotic mutant of Drosophila displaying abnormal spindle poles. Journal of cell science 89 (Pt 1):25-38.

Timmons L, Fire A. 1998. Specific interference by ingested dsRNA. Nature 395(6705):854.

Toya M, Iida Y, Sugimoto A. 2010. Imaging of mitotic spindle dynamics in Caenorhabditis elegans embryos. Methods in cell biology 97:359-372.

Trojer P, Reinberg D. 2006. Histone lysine demethylases and their impact on epigenetics. Cell 125(2):213-217.

Tsai JW, Bremner KH, Vallee RB. 2007. Dual subcellular roles for LIS1 and dynein in radial neuronal migration in live brain tissue. Nature neuroscience 10(8):970-979.

Tsai MC, Ahringer J. 2007. Microtubules are involved in anterior-posterior axis formation in C. elegans embryos. The Journal of cell biology 179(3):397-402.

Tsou MF, Hayashi A, DeBella LR, McGrath G, Rose LS. 2002. LET-99 determines spindle position and is asymmetrically enriched in response to PAR polarity cues in C. elegans embryos. Development 129(19):4469-4481.

Tsou MF, Hayashi A, Rose LS. 2003. LET-99 opposes Galpha/GPR signaling to generate asymmetry for spindle positioning in response to PAR and MES-1/SRC-1 signaling. Development 130(23):5717-5730.

Vagnarelli P, Earnshaw WC. 2004. Chromosomal passengers: the four-dimensional regulation of mitotic events. Chromosoma 113(5):211-222.

van den Heuvel S. 2005. Cell-cycle regulation. WormBook:1-16.

Van Hooser AA, Ouspenski, II, Gregson HC, Starr DA, Yen TJ, Goldberg ML, Yokomori K, Earnshaw WC, Sullivan KF, Brinkley BR. 2001. Specification of kinetochore-forming chromatin by the histone H3 variant CENP-A. Journal of cell science 114(Pt 19):3529-3542.

Villeneuve AM. 1994. A cis-acting locus that promotes crossing over between X chromosomes in Caenorhabditis elegans. Genetics 136(3):887-902.

Wallenfang MR, Seydoux G. 2000. Polarization of the anterior-posterior axis of C. elegans is a microtubule-directed process. Nature 408(6808):89-92.

Walter AO, Seghezzi W, Korver W, Sheung J, Lees E. 2000. The mitotic serine/threonine kinase Aurora2/AIK is regulated by phosphorylation and degradation. Oncogene 19(42):4906-4916.

Wang Y, Liu J, Xia R, Wang J, Shen J, Cao R, Hong X, Zhu JK, Gong Z. 2007. The protein kinase TOUSLED is required for maintenance of transcriptional gene silencing in Arabidopsis. EMBO Rep 8(1):77-83.

Wittmann T, Hyman A, Desai A. 2001. The spindle: a dynamic assembly of microtubules and motors. Nature cell biology 3(1):E28-34.

Wong OK, Fang G. 2005. Plx1 is the 3F3/2 kinase responsible for targeting spindle checkpoint proteins to kinetochores. J Cell Biol 170(5):709-719.

Wong OK, Fang G. 2006. Loading of the 3F3/2 antigen onto kinetochores is dependent on the ordered assembly of the spindle checkpoint proteins. Mol Biol Cell 17(10):4390-4399.

Wong OK, Fang G. 2007. Cdk1 phosphorylation of BubR1 controls spindle checkpoint arrest and Plk1-mediated formation of the 3F3/2 epitope. J Cell Biol 179(4):611-617.

Wood WB. 1988. The Nematode *Caenorhabditis elegans*. Wood WB, editor. Plainview, NY: Cold Spring Harbor Laboratory Press. 667 p.

Yamakawa A, Kameoka Y, Hashimoto K, Yoshitake Y, Nishikawa K, Tanihara K, Date T. 1997. cDNA cloning and chromosomal mapping of genes encoding novel protein kinases termed PKU-alpha and PKU-beta, which have nuclear localization signal. Gene 202(1-2):193-201.

Yeh CH, Yang HJ, Lee IJ, Wu YC. 2010. Caenorhabditis elegans TLK-1 controls cytokinesis by localizing AIR-2/Aurora B to midzone microtubules. Biochemical and biophysical research communications 400(2):187-193.

Zachos G, Black EJ, Walker M, Scott MT, Vagnarelli P, Earnshaw WC, Gillespie DA. 2007. Chk1 is required for spindle checkpoint function. Developmental cell 12(2):247-260.

Zhang J, Yang PL, Gray NS. 2009. Targeting cancer with small molecule kinase inhibitors. Nat Rev Cancer 9(1):28-39.

Zhang K, Lin W, Latham JA, Riefler GM, Schumacher JM, Chan C, Tatchell K, Hawke DH, Kobayashi R, Dent SY. 2005. The Set1 methyltransferase opposes Ipl1 aurora kinase functions in chromosome segregation. Cell 122(5):723-734.

Zonies S, Motegi F, Hao Y, Seydoux G. 2010. Symmetry breaking and polarization of the C. elegans zygote by the polarity protein PAR-2. Development 137(10):1669-1677.

Zwaal RR, Ahringer J, van Luenen HG, Rushforth A, Anderson P, Plasterk RH. 1996. G proteins are required for spatial orientation of early cell cleavages in C. elegans embryos. Cell 86(4):619-629.

Jason Robert Ford was born in Bryan, Texas in 1983. He attended Bryan High School where he graduated in the top two percent of his high school class in 2001, and then went on to matriculate at Texas A&M University in College Station, Texas. He pursued an education in biochemistry and molecular research during his undergraduate studies, gaining valuable research experience as an undergraduate research assistant in the laboratory of Dr. Patricia LiWang. He also participated in the Meyerhoff Undergraduate Summer Research Program in the HHMI laboratory of Dr. Michael Summers. Jason also joined the L.T. Jordan Institute while at Texas A&M and went to study abroad in the United Kingdom in the laboratory of Dr. Paul Brown at King's College London. He then joined the University of Texas Health Sciences Center at Houston Graduate School of Biomedical Sciences and earned his Master of Science degree in cell biology while working in the laboratory of Dr. Jill Schumacher at the University of Texas M.D. Anderson Cancer Center, where he went on to complete his Ph.D. dissertation studying the roles of the Tousled-like kinase during mitosis.

Contact: jasonrobertford@gmail.com